TECHNISCHE UNIVERSITÄT MÜNCHEN

Lehrstuhl für Experimentelle Genetik

Regulation of the *Dll1* gene during mouse embryogenesis: MSD mediated *cis*-regulation and identification of miRNAs

Dipl.-Biol. Univ. Bastian G. Hösel

Vollständiger Abdruck der von der Fakultät Wissenschaftszentrum Weihenstephan für Ernährung, Landnutzung und Umwelt der Technischen Universität München zur Erlangung des akademischen Grades eines

Doktors der Naturwissenschaften

genehmigten Dissertation.

Vorsitzender: Univ.-Prof. Dr. M. Hrabé de Angelis

Prüfer der Dissertation:

1. Priv.-Doz. Dr. J. Beckers
2. Univ.-Prof. A. Schnieke, Ph.D.

Die Dissertation wurde am 24.02.2011 bei der Technischen Universität München eingereicht und durch die Fakultät Wissenschaftszentrum Weihenstephan für Ernährung, Landnutzung und Umwelt am 17.06.2011 angenommen.

For Kolja and Bea.

Special thanks go to Dr. Johannes Beckers, Prof. Dr. Martin Hrabé de Angelis, Dr. Gerhard Przemeck, Sandra Schädler, Zambaralal Bhujabal, Dr. Rashmi Rajendra, Annerose Kurtz-Drexler, Dr. Hendrik Tiedemann, Dr. Ingeborg Klymiuk, Christian Cohrs and Prof. Dr. Angelika Schnieke for their support.

Table of contents

1. Summary

To evaluate the function of MSD, a potential mesodermal *Dll1 cis*-regulatory element, *in vivo* in its endogenous context, we have replaced and deleted MSD through homologous recombination in mouse embryonic stem cells. Two different alleles were generated, the MSD replacement allele (*Dll1*^{tm1leg}), harbouring a selection cassette in place of MSD and the floxed MSD deletion allele (*Dll1*$^{tm1.1leg}$).

Heterozygous and homozygous *Dll1*^{tm1leg} and *Dll1*$^{tm1.1leg}$ MSD deficient mutant mice are viable and fertile. Whole mount *in situ* hybridisations and quantitative PCR data suggest that neither replacement nor deletion of MSD dramatically changes *Dll1* expression during mouse embryonic development. Instead we found that MSD is specifically required for *Dll1* expression in the presomitic mesoderm at 8.5 days post coitum (d.p.c.). A subtle down-regulation of *Dll1* at 8.5 dpc is detected exclusively in the presomitic mesoderm (PSM) of homozygous *Dll1*^{tm1leg} and *Dll1*$^{tm1.1leg}$ MSD mutant mouse embryos. On the morphological level, a common phenotypic alteration in MSD deficient mice, is the presence of ectopic ribs on the 7th cervical vertebra. This skeletal malformation is reminiscent of a posterior homeotic transformation since it co-incides with an anterior shift of *Hoxb6* mRNA expression at 12.5 dpc. We hypothesize that this homeotic transformation could be caused by the observed down-regulation of *Dll1* in the PSM of 8.5 dpc embryos, since this corresponds to the developmental stage, when the somites, contributing to the vertebrae of cervical to thoracic region, bud off from the PSM.

Previous experiments suggested that Tbx6 might be one of the important transcription factors that bind to MSD and control *Dll1* expression *in vivo*. Accordingly, we find that mice heterozygous for a *Tbx6* loss-of-function allele phenocopy most vertebral malformations of MSD deficient mice. It is thus likely that

1. Summary

Tbx6 mediates most functions of MSD *in vivo,* which are associated with the morphogenesis of the vertebral elements at the cervical-thoracic transition. In contrast, genetically combining the *Tbx6* loss-of-function and the MSD deletion alleles leads to a marked increase of split vertebral bodies in the lumbar region of compound mutants, providing evidence for an additive effect of *Tbx6* and MSD alleles during the development of the lumbar vertebrae. We hypothesise that correct *Dll1* and *Tbx6* expression most likely requires a feedback loop of *Tbx6*, MSD and *Dll1*.

In order to begin to unravel additional and novel regulatory mechanisms for *Dll1* gene expression, we performed a combined *in silico* analysis and *in situ* hybridisation approach, to identify miRNAs that are spatially and temporally co-expressed with the *Dll1* mRNA. We identified 7 miRNAs (miR-34a, miR-103, miR-107, miR-130a, miR-130b, miR-449a and miR-449c) that overlap with *Dll1* expression in the paraxial mesoderm, the neural tube and hindbrain region and in cranial ganglia during mouse embryogenesis. Studies of the functional role of miRNAs in the regulation of *Dll1* during mouse embryogenesis may now focus on the miRNAs identified as candidates in our study.

2. Zusammenfassung

Um die Funktion von MSD, einem potenziellen mesodermalen *Dll1* Enhancer an seiner endogenen Position aufzuklären, haben wir ihn durch homologe Rekombination in embryonalen Mausstammzellen ausgetauscht und deletiert. Zwei verschiedene Allele wurden generiert, das MSD Austauschallel (*Dll1*^{tm1leg}), welches anstatt von MSD eine Selektionskassette trägt, sowie das gefloxte MSD Deletionsallel (*Dll1*$^{tm1.1leg}$).

Heterozygote und homozygote *Dll1*^{tm1leg} und *Dll1*$^{tm1.1leg}$ MSD defiziente Mäuse sind lebensfähig und fruchtbar. *In situ* Hybridisierungen und quantitative PCR Daten weisen darauf hin, dass weder der Austausch noch die Deletion von MSD die *Dll1* Expression während der embryonalen Entwicklung dramatisch ändern. Wir können jedoch zeigen, dass MSD nötig ist, um die *Dll1* Expression im präsomitischen Mesoderm von 8,5 Tage alten Embryonen zu steuern. Eine schwache Herrunterregulation der *Dll1* Expression ist im präsomitischen Mesoderm von *Dll1*^{tm1leg} und *Dll1*$^{tm1.1leg}$ MSD defizienten 8,5 Tage alten Embryonen zu finden. Die gemeinsame morphologische Veränderung in Mäusen, die einen Austausch oder eine Deletion für MSD tragen, ist eine zusätzliche Rippe am siebten cervikalen Segment. Diese morphologische Veränderung erinnert an eine posteriore homöotische Transformation, da sie zusammen mit einer Veränderung der anterioren *Hoxb6* Expressionsgrenze in 12,5 Tage alten Embryonen auftaucht. Wir hypothetisieren, dass diese homöotische Transformation auf die Herunterregulation der *Dll1* Expression im präsomitschen Mesoderm in 8,5 Tage alten Embryonen zurückzuführen ist, da das dem Entwicklungszeitpunkt entspricht, an welchem die Somiten vom präsomitischen Mesoderm abgespaltet werden, welche zum cervikal nach thorakalen Übergang beitragen.

2. Zusammenfassung

Frühere Experimente wiesen darauf hin, dass Tbx6 ein wichtiger Transkriptionsfaktor ist, welcher an MSD bindet und die *Dll1* Expression *in vivo* kontrolliert. In Übereinstimmung damit, phänokopieren Mäuse die heterozygot für *Tbx6* sind, die meisten Wirbelmissbildungen von MSD defizienten Mäusen. Es ist somit wahrscheinlich, dass Tbx6 den größten Teil der Funktion von MSD, welche mit der Morphogenese der Bildung der cervikalen nach thorakalen Transition assoziiert sind, *in vivo* vermittelt. Im Gegensatz dazu führt genetische Kombination von *Tbx6* und MSD Allelen zu einer Zunahme gespaltener Wirbelkörper im lumbaren Bereich der Wirbelsäule, was einen additiven Effekt von Tbx6 und MSD Allelen während der Entwicklung der lumbaren Wirbel andeutet. Wir hypothetisieren, dass korrekte *Dll1* und *Tbx6* Expression wahrscheinlich von einer Rückkopplungschleife, welche aus *Tbx6*, MSD und *Dll1* besteht, abhängig ist.

Außerdem haben wir angefangen neue und zusätzliche regulatorische Mechanismen für die *Dll1* Expression zu identifizieren. Dafür haben wir eine kombinierte *in silico* und *in situ* Studie durchgeführt, um miRNAs zu identifizieren, die räumlich und zeitlich mit der *Dll1* mRNA co-exprimiert sind. Wir identifizieren sieben miRNAs (miR-34a, miR-103, miR-107, miR-130a, miR-130b, miR-449a und miR-449c), welche mit der *Dll1* Expression im paraxialen Mesoderm, dem Neuralrohr und dem Hinterhirnbereich, sowie in den kranialen Ganglien überlappen. Studien der funktionellen Rolle von miRNAs in der Regulierung von *Dll1* während der Mausembryogenese sollten sich jetzt auf die miRNAs konzentrieren, welche als Kandidaten in unserer Studie identifiziert wurden.

3. Publications

Hoesel, B., Bhujabal, Z., Przemeck, G. K. H., Kurz-Drexler, A., Weisenhorn, D. M. V., de Angelis, M. H., Beckers, J., 2010.

Combination of *in silico* and *in situ* hybridisation approaches to identify potential *Dll1* associated miRNAs during mouse embryogenesis.

Gene Expression Patterns 10 (2010) 265–273

Nicola Rath, Sarah Abdul-Wajid, Molly Thomas, Christian Cohrs, Frauke Neff, Bastian Hoesel, Eric Yanni, Kimie Hattori, Zhibin Chen, Valerie Gailus-Durner, Johannes Beckers, Irene Esposito, Wolfgang Hans, Helmut Fuchs, Martin Hrabé de Angelis, Anjana Rao, Vigo Heissmeyer, K. Mark Ansel

Eri1 inhibits RNAi and the miRNA pathway in T cell differentiation and skeletal patterning

Manuscript in preparation.

Hendrik B. Tiedemann, Elida Schneltzer, Bastian Hösel, Johannes Beckers, Gerhard K. H. Przemeck and Martin Hrabé de Angelis

From Dynamic Expression Patterns to Boundary Formation in the Presomitic Mesoderm

Manuscript in preparation.

Bastian Hoesel, Christian Cohrs, Sonja Becker, Martin Hrabé de Angelis and Johannes Beckers

Regionalization is coupled to the *Dll1* enhancer MSD

Manuscript in preparation.

4. Introduction

Embryonic development is a process that requires the functioning of many different signalling pathways. It is characterized by dynamic and complex gene expression patterns, which are generated by the modulation of multiple regulatory stages.

Many novel mechanisms of gene regulation have been added to the “dashboard“ since the discovery of *cis*-mediated gene regulation, when Jacob and Monod characterized the lacZ operon (Jacob et al., 1960). Besides *cis*-mediated gene regulation, especially non-coding RNAs have been a focus of many research groups in recent years (Guo et al., 2010; Zinzen et al., 2009). It is becoming clear that gene regulation has a far-reaching impact for embryogenesis and that it must be considered as a functional part of most genes and gene networks.

One important signalling pathway required for many differential aspects of mouse embryonic development is the Delta-Notch signalling pathway. The proteins involved and their functions are highly conserved between many species. Especially the *Delta-like 1* (*Dll1*) gene has been shown to be essential for a variety of developmental processes such as, for example somitogenesis, neurogenesis and left -right development (Hrabě de Angelis et al., 1997; Marklund et al., 2010; Przemeck et al., 2003). During these developmental processes the *Dll1* gene is expressed in a complex and dynamic pattern (Beckers et al., 1999; Bettenhausen et al., 1995; Morrison et al., 1999), which is indispensable for its function (Teppner et al., 2007). Little is known however about *cis*- and miRNA mediated regulation of *Dll1* during mouse embryonic development. It is the aim of this work to provide novel insights into *cis*- and miRNA mediated *Dll1* gene regulation. The underlying biological and molecular processes, which are essential to understand the presented work and interpret the obtained results are introduced on the next pages.

4.1 Somitogenesis

Somites are epithelial blocks of tissue that are generated in an anterior to posterior fashion by mesenchymal to epithelial transition (MET) from the presomitic mesoderm (PSM) at the posterior end of the developing embryo (Duband et al., 1987; Tam and Trainor, 1994). Early in development, PSM cells migrate through the primitive streak. In the mouse, around 9.5 days post coitum (d.p.c.), a new tissue called the tailbud is formed. After its formation PSM cells are derivatives of this structure (Tam, 1981; Tam and Trainor, 1994). Soon after somites are formed, they de-epithelialize into the ventral sclerotome, which develops into the precursors of the axial skeleton and form the dorsal dermomyotome, which contributes to the myotome and dermatome (Christ and Ordahl, 1995). Later in development these structures form the skeletal muscles and dermis of the back, respectively (Stern et al., 1988). Somites are subdivided into cranial and caudal half-segments, which show differences in gene expression patterns and functional properties. This partitioning is, for example, essential for the definitive patterning of vertebrae. During a process called resegmentation, the definite precursors of the vertebrae form, when the posterior part of one somite fuses to the anterior part of the consecutive somite (Aoyama and Asamoto, 1988, 2000; Bagnall et al., 1988). Thus, the metamerism of the somites provides the basis for the segmented arrangement of the axial skeleton (Christ and Wilting, 1992).

Somites form pair wise on both sides of the neural tube in a coordinated fashion. The time period, which is needed to form one pair of somites is characteristic for each species, ranging from 30 minutes in zebrafish, 90 minutes in chicken and 120 minutes in mouse, to approximately 4–5 hours in humans (Richardson et al., 1998). The number of somites, and therefore the number of vertebrae, can vary greatly among species. Frogs have up to ~10, humans have 33 and snakes can have more

than 300 vertebrae.

In the mouse the first 4.5 somites fuse to form the occipital bone of the skull. The more posterior somites form the definite vertebral column including cervical, thoracic, lumbar and tail segments (Couly et al., 1993). Somitogenesis begins caudally to the otic vesicle. It can principally be subdivided into three main phases. During the specification phase the cells of the epiblast and later on of the tailbud receive their paraxial mesoderm identity. In the second phase a blueprint for the segmentation is generated in the anterior PSM, which is in the third phase translated into morphological segments, the somites (Dequéant and Pourquié, 2008). In chicken, mouse, snake and zebrafish embryos, termination of somitogenesis is mediated by shrinking of the PSM, which presumably reflects a gradual extinction of signals (Gomez et al., 2008).

Nowadays, the most widely accepted model for somitogenesis is the clock and wavefront model, which was initially proposed by Cooke and Zeeman in 1976, long before the molecular factors were identified (Cooke and Zeeman, 1976). The key elements of this model are a molecular clock in the PSM and a maturation wave front, which moves posterior as the embryo grows (Figure 1).

In situ hybridisations provided the first experimental evidence for an oscillator coupled to somitogenesis, which showed transcriptional bursts of an mRNA encoding the transcription factor *c-hairy1* in the PSMs of chicken embryos (Figure 1 B). These expressional bursts temporally correlated with somite formation. *C-hairy1* is a transcription factor homologous to the Drosophila segmentation gene *hairy1* (*HES 1*) (Palmeirim et al., 1997). Subsequently, several other genes exhibiting a cyclic behaviour were identified in fish, frog and mouse, indicating that the segmentation clock is conserved among vertebrates. The first genes identified exhibiting a periodic

mRNA expression in the PSM, belong to the Delta-Notch signalling pathway, e.g lunatic fringe (*Lfng*), which is a glucosyl-transferase that modifies the Notch receptor, or the *Hes* genes, which are the murine homologues of *c-hairy1* (Aulehla and Johnson, 1999; Forsberg et al., 1998; McGrew et al., 1998). However, not all Delta-Notch pathway genes, are characterized by periodic mRNA expression in the PSM, but defects in somitogenesis occur, for example in *Notch1* (Conlon et al., 1995), Delta-like 1 (*Dll1*) (Hrabě de Angelis et al., 1997), Delta-like 3 (*Dll3*) (Kusumi et al., 1998), Presenilin 1 (*Psen1*) (Wong et al., 1997) , *RBPJk* (Oka et al., 1995) and *Lfng* (Aulehla and Johnson, 1999; Evrard et al., 1998) loss-of-function mutants.

The first indication that pathways other than the Delta-Notch signalling pathway are necessary for somitogenesis came from the observation, that *Axin2,* a negative regulator of the Wnt pathway, also shows cyclic gene expression in the PSM. Further, a hypomorphic mutant for Wnt3a, vestigial tail (vt), showed disrupted *Axin2* and *Lfng* expression (Aulehla et al., 2003).

A microarray based study of mouse PSMs lead to the identification of a much larger number of genes with periodic expression patterns (Dequéant et al., 2006). Although *Axin2* deficient mice do not show disturbed somitogenesis (Yu et al., 2005), many of the newly identified genes that belong to the Wnt pathway, for example *Dkk1* (MacDonald et al., 2004) or *Sp5* (Harrison et al., 2000), which cycle in anti-phase with respect to Delta-Notch signalling (Dequéant et al., 2006), have an abnormal somite phenotype, when the genes are mutated. These results support an essential role of the Wnt pathway for the segmentation clock in the mouse. In this study a large number of cycling genes that belong to the Fgf signalling pathway were also identified (Dequéant et al., 2006).

The maturation wavefront, which was initially postulated by Cooke and Zeeman

(Cooke and Zeeman, 1976), is also characterized on the molecular level, albeit partially (Figure 1 A). It consists of specific *Fgf8*, *Mesp2* (mesoderm posterior 2) and *Wnt3a* expression domains in the PSM. *Wnt3a* and *Fgf8* are expressed in the growth zone of the posterior PSM, thus resulting in posterior to anterior expression gradients of their respective mRNAs in the PSM (Aulehla et al., 2003; Dubrulle et al., 2001). These gradients control the conversion of the clock pulse into the spatial periodicity of somites (Dequéant and Pourquié, 2008). The size of a somite is thus determined by the distance traveled by the wavefront during one period of the segmentation clock oscillation (Iimura et al., 2009). In contrast, *Mesp2* is periodically expressed in a specific stripe pattern in the first nascent somite (Morimoto et al., 2005; Takahashi et al., 2000). Somite boundary formation is lost in *Mesp2* deficient mouse embryos (Saga et al., 1997; Takahashi et al., 2007). In addition, Mesp2 was shown to induce *Eph4a* (Nakajima et al., 2006), by probably controlling mesenchymal to epithelial transition (Barrios et al., 2003; Cooke et al., 2005; Durbin et al., 1998). However, Epha4 deficient mice do not show a somitic phenotype, indicating that additional factors may be needed, which act downstream of *Mesp2* (Dottori et al., 1998; Kullander et al., 2001; Nakajima et al., 2006). Nevertheless, morphological segmentation is accompanied by dynamic METs (Duband et al., 1987), resulting in each somite having a ephitelialized layer wherein an internal mesenchyme is located, termed the somitocoel (Mittapalli et al., 2005). The transition state between epithelial and mesenchymal is pivotal for most organogenic processes. MET takes place for example during kidney development and coelomic cavity formation (Funayama et al., 1999; Nakaya et al., 2004 and references therein). The reverse process, termed epithelial to mesenchymal transition (EMT) takes place for example during wound healing and cancer progression (Dale et al., 2006; Martello et al., 2010).

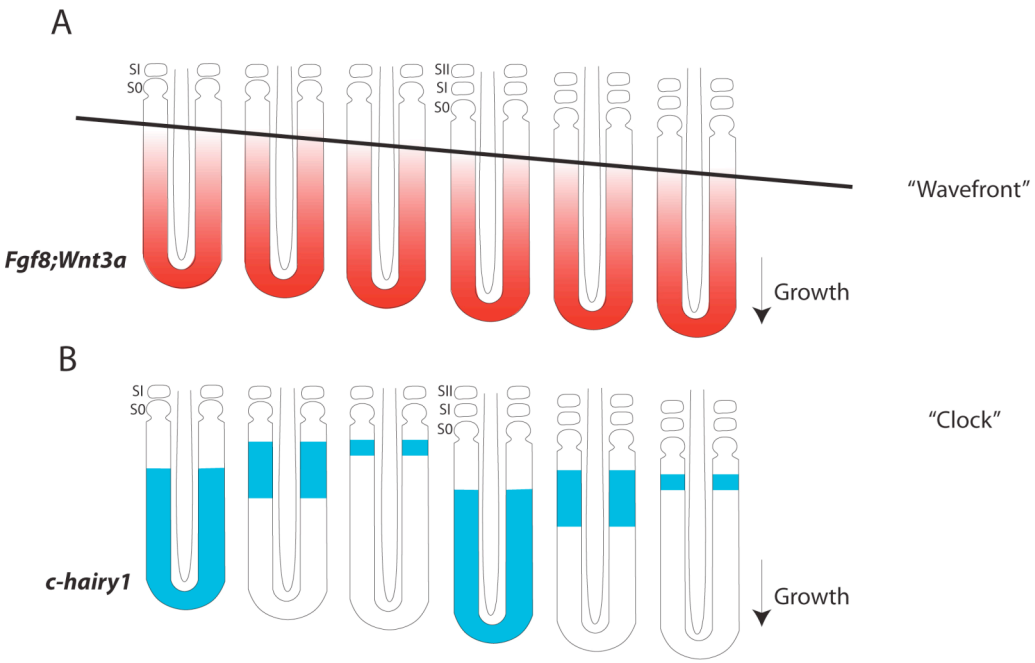

Figure 1: The clock and wavefront model for somitogenesis (modified from (Dequéant and Pourquié, 2008; Pourquié, 2004))

(A) *Fgf8* and *Wnt3*a are expressed in a posterior to anterior gradient in the PSM, which sets a window of determination (determination front), where a new somite is formed. This window is moving posterior during development.

(B) A molecular clock in the PSM sets the pace for somite formation.

4.2 Establishment of anterior-posterior identities in axial tissues

Although all recently formed somites appear extrinsically similar, vertebrae acquire distinct morphology along the anterior-posterior axis, as the vertebrate column is partitioned into domains such as cervical, thoracic, sacral and caudal.

This acquisition of vertebral identities is controlled by homeotic genes (Hox), which provide anterior-posterior identity to structures during embryogenesis (Wellik, 2007). During formation of the vertebral column, each somite receives its identity based on its axial position. In amniotes, Hox genes can be subdivided into four groups (Hoxa; Hoxb; Hoxc; Hoxd (Figure 2 A)), which each are organized into clusters (Liu et al., 2007). Each cluster contains up to 11 Hox genes of one paralogous group, mammals do have 39 Hox genes in total (Duboule, 2007). Genes from these clusters are

expressed at specific boundaries during development. The most anteriorly expressed *Hox* genes reside at the 3´end of the cluster and are expressed first during development, whereas *Hox* genes that have a more 5´ orientation in the cluster are expressed sequentially (Figure 2 B), thus providing tissues with there unique " Hox code" (Deschamps and van Nes, 2005). This remarkable correlation between the spatiotemporal expression of the genes and their linear order on the chromosome has been termed spatiotemporal colinearity (Duboule and Morata, 1994). This spatiotemporal colinearity leads to convoluted expression domains of *Hox* genes along the anterior-posterior axis (Figure 2 C), which results in specific combinations of individual *Hox* genes expressed in each somite (Kessel and Gruss, 1991).

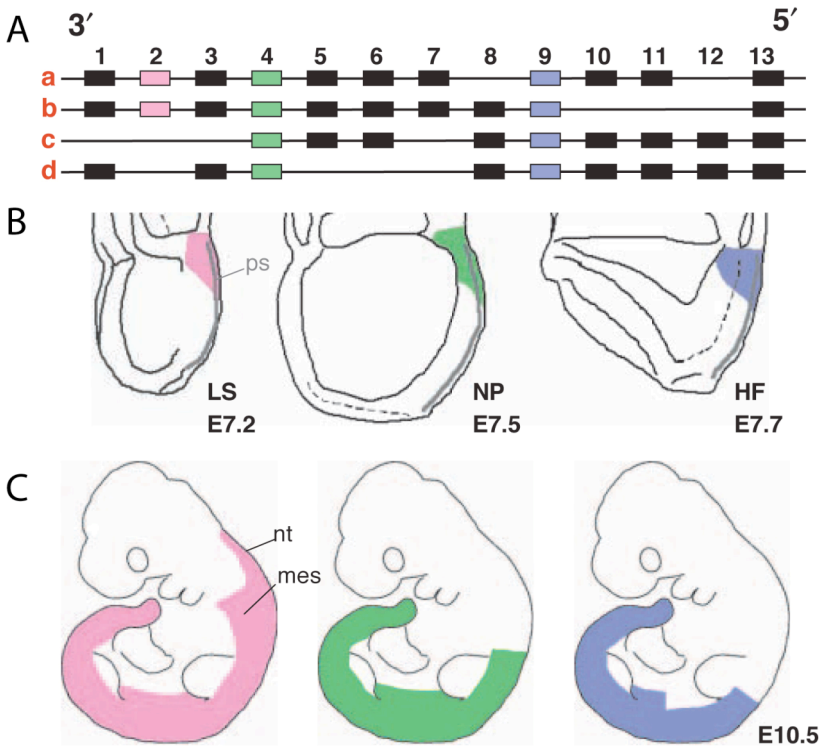

Figure 2: The mouse Hox clusters and *Hox* gene expression during mouse embryonic development (modified from (Deschamps and van Nes, 2005))

(A) The four Hox clusters in the mouse (a, b, c, d) are displayed in their clustered organisation on the respective chromosomes.

(B) *Hox* gene expression starts early during mouse development and the expression is activated sequentially, which reflects the linear organisation on the respective

chromosomes. Thus, 3` Hox2 paralogues are activated first (pink) followed by the more 5` Hox4 (green) and Hox9 paralogues (blue).
(C) Later in development Hox genes display expression domains with distinct anterior limits, thus leading to a unique combination of Hox gene expression ("Hox code") in derivatives of the paraxial mesoderm.

Another remarkable feature of *Hox* genes is termed posterior prevalence in vertebrates. Posterior prevalence or phenotypic suppression was first characterized in a temperature sensitive *Drosophila* mutant for the Polycomb gene *extra-sex combs* (*esc*) (Struhl, 1983). In mice with loss-of-function mutations for *Hox* genes, vertebral malformations along the anterior-posterior axis are usually restricted to a narrow region in the anterior-most expression domain of the mutated *Hox* genes (Horan et al., 1994; van den Akker et al., 2001; Wellik and Capecchi, 2003). In more posterior regions where the other *Hox* genes are normally expressed but the mutated gene is lacking, mice usually show a normal skeletal morphology. Over-expression of *Hox* genes anterior to their normal expression domains in transgenic mice, leads to posterior homeotic transformations in those vertebrae, which ectopically express the transgene (Kessel et al., 1990; Lufkin et al., 1992). The posterior-most *Hox* genes expressed in a somite is thus considered to play a prevalent role in specifying its future vertebra identity.

The onset of *Hox* gene activation has been studied in detail in chicken and mouse embryos (Forlani et al., 2003; Iimura and Pourquié, 2006). During mouse development *Hox* gene expression starts around 7.2 dpc in the primitive streak and expands rostrally towards the node. However, *Hox* codes are not fixed at the node, but must be acquired later and anterior to the node in the neuroectoderm, and independently in the mesoderm (Forlani et al., 2003). *Hoxb8* expression starts, for

example, around 7.5 dpc in the primitive streak and subsequently expands towards the node. After the *Hox* gene expression reaches the node, it migrates further anterior through the presomitic mesoderm, until it reaches its final expression boundary in the somites (Iimura and Pourquié, 2006). Interestingly, the corresponding primitive streak cells do have their anterior most localization at the level of somites 6/7, whereas the anterior most *Hoxb8* expression domain resides more posterior, at the level of somites 10/11 (Forlani et al., 2003). This data indicates that the position of the definitive *Hox* gene expression boundaries requires modification after cells exit the primitive streak and before they are incorporated into a somite, hence, while located in the PSM (Deschamps and van Nes, 2005; Forlani et al., 2003; Iimura et al., 2009).

4.3 The canonical Delta-Notch signalling pathway

Dll1 is a type 1 transmembrane protein (Artavanis-Tsakonas et al., 1999) and both the Delta ligand and its receptor Notch contain Epidermal Growth Factor (EGF) like repeats in their extra cellular domain, through which they are thought to interact (Bettenhausen et al., 1995). Early experiments in fly led to one of the first known function of Delta and its receptor Notch. They act in a process called lateral inhibition, where a Delta expressing cell prevents the adjacent Notch expressing cells from assuming the same fate (Artavanis-Tsakonas et al., 1995; Artavanis-Tsakonas et al., 1999). It proposes a function of Delta Notch signalling in neuronal differentiation, in which the Delta expressing neuronal cell inhibits the Notch expressing cells and changes its fate to that of an epidermal progenitor cell. This has also been confirmed in Xenopus (Chitnis et al., 1995) and teleost fish (Appel et al., 2001). Homologues of the Delta-Notch pathway have also been identified in the mouse. There are at least four known Notch (Notch 1-4) receptors (Ellisen et al., 1991; Lardelli et al., 1994;

Uyttendaele et al., 1996; Weinmaster et al., 1992), and two Jagged and three Delta-like ligands (Bettenhausen et al., 1995; Dunwoodie et al., 1997; Lan et al., 1997; Lindsell et al., 1995) of which *Dll1* and *Dll3* are known to be essential for normal somitogenesis (Hrabě de Angelis et al., 1997; Kusumi et al., 1998). Dll4, the third Delta-like protein is thought to play a role in vascular development (Gale et al., 2004).

In the canonical view of the Notch signalling pathway one of the Delta ligands binds to one of the Notch receptors of an adjacent cell (Figure 3 A). This ligand-receptor interaction leads to three induced proteolytic cleavages of the Notch receptor. The first and second proteolytic cleavage is mediated by ADAM-metalloproteases (Figure 3 B and not shown), whereas the third proteolytic cleavage is mediated by the γ-secretase complex (Figure 3 C). This leads to the release of the Notch intracellular domain (NICD). NICD then translocates into the nucleus and binds to the transcriptional repressor RBPjk (CSL) turning it into a transcriptional activator. Together with its co-activator mastermind, RBPjk subsequently induces expression (Figure 3 D) of downstream target genes (Bray, 2006). Many of the most well defined Delta-Notch target genes belong to the Hes/Hey family of basic helix-loop-helix transcription factors: *Hes1, Hes5, Hes7 Hey1*, *Hey2* and *HeyL*, which are considered to mediate most of the Notch functions (Fischer and Gessler, 2007). The Hes genes *Hes7, Hes1, Hes5* and *Hey2* are expressed periodically in the PSM, albeit only mice deficient for Hes7 show defective somitogenesis (Bessho et al., 2001; Jouve et al., 2000; Leimeister et al., 2000). Nevertheless, the Hes genes are still considered to play a major role in controlling oscillatory gene expression in the PSM as *Hes7* protein half-life is essential for correct somite segmentation and oscillatory gene expression in the PSM (Hirata et al., 2004).

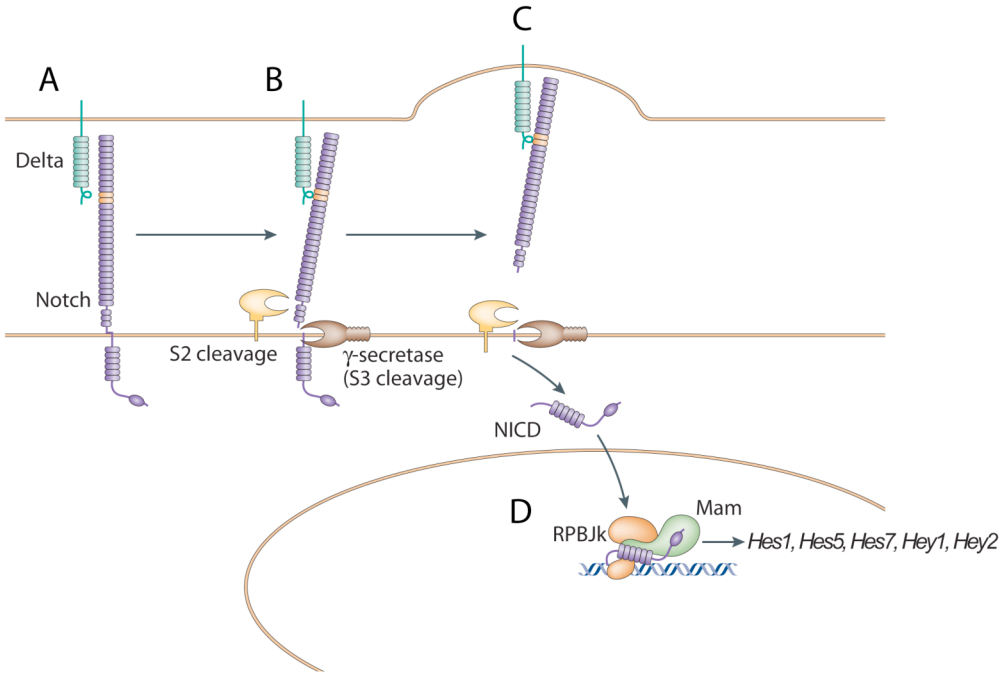

Figure 3: The canonical Delta-Notch pathway (modified from (Bray, 2006)).
(**A**) In the canonical Delta Notch pathway the Delta ligand first binds to the Notch receptor. This ligand-receptor interaction leads to induced proteolytic cleavages (**B**, **C**) of the Notch receptor. (**B**) The second proteolytic cleavage is mediated by ADAM-metalloproteases. (**C**) The third proteolytic cleavage is mediated by the γ-secretase complex, which leads to the release of the Notch intracellular domain (NICD). (**D**) NICD then translocates into the nucleus and binds to the transcriptional repressor RBPjk (CSL) turning it into an activator. Together with its co-activator mastermind (Maml1), RBPjk subsequently induces expression of downstream target genes (*Hes1, Hes5, Hes7, Hey1, Hey2*).

4.4 Regionalization and segmentation

Potential connections between the acquisition of vertebral identity (regionalization) and the segmentation process are under current dispute in the literature. Some studies postulated a direct link between the segmentation clock and the establishment of anterior to posterior identities. In an early study, it was shown that the *Hoxd1* gene is expressed in dynamic stripes within the PSM. These *Hoxd1* stripes were abolished when *RBPjk* was inactivated (Zákány et al., 2001), suggesting

a functional relation between Delta-Notch signalling and the expression of *Hox* genes. Using Fgf8 soaked beads, which lead to the development of smaller somites anterior to the bead, others could show that the anterior expression limits of some Hox genes were changed correspondingly to the appropriate somite number (Alvares et al., 2003; Dubrulle et al., 2001). Based on this data a counting mechanism was proposed, where the numbers of oscillations of the segmentation clock do have an instructive role on the determination of the establishment of anterior Hox gene expression (Jouve et al., 2002). Furthermore, precisely regulated Notch activity in the PSM was shown to be essential for correct regionalization (Cordes et al., 2004).

Other studies, however, indicate that segmentation and regionalization could be independent processes. Some *Hox* genes appear to control their anterior expression limits by themselves, as over-expression of *Hox* genes in chick epiblast cells could delay the time these cells needed to reach the primitive streak. The authors suggest, that this delay could result in the nested expression domains of Hox genes in the somites, as the time needed to reach the primitive streak was longer for cells over-expressing more 5´Hox genes compared to 3´Hox genes. This would imply that the acquisition of regional identities is mainly determined prior to the ingression of cells in the PSM (Iimura and Pourquié, 2006). Another study highlights the importance of a precise temporal activation of *Hox* gene expression. In this study a *Hoxc8 cis*-regulatory element was mutated. The mutation of this early enhancer region leads to an initial delay of Hoxc8 expression, but somitic *Hox8* expression appeared recovered at later embryonic stages. These mice do, however, show skeletal malformations of the axial skeleton, which are reminiscent of the Hoxc8-null mutant. (Juan and Ruddle, 2003). In another study, presacral vertebral counts and size variations were determined across amniotes. The authors then used statistical

methods to determine potential correlations between the regionalization and somitogenesis process. They could, however, not detect any correlation in most cases, suggesting that regionalization and somitogenesis are independent processes (Müller et al., 2010).

4.5 miRNAs in mouse development

miRNAs (miRNAs) are short ~21bp long, endogenous, single-stranded RNAs, that base-pair to specific sites in the 3´untranslated regions (UTRs) of protein coding mRNAs, typically leading to translational repression of their respective targets or enhanced mRNA degradation (Bartel, 2004). Initially, miRNAs were identified in their role as developmental switches, when the miRNA founding member *lin-4* was discovered in a screen for genes, which control post-embryonic development in *C.elegans* (Chalfie et al., 1981). Today, it is known that miRNAs have far more roles than just timing developmental transitions and they are considered to act as important players in many biological processes including for example proliferation, apoptosis (Calin and Croce, 2006) and the evolution of species (Berezikov et al., 2006). miRNAs are transcribed from the genome and processed by the RNAse III enzyme Dicer. In the mouse, complete inactivation of Dicer leads to early embryonic lethality (Bernstein et al., 2003). Later functions for Dicer during mouse embryogenesis have also been shown (Chen et al., 2004; Harris et al., 2006; Zhao et al., 2007), suggesting that miRNAs do also have essential functions throughout mouse development. More important than a functional characterization of miRNA presence or absence, however, is the precise determination of the localized expression of each miRNA and its mRNA targets. This can be illustrated by the example of miR-1, which is expressed in heart and skeletal muscle of the developing mouse embryo (Kloosterman et al., 2006). Hdac4 is a repressor of muscle

differentiation and miR-1 is thought to target Hdac4 in muscles and thus promote muscle differentiation (Chen et al., 2006). In the heart, however, miR-1 is essential to regulate ventricular cardiomycytes through targeting the cardiac transcription factor Hand2 (Yang et al., 2005). This example also demonstrates that the characterization of a miRNA is also highly dependent on the knowledge of its target mRNA(s).

Many different *in silico* prediction tools have been developed in recent years, which can be used to identify potential target mRNAs for specific miRNAs (Griffiths-Jones et al., 2008; Lewis et al., 2005). In vertebrates these predictions turned out to be difficult to interpret, as the miRNA-mRNA pairings are not entirely complementary (in contrast to plants where the miRNA-mRNA binding is normally highly complementary) (Galceran et al., 2004). Therefore, it is essential to narrow down potential miRNA targets. During complex and highly dynamic processes like embryonic development the most useful approach is to generate individual expression profiles of each detectable miRNA and to determine whether the miRNA is temporally and spatially co-expressed with its potential target mRNA(s), since this is a prerequisite for a miRNA mRNA interaction.

4.6 *cis*- mediated *Dll1* gene regulation

Previous work suggested *cis*-mediated *Dll1* regulation during mouse embryogenesis. A 4.3 kb region of the *Dll1* 5´ upstream region was screened by a transgenic reporter gene approach for regulatory elements. Several elements were identified, including two potential neuronal enhancers termed HI and HII and a potential mesodermal enhancer region (MSD). The 3´ end of the mesodermal *Dll1* enhancer is located 2 kb upstream from the mouse *Dll1*-coding region. This 1678 bp long MSD fragment was sufficient to direct reporter gene expression in the PSM, in the somites, as well as in derivatives of the paraxial mesoderm, like the rib primordia and muscle precursors of

the developing limb of transgenic mice. Reporter gene expression did thus reproduce major aspects of the endogenous *Dll1* expression pattern during somitogenesis (except the fact that the restriction of *Dll1* to the caudal part of somites was not recapitulated in these experiments) (Beckers et al., 2000). This indicates that MSD could be an important endogenous element for *Dll1* expression and could have a major regulatory function for controlling *Dll1* expression during somitogenesis.

The MSD sequence further contains multiple putative Tbx6 and Lef1/Tcf binding sites, which where found by means of sequence analysis and functionally tested by reporter gene expression in transgenic mice (Galceran et al., 2004; Hofmann et al., 2004). *Tbx6* and *Lef1/Tcf* transcription factors are co-expressed in the PSM and have been identified as nuclear mediators of the Wnt pathway. Complete loss of either *Tbx6* or *Lef1/Tcf* leads to a lack of paraxial mesoderm and in the generation of three neural tubes, a phenotype, which is close to the *Wnt3a* null mutation (Chapman and Papaioannou, 1998; Galceran et al., 2004; Takada et al., 1994; Yoshikawa et al., 1997). In addition, *Dll1* expression is down-regulated or lost in these mutants (Galceran et al., 2004; Hofmann et al., 2004). Tbx6 is a T-Box transcription factor and Tbx6 protein was shown to bind to the MSD sequence *in vitro* (White and Chapman, 2005). Furthermore, a hypomorphic mutant of Tbx6 termed rib-vertebrae (rv), was shown to genetically interact with a *Dll1* loss-of-function allele *in vivo* (Watabe-Rudolph et al., 2002; White et al., 2003). Interestingly, the *Tbx6* 5´ upstream regulatory region itself contains a RBPjk binding site, suggesting a feedback loop between *Dll1,* NICD and *Tbx6* (Shifley and Cole, 2007; White et al., 2005). This supports the idea that MSD could play an important role for the interconnectivity of the Wnt and the Delta–Notch signalling pathway.

Furthermore, the MSD sequence has been used to generate several transgenic

mouse lines, which constitutively express certain mRNAs in the presomitic and somitic mesoderm, as for example: *Dll1*, *Cre*, *Lnfg, Axin2*, *Tbx18 and Hoxa11* (Aulehla et al., 2003; Bussen et al., 2004; Carapuço et al., 2005; Serth et al., 2003; Teppner et al., 2007; Wehn et al., 2009). The MSD sequence has also been used in a proof of principal experiment for an *in silico* prediction tool, which is able to differentiate between neuronal and mesodermal enhancers in mammals (Brody et al., 2007).

4.7 miRNA mediated *Dll1* gene regulation

Experimental data suggest that *Dll1* is also a target for miRNA-mediated regulation. It has been shown in *Drosophila* that dmiR-1 targets the *Dll1* orthologue *Dl* (Kwon et al., 2005) and additional evidence suggests that mmu-miR1 might regulate *Dll1* expression during cell lineage decision of pluripotent embryonic stem cells (Ivey et al., 2008). It has been recently shown that miRNAs have a conserved function in the segmentation process through post-transcriptional regulation of oscillatory genes, as blocking the binding sites using Target Protectors for miR-125a-5p and miR-200b in the *Lfng* 3´UTR in chicken embryos disrupts its oscillatory gene expression and results in disrupted somite formation (Riley, 2010). In addition, miRNAs have been shown to play a role in EMT (Gregory et al., 2008). *Dll1* in turn is essential for the development of epithelial somites (Hrabě de Angelis et al., 1997), suggesting an function for miRNAs in controlling *Dll1* expression during mesenchymal to epithelial transition.

4.8 Project aims

4.8.1 *cis*- mediated *Dll1* gene regulation

The aim of the first part of this work is to get further insights into functional *cis*-mediated *Dll1* regulation.

We selected the MSD enhancer for a functional analysis, as it was shown to drive reporter gene expression in the PSM and somites in transgenic mice, indicating an endogenous *cis*-regulatory function for MSD in regulating *Dll1* in these tissues during mouse development. This prompted us to analyze, whether the MSD enhancer is necessary for correct *Dll1* expression and has a function as an endogenous genomic regulatory element for *Dll1*.

To answer this question, we deleted the *Dll1* MSD enhancer through homologous recombination by means of ES cell targeting. Two different alleles were generated: the MSD replacement allele, which is referred to as $Dll1^{tm1leg}$ and the MSD deletion allele, which is referred to as $Dll1^{tm1.1leg}$, subsequently. Wild type, heterozygous and homozygous $Dll1^{tm1leg}$ and $Dll1^{tm1.1leg}$ mice, respectively, were analyzed by skeletal preparation, whole mount *in situ* hybridisations and qRT-PCR for *Dll1* and selected Delta-Notch target genes. Since Tbx6 was shown to bind to MSD *in vitro* and mediate *Dll1* expression *in vivo* we also analyzed mice heterozygous for a loss-of-function allele for the *Tbx6* transcription factor (Chapman and Papaioannou, 1998). To unravel potential genetic interactions of *Tbx6* and MSD alleles we additionally analyzed mice, which carry combinations of $Tbx6^{tm1Pa}$ and $Dll1^{tm1.1leg}$ alleles ($Tbx6^{tm1Pa/+}$ $Dll1^{tm1.1leg/+}$ and $Tbx6^{tm1Pa/+}$ $Dll1^{tm1.1leg/tm1.1leg}$, respectively).

4.8.2 miRNA mediated *Dll1* gene regulation

The second part of this work describes a novel strategy to identify miRNAs that can potentially regulate *Dll1* during mouse embryogenesis by targeting its endogenous 3´UTR.

By interspecies *in silico* comparisons between mouse, human and chicken *Dll1* 3´UTRs 16 miRNAs were identified that have evolutionary conserved binding sites among these three species. To analyze whether these miRNAs could regulate *Dll1*

gene expression during embryogenesis, we performed a systematic whole mount *in situ* hybridisation screen using DIG labelled LNA modified DNA probes in wild-type mouse embryos at 9.5 dpc and 10.5 dpc, to unravel whether any of these miRNAs is/are spatially and temporally co-expressed with the *Dll1* mRNA. Selected positive miRNAs that were found to be co-expressed with *Dll1* in the latter study were further analyzed on histological sections of 12.5 dpc mouse embryos using radioactive *in situ* hybridisation.

5. Materials and Methods

5.1 Methods

5.1.1 Mice

Sonja Becker initially generated the *Dll1*^{tm1leg} founder mouse line. For constructing the MSD replacement vector a Diphterie-toxin A (DT_A) fragment was first ligated into a pBluescript vector.

A genomic clone containing parts of the 5´*Dll1* upstream regulatory sequence (Beckers et al., 2000), was digested with XbaI/SalI and the 4.1 kb long MSD flanking left arm sequence was isolated. This left arm sequence was ligated into the previously constructed pBluescript/DT_A. Another genomic clone containing parts of the 5 ´*Dll1* upstream regulatory sequence (Beckers et al., 2000), was digested with FokI and the 1.9 kb long MSD flanking right arm sequence was isolated. This fragment was subsequently subcloned and then ligated into the pBluescript/DT_A /Left Arm vector.

The Hygromycin/loxP sequence was isolated and cloned in between the left arm and the right arm sequence in the pBluescript /DT_A/Left Arm/Right Arm vector (for detailed vector map see Figure 4 A). The vector was transfected into mouse ES cells, resulting in two chimeric mouse lines. In one chimeric mouse line the ES cells successfully contributed to the germ line, generating the *Dll1*^{tm1leg} founder mouse line. In order to generate the *Dll1*$^{tm1.1leg}$ MSD mouse line, homozygous *Dll1*^{tm1leg} mice were crossed to a heterozygous C57BL/6$^{rosa26(SA\text{-}CrepA)ARTE}$ general Cre deleter strain. *Dll1*^{tm1leg} mice were maintained on a mixed C57BL/6J x C3HeB/FeJ background. *Dll1*$^{tm1.1leg}$ were first maintained on a mixed C57BL/6J x C3HeB/FeJ and then backcrossed to C57BL/6J for five generations.

Dll1^{tm1leg} and *Dll1*$^{tm1.1leg}$ mice and embryos were genotyped using allele specific duplex polymerase chain reaction (PCR) (For details see 2.1.3).

Generation of *Dll1*^{tm1Gos} mice has been described (Hrabe de Angelis et al., 1997). *Dll1*^{tm1Gos} mice were maintained on a C3HeB/FeJ background. The *Dll1*^{tm1Gos} allele was genotyped using allele specific duplex polymerase chain reaction as previously described (Rubio-Aliaga et al., 2007) (for details see 2.1.3).

Generation of *Tbx6*^{tm1Pa} has also been described (Chapman and Papaioannou, 1998). *Tbx6*^{tm1Pa} mice were initially obtained on a mixed C57BL/6J x NMRI background and then backcrossed to C57BL/6J for five generations. The *Tbx6*^{tm1Pa} allele was genotyped using allele specific duplex polymerase chain reaction as previously described (Wittler et al., 2007) (for details see 2.1.3).

Mouse husbandry was conducted under specific pathogen-free (SPF) conditions in compliance with the Federation of European Laboratory Animal Science Associations (FELASA) protocols. Mice received standard rodent nutrition and water *ad libitum* and all animal experiments were performed under the approval of the responsible animal welfare authority.

5.1.2 Genotyping

Genomic DNA was isolated either from mouse-tails, liver or yolk sac. The respective tissue was incubated at 60 °C over night in 400 µl tail buffer, containing 10 µl Proteinase K (20 mg/ml). Tail buffer was prepared according to the scheme below. For smaller amounts of tissue, mainly for yolk sacs of 8.5 and 9.5 embryos, only 100 µl of tail buffer and 5µl Proteinase K 20 mg/ml were used, to increase genomic DNA concentration.

50 mM KCL

10 mM Tris-HCL (pH 8,3)

0,1 mg/ml Gelatin

0,45 % Nonidet NP-40

0,45% Tween 20

After over night incubation, Proteinase K was heat inactivated for 20 min at 95° C. The template was centrifuged for 5 min at full speed and the supernatant was transferred to a new tube. Then the isolated genomic DNA was used for PCR reactions.

5.1.3 PCR cycling schemes and primers for genotyping

5.1.3.1 *Tbx6*^{tm1Pa}

94°C	3min
94°C	30 sec
62,7°C	30 sec
72°C	1 min
40 cycles	
72°C	10min
12°C	Hold

Tbx_for:	5´- GCC AAA CTG CGT CCC TGT CTT - 3´
Tbx_rev:	5´- GGC GCC CGG TTC TTT TTG TC - 3´

TbxMut_rev: 5´- GGG GGT GGC GGT GCT GTC TC - 3´

5.1.3.2 *Dll1^{tm1Gos}*

94°C	4min
94°C	30sec
60°C	30sec
72°C	40sec

45 cycles

12°C	hold

Dll1_for: 5’ - CAA GGG CGT CCA GCG GTA C - 3’
Dll1_rev: 5’ - CCT TGC TAG GAC GCA GAG GC - 3’
LacZ3_rev: 5’ - GCA CCA CAG ATG AAA CGC CG - 3’

5.1.3.3 *Dll1^{tm1leg}*

94 ° C	4 min
94 ° C	30 sec
60 ° C	30 sec
72 ° C	40 sec

45 Cycles

72 ° C	5 min

12°C	Hold

MSD_1: 5´- TTT CCC GGT GTA CAC ACC CTC TCC- ´3,
MSD_2: 5´- GAG CTT GTA ACC AGG GGA GCC GTT- ´3
MSD_3: 5´- CGC CTA CCG GTG GAT GTG GAA T- ´3

Tbx6^{tm1Pa}, *Dll1*^{tm1Gos} and *Dll1*^{tm1leg} allele specific PCR reactions were prepared according to following scheme:

25 µl reaction volume (one reaction)

2,5	µl	Q-10xB
5,0	µl	Q-Solution
0,5	µl	dNTPs (10mM)
1,0	µl	PRIMER 1
2,0	µl	PRIMER 2 (respective reverse Primer)
1,0	µl	PRIMER 3
0,3	µl	Taq Polymerase (Qiagen)
1,0	µl	DNA
11,7	µl	H_2O

5.1.3.4 *Dll1*$^{tm1.1leg}$

94 ° C	5 min

94 ° C	30 sec
63 ° C	30 sec
72 ° C	1 min

35 Cycles

72 ° C	5 min
12°C	hold

Dll1^{tm1leg} allele specific PCR reactions were prepared according to following scheme:

25 µl reaction volume (one reaction)

2,5	µl	10xB
0,625	µl	dNTPs (10mM)
0,75	µl	PRIMER 1
1,5	µl	PRIMER 2 (respective reverse Primer)
0,75	µl	PRIMER 3
0,4	µl	Taq Polymerase (Biotherm)
3,0	µl	$MgCl_2$ (15mM)
1,0	µl	DNA
11,7	µl	H_2O

Flox_1:	5´- CTG TTA TTG TGC GAG GCT GA- ´3
Flox_2:	5´- GCT GGG TCA TCA GAA AAG GA- ´3
Flox_3:	5´- CGA TAC CGA GGG ATC CAT AA- ´3.

5.1.4 Embryo dissection

Embryos were obtained from timed pregnancies, dissected in phosphate buffered saline (PBS, pH 7.3) and fixed at 4°C overnight in 4% paraformaldehyde (PFA) in PBS.

5.1.5 Skeletal preparation

Skeletal preparation was done with an Alcian-Blue/Alizarin-Red staining solution, which stains cartilage blue and ossified calcium rich tissue red. Alcian blue is a

cationic dye, for the demonstration of glycosaminoglycans. It is thought to work by forming reversible electrostatic bonds between the cationic dye and the negative (anionic) sites on the polysaccharide.

Alizarin Red is used for the demonstration of calcium and forms an alizarin red S-calcium complex, in a chelation process.

First, newborn mice were killed by ether. Afterwards the skin and the inner organs were removed. A small piece of liver was used for genotyping and the rest of the liver was frozen at -20 °C as resource for the isolation of additional genomic DNA. After preparation, mice were dehydrated in 100% Ethanol for 4 days and fixed in 100% Aceton for 3 days. Then mice were stained for 10 days, in the Alcian-Blue/Alizarin-Red staining solution.

Alcian-Blue/ Alizarin-Red Staining Solution

0,3% Alcian-Blue in 70% Ethanol 1 Volume

0,1% Alizarin-Red in 95% Ethanol 1 Volume

100% Acetic Acid 1 Volume

100% Ethanol 17 Volumes

After 10 days of staining, mice were incubated for 1 Day in 1% KOH/20% Glycerin at 37 ° C. Then mice were stored in 1% KOH/20% Glycerin at RT, until all tissue was removed and the bones were clearly visible (~2 - 4weeks). Axial skeletons were then stored and dissected in 50% Glycerin.

5.1.6 Long-range PCR and sequencing

To confirm correct homologous integration of the targeting vector and deletion of the

hygromycin selection cassette, we performed long-range PCR on *Dll1*^{tm1leg} and *Dll1*$^{tm1.1leg}$ mutant mice (for details see Figure 4). All PCR fragments were partially sequenced (~600bp) from both sides to confirm correct integration of the targeting vector and deletion of the hygromycin resistance cassette. Genomic DNA for long range PCR was extracted from liver tissue using the Qiagen QuiaAMP Kit according to the manufacturer's protocol. Genomic DNA concentration was adjusted to 50ng.

5.1.6.1 PCR cycling scheme and primers for long-range PCR

Preheat Block to 93°C and add tubes (simplified Hot Start)

93°C	3 min

First 10 cycles:

93°C	15 sec
55°C	30 sec
68°C	10 min

Next 30 cycles:

93°C	15 sec
55°C	30 sec
68°C	10 min + 20 sec additional per cycle

40 cycles total

68°C	10 min
12°C	Hold

F1: 5´- CCT GCA GC TTC AGC TCA AAT -´3

F2: 5´- CGA TAC CGA GGG ATC CAT AA- ´3

R1: 5´- AGT CAA GAC CTC AGG CGT GT- ´3

R2: 5´- AGT CAA GAC CTC AGG CGT GT- ´3

50 µl reaction volume (one reaction)

5,0	µl	Q-10xB
10,0	µl	Q-Solution
2,5	µl	dNTPs (10mM)
2,0	µl	PRIMER 1
2,0	µl	PRIMER 2
0,4	µl	Long Range Enzyme Mix (Qiagen)
2,0	µl	DNA (50ng)
26,1	µl	H_2O

The PCR was checked afterwards on a 1.5% agarose gel (TAE). The remaining PCR reaction volume was further processed for sequencing.

5.1.6.2 Long Range PCR Purification

Purification was performed using the Agencourt AMPure PCR Purification Kit according to the manufacturer´s instructions.

5.1.6.3 BigDye PCR

1 µl Primer (forward or reverse) and 2 µl purified DNA were applied to a new plate and dried by using a speed-vac for 15 min. Afterwards 5 µl H2O, 4 µl 5x Sequencing buffer and 1 µl BigDye v.3.1 were added to the dry samples. Big Dye PCR was performed according to following cycling scheme.

94 ° C	1 min
94 ° C	5 sec
50 ° C	10 sec
60 ° C	4 min

39 Cycles

12°C	hold

5.1.6.4 Purification of the BigDye PCR

The PCR was purified with the Agencourt CleanSEQ Purification Kit according to the manufacturer´s instructions.

5.1.6.5 Sequencing and evaluation

The sequence detection was performed using an ABI-3730. Sequences were analysed using Sequencer 4.6.

5.1.7 *In situ* hybridisations for detecting endogenous mRNAs

5.1.7.1 RNA probe preparation

For RNA probe preparation, the respective linearized Plasmid was first cleaned using the QiaQuick Nucleotide Removal Kit and eluated in 30 µl ddH_2O.

Then RNA was transcribed according to following scheme:

10µl Plasmid DNA

3µl ddH_2O (Ampuwa)

2µl Transcription Buffer (Roche)

2µl DIG RNA Labelling Mix (Roche)

1µl RNase Inhibitor (Roche)

2µl RNA-Polymerase T7, T3 or Sp6 (Roche)

After 2 hours of incubation at 37 ° C, 2 µl RNase free DNase were added to the reaction mix, to remove Plasmid DNA. The DNase digest was performed for 15 min at 37 ° C. Finally RNA probes were cleaned using the Rneasy Mini Kit and eluated in 50 µl Ampuwa. Then 1µl of RNase inhibitor was added, 5 µl of each probe was checked on a 1% Agarose Gel and the rest was frozen at -80 °C.

5.1.7.2 Whole mount *in situ* hybridisation (mRNA)

On the first day embryos were hybridised with the prepared antisense RNA. Therefore, embryos were first rehydrated through a series of 75%, 50%, and 25% Methanol on ice. Then embryos were washed in PBT on ice for 2 x 10 and 1 x 5 minutes. For embryos <10.5 dpc, embryos were treated with Proteinase K at 10 µg/ml in Proteinase K buffer at 37 °C. 10.5 dpc embryos were treated for 3 minutes whereas and 11.5 dpc embryos were treated for 4 minutes with Proteinase K. After that, embryos were incubated in RIPA buffer for 10 minutes and washed 2 x 5 minutes with PBT both on ice. Then embryos were fixed in 4% PFA/0,2% glutaralaldehyd on ice, which was freshly prepared. Embryos were washed again in PBT for 2 x 5 minutes. Afterwards embryos were washed in a 1:1 mixture of hybe-buffer/PBT for 10 minutes at RT, washed again, for 10 minutes in hybe-buffer only at RT and finally prehybridised in hybe-buffer + tRNA at 100 µg/ml at 68° C for 3 hours. Shortly before the end of prehybridisation, the frozen RNA was thawn and denatured

for 3 minutes at 90° C. As a last step, the embryos were hybridised in a 1:50 dilution of the RNA probe in hybe-buffer at 68° C over night.

On the second day, the unbound probe was removed. Therefore, embryos were first washed at 65° C with hybe-buffer for 2 x 30 minutes. Then embryos were cooled down to RT and washed two times for 5 minutes. First, using a 1:1 mixture of hybe-buffer/RNase solution, then with RNase solution alone. Then an RNase digest was performed, with RNase A at 100 µg/ml in RNase solution at 37° C for 1 hour. After that, embryos were washed in a 1:1 mixture of RNase solution/SSC/FA/Tween 20 for 5 minutes at RT. Then embryos were heated in SSC/FA/Tween 20 from RT to 65° C. After that several SSC/FA/Tween 20 washing steps were performed at 65° C. Embryos were washed for 2 x 5, 3 x 10 and 5 x 30 minutes in SSC/FA/Tween 20 and cooled down to RT again. After cooling down to RT, embryos were washed in a SSC /FA/ Tween 20/TBST mixture. Afterwards they were washed with TBST for 2 x 10 minutes at RT. Thereafter embryos were washed 2 x 10 minutes in MABT and then blocked in 10% Blocking Solution in MABT at RT. Meanwhile DIG antibodies were preabsorbed at a 1:5000 dilution in 1% Blocking Solution in MABT at 4° C and finally embryos were incubated in that solution at 4° C over night. On the third day, the unbound antibody was removed. Therefore embryos were washed in TBST for 3 x 5 minutes and 8 x 1 hour at 4 ° C. Embryos were left in TBST at 4° C for two days. After that, TBST was changed one last time. In the evening of that day, embryos were first washed in alkaline phosphatase buffer for 2 x 5 minutes and then incubated in staining solution at 4° C over night. If the staining was sufficient embryos were fixed in 4 % PFA/PBS.

5.1.7.3 Solutions for whole mount *in situ* hybridisation (mRNA)

- Alkaline phosphatase buffer: 200 µl 5 M NaCl, 2.5 ml 1 M $MgCl_2$, 50 µl Tween20, 5 ml 1 M Tris- HCl pH 9.5 and 100 µl 1M Levamisole were mixed. The total volume was filled up to 50 ml with double distilled water.
- Ampuwa/Levamisole: 1 M Levamisole was prepared in Ampuwa.
- Blocking stock solution: 10% Blocking reagent in MAB
- Citric acid was prepared in DEPC water.
- DEPC-H_20: 1 ml diethylpyrocarbonate was added to 1 litres of Millipore water. The solution was mixed and incubated over night at room temperature under the fume hood. Afterwards, it was autoclaved.
- Detection buffer: Consists of 1 M NaCl, 1 M Tris-HCl, pH 9.5
- Heparin: 100 mg/ml Heparin were dissolved in DEPC water.
- Hybe-buffer: Consists of 50% deionised formamide, 4.5 x SSC, Heparin solution, 0,1% Tween20 and DEPC water.
- Maleic acid buffer (MAB): 0.1 mol maleic acid, 0.15 mol NaCl and double deionised water were mixed. The pH was adjusted to 7.5 with solid NaOH and solution was autoclaved.
- MABT: MAB was drugged with 0.1 % Tween20.
- Phosphate buffered saline (PBS): Phosphate buffered saline concentrate was used. Phosphate buffered saline consists of 137 mM NaCl, 2.7 mM KCl, 10 mM Na_2PO_4, 2 mM KH_2PO_4 and 1 mM $MgCl_2$. Solution was autoclaved.
- Phosphate buffered saline with Tween20 (PBST): 10x PBS was diluted 1:10 with DEPC water 0.1 % Tween20 were added.
- 4 % PFA/PBS: 2 g PFA, 50 ml 1x PBS-DEPC and a few drops 10 N NaOH were heated to 55 °C until the PFA was dissolved. Afterwards, the solution

was cooled on ice and the pH was adjusted to 7 with HCl.

- RIPA (500 ml): 2.5 ml 10 % SDS, 15 ml 5 M NaCl, 5 ml IGEPAL CA-630, 25 ml 10% Deoxycholate, 1 ml 0.5M EDTA, 25 ml 1 M Tris-HCl pH 8.0 and 500 ml DEPC water were mixed.
- RNase A: RNase A was dissolved at a concentration of 10 µg/µl in 0.01 M NaAc (pH 5.2), heated to 100 °C for 15 min and cooled down slowly to room temperature. The pH was adjusted, adding 0.1 volumes of 1 M Tris-HCl pH 7.4. RNase A was stored in aliquots at -20 °C
- RNase solution: Consists of 0.5 M NaCl, 0.01 M Tris pH 7.5 and 0.1 % Tween20.
- Standard saline citrate, 20x conc. (20x SSC): Consists of 3.0 M NaCl and 0.3 M sodium acetate. The pH was adjusted to 7 with a few drops of concentrated hydrochloric acid. The solution was autoclaved.
- SSC/FA/Tween20: Consists of 2 x SSC, 50 % deionised formamide, 0.1% µl Tween 20 and double distilled water.
- Staining solution BM purple AP (Roche) substrate was used. Per 1 ml BM purple 2 µl 1 M Levamisole and 1 µl Tween20 were added. The solution was centrifuged at full speed for 5 minutes.
- Tris buffered saline, 10x conc. (10x TBS): Consists of 0.15 M NaCl and 0.01 M Tris-HCl, pH 7.5.
- 1x TBST: 25 ml 10x TBS, 250 µl Tween20 and 250 ml double distilled water were mixed.
- 10x Tris EDTA: Consists of 100 mM Tris-HCl pH 7.6 and 10 mM EDTA pH 8.0

5.1.7.4 *In situ* hybridisation on sections (mRNA)

On the first day sections were hybridised with the prepared antisense RNA. Therefore, sections were dewaxed for 2 x 30 minutes in Rotihistol. Then slides were rehydrated through a graded series of 2 x 5 minutes 100% ethanol, 2 x 5 minutes 70% ethanol and 3 minutes DEPC water. After that, sections were washed 1 x 5 minutes in PBS refixed in 4% PFA for 1 x 10 minutes and again washed 2 x 5 minutes in PBS. After that slides were treated in 0.2 M HCL, washed again for 2 x 5 minutes in PBS and incubated in Proteinase K Buffer containing 20μg/ml Proteinase K for 5 minutes. After that slides were washed 2 x 5 minutes in PBS and fixed for 15 minutes in 4% PFA using the same solution as before. Then slides were treated in 1 x TEA buffer containing 2.5% acetic anhydride for 10 minutes and again washed for 2 x 5 minutes in PBS. Then slides were quickly dehydrated through a graded series of DEPC water, 70 % ethanol and 100% ethanol one minute each. Slides were then prehybridised for 2h at 56°C in hybridisation mix containing 100μg/ml tRNA and after at incubated at 56 ° C over night in hybridisation mix containing 100μg/ml tRNA and mRNA probe at 1:100. Hybridisation chambers used contained hybridisation chamber fluid to avoid drying of sections. Before use, probe was incubated at 90°C for 3 minutes. Hybridisation mix was prepared according to the table below:

50 % formamide

20 mM Tris-HCl pH 8.0

300 mM NaCl

5 mM EDTA pH 8.0

10 % dextran sulphate

0.02 % Ficoll 400

0,02 % PVP40

0.02 % BSA

0,2 mg/ml carrier DNA

200 mM DTT

On the second day unbound probe was removed, antibody detection was performed and the staining reaction was started. Therefore slides were first washed in 5 x SSC / 0,05 % Tween for 20 min at 62°C. Then the slides were incubated in 1 x NTE Buffer containing RNase A at a concentration of 20μg/ml for 20 min at 37°C. After that slides were washed in 50% deionised formamide / 2 x SSC / 0,05 % Tween, 50 % deionised formamide / 1 x SSC / 0,05 % Tween and 0,1 x SSC / 0,05 % Tween for 30 minutes each at 62°C. Then slides were incubated in 1 x NTE Buffer for 5 minutes at RT, followed by a 3 x 5 minutes MABT washing at RT. Then slides were blocked in 10% Blocking solution in MAB for 2 hours at RT. Then preabsorded Anti-DIG-AP in 2% Blocking solution was applied and slides were incubated for 2 hours at RT in that solution. After the antibody steps slides were washed in MABT for 3 x 10 minutes at RT. Then slides were washed in Alkaline phosphatase buffer for 2 x 10 minutes at RT. Finally staining reaction was started. For that BM purple was applied and sections were stained for 3 days at 4°C followed by staining for 2-3 days at RT until proper signal intensity was reached. Sections were then washed in PBS and mounted in Kaiser´s Glycerol Gelatine.

5.1.7.5 Additional solutions used for *in situ* hybridisation on sections (mRNA)

Some buffer used for *in situ* hybridisation on sections, were the same as used for whole mount *in situ* hybridisation and are stated in 2.5.2. Additional buffers used were prepared as follows:

- 10 x TEA/DEPC-stock solution (pH 8.0)

  84 ml of 1 M triethanolamine were dissolved in 300 ml H_2O-DEPC. pH was adjusted to 8.0 with 32 % HCl . Proper volume was adjusted with DEPC-water. Solution was autoclaved afterwards
- 20 x SSC/DEPC-stock solution (pH 7,4). Was prepared as stated in 2.5.2 only pH was adjusted differently. Solution was autoclaved afterwards.
- 10 x Proteinase K buffer/DEPC-stock solution (pH 8,0)

  Consists of 0.5 M Tris-HCl pH 7.6; 50 mM EDTA pH 8.0. Solution was autoclaved afterwards.
- Hybridisation Chamber Fluid

  Consists of 50% deionised formamide and 2 x SSC and double distilled water.
- 0.5 M EDTA/DEPC-stock solution (pH 8.0).

  Solution was autoclaved afterwards.
- 5 x NTE stock solution

  Consists of 2.5 M NaCl, 50 mM Tris-HCl pH 8.0, 25 mM EDTA ph 8.0. Solution was autoclaved afterwards.
- 10 x Polymers-Mix

  1 g of Ficoll 400, 1 g of polyvinyl pyrrolidone, and 1 g BSA were added to a total volume of 50 ml with autoclaved DEPC-H_2O.
- 50 % Dextran sulphate in DEPC water.
- 5 M DTT solution

5.1.8 *In situ* hybridisation for detecting endogenous miRNAs

5.1.8.1 Probes

All unlabeled and double DIG labelled (**DL**) LNA modified DNA probes used were purchased from Exiqon. For whole mount *in situ* hybridisation unlabeled probes were labelled using the 3´DIG labelling Kit (Roche) (**SL**) according to the manufacturer's instructions and cleaned up using MicroSpin G25 columns (GE Healthcare) according to the manufacturer's instructions. For *in situ* hybridisation on sections probes were radioactively labelled [^{35}**S**] using the terminal transferase labelling Kit (Roche) according to the manufacturer´s instructions. All probe sequences can be obtained from www.exiqon.com. All probes were hybridised 20-21°C below their respective melting temperature. Melting temperatures for the respective probes can also be obtained from www.exiqon.com.

5.1.8.2 Whole mount *in situ* hybridisation (miRNA)

In situ hybridisations were performed as previously described (Kloosterman et al., 2006; Sweetman et al., 2008). The miR-1 probe was used as a positive control for *in situ* hybridisations. Hybridisation with a scrambled miR probe was used as a negative control.

For SL probes standard incubation time until proper signal development was approx. 2 - 4 weeks with weekly intervals of TBST washing and exchange of BM Purple solution. MiR-103, miR-130a/b initially developed comparable to previously published data in chicken embryos with strong ubiquitous expression without the heart in 10.5 dpc embryos, when probes were processed manually (Darnell et al., 2006). We thus assumed a high signal to noise ratio of these probes, which we tried to reduce. Our attempts included higher post hybridisation washing temperature, longer and shorter

Proteinase K treatment, prehybridising or reusing probe and EDC fixation, which were all unsuccessful. Automatic tissue procession using an Intavis *In Situ* Pro robot clearly improved the signal to noise ratio, resulting in more restricted and reproducible expression patterns for these probes at 10.5 dpc. For 9.5 dpc embryos automatic tissue processing reduced the staining to an undetectable level.

For DL probes the mean incubation time until proper signal development was much shorter compared (approx 1-2 days), but they developed more background compared to SL probes. All *in situ* hybridisations for DL probes were performed using an Intavis *In Situ* Pro robot.

General protocol:

On the first day embryos were hybridised with the purchased miRNA probes.

Therefore, embryos were first rehydrated through a series of 75%, 50% and 25% Methanol on ice and then washed for 5 minutes in PBST. Embryos were then incubated in PBST containing 10μg/ml Proteinase K for 45 min at 37°C. Embryos were refixed in 4% PFA/0.2 % glutaraldehyde and washed in PBS 3 x 5 minutes. Embryos were subsequently washed in water for 5 minutes and incubated in 1 x TEA buffer containing 2.5% Acetic anhydride for 10 minutes. Embryos were again washed in water for 5 minutes and subsequently washed for 5 x 5 minutes in PBST. Embryos were then prehybridised in hybridisation buffer containing 500μg/ml tRNA at the respective hybridisation temperature for 2-3 hours and subsequently incubated in hybridisation buffer containing 500μg/ml tRNA and the respective miRNA probe over night.

On the next day unbound miRNA probe was removed. For that embryos were washed in a graded series of hybridisation buffer and 2 x SCC for 15 minutes each at the respective temperature as follows:

100 % hybridisation mix

75 % hybridisation mix – 25 % 2 x SSC.

50 % hybridisation mix – 50 % 2 x SSC.

25 % hybridisation mix – 75 % 2 x SSC .

Embryos were then washed for 15 min in 2 X SSC followed by a 15 minutes wash in 0.2 x SSC. Embryos were then washed at RT in a graded series of 0.2 x SCC and PBST for 15 minutes each as follows:

75 % 0.2 x SSC – 25 % PBST

50 % 0.2 x SSC – 50 % PBST

25 % 0.2 x SSC – 75 % PBST

Embryos were then washed for 10 minutes in PBST and incubated in PBS containing 2% sheep serum and BSA at a concentration of 2 mg/ml for 2 hours at RT. Embryos were then incubated in pre-absorbed anti-DIG for final conc. of 1:5000 in PBST containing 2% sheep serum and BSA at a concentration of 2 mg/ml, overnight with agitation at 4° C.

After over night antibody incubation embryos were washed at RT for 3 x 5 min and 5 x 1 hour in TBST containing 2mM Levamisole. Embryos were subsequently washed in the same solution for 2 days at 4°C with regular exchanges of TBST. After these two days of washing the staining reaction was started. For that embryos were first washed in alkaline phosphatase buffer for 2 x 5 minutes and then incubated in staining solution at 4° C over night. If the staining was sufficient embryos were fixed in 4 % PFA / PBS.

For antibody pre-absorbation 5 to 6 10.5 dpc embryos were rehydrated to PBST and the anti-DIG antibody was applied at a 1:1000 dilution in PBS containing 2 % sheep

serum and BSA at a concentration of 2 mg/ml. Antibody and embryos were then subsequently incubated for several hours at RT.

5.1.8.3 *In situ* hybridisation on sections (miRNA)

In situ hybridisations on sections were done as previously described (Delic et al., 2008; Thomsen et al., 2005), with modifications to tissue treatment as described in mice and embryo dissection and by the use of a commercially purchased *in situ* hybridisation buffer (# B8807 G Lot / # 106B13 Ambion). The miR-124 probe was used as a positive control for *in situ* hybridisations. Hybridisation with a scrambled miR probe was used as a negative control. All probes were hybridised 20-21°C below their respective melting temperature.

5.1.9 qPCR

For qPCR analysis embryos were first dissected and washed once in PBS pH 7.3. PSMs were separated from embryos behind the first formed somite, frozen in liquid Nitrogen and stored at -80°C. RNA isolation of PSMs was performed as previously described (Horsch et al., 2008) using a RNeasy Mini Kit and Trizol reagent.

5.1.9.1 cDNA synthesis

cDNA synthesis was performed with SuperScript II Reverse Transcriptase Kit and Oligo $(dT)_{15}$ primers.

The following reaction mix was first incubated (preannealing) for 5 min at 65°C

15 µl	RNA
2 µl	Oligo (dT) primer

The following ingredients were subsequently added to the reaction mix.

10 µl	5x buffer
2,5 µl	dNTPs (Fermentas)
2 µl	RNAseOut Ribonuclease Inhibitor (Invitrogen)
2 µl	SuperScript II
16,5 µl	RNAse free water

The reaction was subsequently incubation at 42°C for 60 min.

qRT-PCR was conducted using ABI Prims 7900HT Sequence Detection System and Power SYBR Green (Applied Biosystems) and QuantiTect Primer Assays (Qiagen) according to the manufacturer's instructions. Determination of gene expression was performed as relative quantification and calculated as previously described (Livak and Schmittgen, 2001; Pfaffl, 2001).

5.1.9.2 qPCR master mix

20 µl reaction volume (one reaction)

10,0	µl	Power SYBR Green PCR Master Mix
1,0	µl	forward primer (10 pmol/µl)
1,0	µl	reverse primer (10 pmol/µl)
2,0	µl	1:10 cDNA dilution
6,0	µl	H_2O

5.1.9.3 qPCR cycling profile

95 ° C	10 min

94 ° C	25 sec
60 ° C	1 min

40 Cycles

55°C – 95°C for evaluation of the melting curve

5.1.10 Immunohistochemistry

For HRP or AP detection we used the respective vectastain elite goat kits (see 2.2.1). For Immunofluorescence we principally used the same protocol with minor modifications in regards to signal detection by the use of a fluorescence labelled secondary antibody. Generally, for IHC on sections 12.5 dpc wild type embryos were fixed for 2h in 4 %PFA at 4°C. Then embryos were incubated in 30% sucrose in PBS O/N at 4°C. On the next day embryos were incubated in a 1:1 mixture of Tissue Tek and 30% sucrose at RT for 2h. Embryos were then incubated in the same mixture for 1 - 2h at 4°C. Embryos were subsequently frozen in Tissue Tek and sectioned.

After sectioning the tissue was incubated for 30 min in PBS. For HRP detection sections were incubated for 30 min in Methanol with 0.3% H_2O_2 afterwards. Sections were subsequently washed in PBS and then placed for 10 min in boiling 10 mM citrate buffer. Sections were then washed in PBS and blocked for 30 in PBS containing 3% of respective blocking serum. Sections were then incubated O/N at 4°C with Hoxb6 primary antibody diluted in PBS at 1:400 in a humidified chamber. Sections were then washed in PBS for 10 min. For HRP and AP detection sections were then incubated for 1 hour at RT with 0,5 % biotinylated secondary antibody solution and 1,5% goat serum in PBS in a humidified chamber. Sections were washed in PBS for 10 minutes. Then avidin coupled HRP or AP was added to the

sections and incubated for 30 minutes at RT. After two washes for 5 minutes sections were incubated in DAB or BM purple solution, respectively until proper signal intensity was reached. Then sections were briefly rinsed under tap water and counterstained with Haematoxylin solution for 30 sec. Sections were then dehydrated in a graded series of 5 min 25%, 50%, 75% and 100% EtOH and finally cleared in 100% Xylol for 5 minutes. Sections were mounted in Entellan.

For immunofluorescence sections were counterstained with DAPI dehydrated in the same way as described above and mounted.

Antibodies used:

Hoxb6 (Abcam, ab26077)

Hoxb6 (Santa Cruz, SC-17171)

Donkey Anti Goat Alexa Fluor 488 (Invitrogen, A11055)

5.1.11 *In silico* analysis of *Dll1* 3´UTRs

Transcripts were analyzed using the miRBase Targets Version 5.1. Transcripts used were ENSMUST00000014917, ENST00000366756 and ENSGALT00000037704 for mouse, human and chicken *Dll1*, respectively. For *Dll3* transcript ENSMUST00000050191 was analyzed. For *Jagged1*, *Jagged2* and *Dll4* transcripts ENSMUST00000028735, ENSMUST00000075827 and ENSMUST00000102517 were used, respectively.

5.1.12 *In silico* analysis of the *Dll1* 5´ upstream regulatory region

The *Dll1* 5´upstream regulatory region was analyzed using Genomatix MatInspector software (www.genomatix.de), which detects DNA consensus binding motifs for certain transcription families. All T/Tbx6 and Lef1/Tcf consensus binding sites were documented and matched to their linear distribution on the chromosome.

5.1.13 Microscopy

For whole mount *in situ* hybridisation pictures of embryos were taken using a Leica MZ16F microscope equipped with a Leica DFC320 camera. Pictures of sections were taken using a Zeiss Axioplan 2 microscope or a Zeiss Stemi SV6 binocular an AxioCam camera and Axiovision software.

All pictures were processed using Adobe Photoshop.

5.1.14 Statistical analysis

Statistical significance was calculated using Fisher's Exact test (T-test) or one-way ANOVA. $P<0.05$ was taken to be statistically significant. Error bars are depicted in SEM.

5.2 Materials

5.2.1 Kits

- 3´DIG labelling Kit (03353575910, Roche)
- Agencourt AMPure PCR Purification Kit (A63880, Agencourt Bioscience Corporation)
- Agencourt CleanSEQ Purification Kit (A29151, Agencourt Bioscience Corporation)
- Long Range PCR Kit (206401, Qiagen)
- Nucleotid Removal Kit (28304, Qiagen)
- QuiaAMP Kit (51304, Qiagen)
- RNeasy Mini Kit (74104, Qiagen)
- Terminal transferase labelling Kit (03333566001, Roche)
- Vectastain Elite kits:
    - HRP Goat IgG: PK-6105
    - AP Goat IgG: AK-5005

5.2.2 Chemicals

- Agarose (15510-027, Invitrogen)
- Alcian-Blue (A-3157, Sigma)
- Alizarin-Red (A-5533, Sigma)
- Ampuwa (1654198, Fresenius Kabi Deutschland GmbH)
- Anti-Digoxigenin-AP Fab fragments (1 093 274, Roche)
- Blocking reagent (11096176001, Roche)
- BM Purple AP substrate, precipitating (1 442 074, Roche)

- BSA (A-6793, Sigma)
- Citric acid (0759, Sigma)
- DAB staining set (Sigma #D-4293)
- Deoxycholic acid, 97% (D-6750, Sigma)
- Deoxyribonucleic acid, single stranded from salmon testes (D-7656, Sigma)
- Dextran sulphate (D-8906, Sigma)
- Diethyl pyrocarbonate (D-5758, Sigma)
- DIG RNA labelling mix (1 277073, Roche)
- DNase I, RNase free (776785, Roche)
- Double DIG labelled LNA modified DNA (miRNA) probes (Exiqon)
- DTT (43815, Fluka)
- EDTA (ES2SS, Sigma)
- Ethanol (1.00983.2500, Merck)
- Ethidium bromide, 1% in water (1.11608.0030, Merck)
- Entellan (1.07961.0100, Merck)
- Ficoll 400 (F-2637, Sigma)
- Formaldehyde (F-1635, Sigma)
- Formamide, deionised, 99.5 % (P040.1, Roth)
- Gelatin (G-8150, Sigma)
- Gene Ruler 1 kb DNA ladder (85.110.0050, Bio&Sell, Germany)
- Gene Ruler 100bp ladder (85.230.0050, Bio&Sell, Germany)
- Glutaraldehyde, grade II, 25% aqueous solution (G-6257, Sigma)
- Glycerin (3783.1, Roth)
- Heparin, sodium salt, grade I-A (H-3149, Sigma)
- Hydrochloric acid, 32% (1.00319.1000, Merck)

- Hydrogen peroxide, 30% (H-1009, Sigma)
- *In situ* hybridisation buffer (# B8807 G Lot / # 106B13 Ambion)
- IPEGAL CA-630 (I-3021, Sigma)
- Kaiser´s Glycerol Gelatine (1.09242.011, Merck)
- Levamisole, 99% (L-9756, Sigma)
- Maleic Acid (M-0377, Sigma)
- Methanol (1.06009.2500, Merck)
- MicroSpin G25 columns (27-5325-01, GE Healthcare)
- Oligo(dT)$_{15}$ primer (# C1101, Promega)
- Paraformaldehyd (P-6148, Sigma)
- Phosphate buffered saline, Dulbecco (L-182-10, Biochrom AG)
- Polyvinyl Pyrrolidone (PVP-40, Sigma)
- Power SYBR Green (4367659, Applied Biosystems)
- Proteinase K (P-2308, Sigma)
- Qiagen QuantiTect Primer Assays (Qiagen)
- Restriction enzyme buffers (MBI, Fermentas)
- Restriction enzymes (MBI, Fermentas)
- Ribonucleoside triphosphate set (1 277 057, Roche)
- RNA polymerases (10881767001, 810 274, 11031163001, Roche)
- RNase A (R-4875, Sigma)
- RNase Inhibitor (03 335 399 001, Roche)
- RNase OUT (10777-019, Invitrogen)
- Sheep Serum (S-2382, Sigma)
- Sodium chloride (1.06404.1000, Merck)
- Sodium citrate, tribasic, dihydrate, ACS reagent (S-4641, Sigma)

- Sodium dodecyl sulphate (L-4509, Sigma)
- Sodium hydroxide, 98 % (S-5881, Sigma)
- Superscript II Reverse Transcriptase (18064-022, Invitrogen)
- Taq DNA Polymerase (201203, Quiagen)
- Taq Polymerase (GC-002-0100, Biotherm)
- Tissue Tek, O.C.T compound (25608-930, VWR)
- Transcription buffer, 10x conc. (1 465 384, Roche)
- Triethanolamine (T-1377 Sigma; 1.08377 Merck)
- Tris (hydroxymethyl) –aminomethan (1.08382.2500, Merck)
- Trizol (15596-0266, Invitrogen)
- tRNA, yeast (R-8759, Sigma)
- Tween20 (P9416, Sigma)
- Unlabeled LNA modified DNA (miRNA) probes (Exiqon)

5.2.3 Equipment

- Binoculars
    - Leica MZ 16F
    - Leica MZ 9
    - Zeiss Stemi SV6
- Cameras
    - AxioCam Camera
    - Leica DFC320
- Centrifuges
    - Eppendorf 5810R
    - Eppendorf Centrifuge 5415 R
    - Heraeus Biofuge pico
    - Sorvall Evolution RC
    - Univapo 150ECH
- Histology
    - Leica Cryostat CM1850
    - Leica Hot Plate HI1220
    - Leica Microtom RM2165
    - Leica Paraffin Embedding Station EG 1140H
    - Leica Watherbath HI1210
- Homogeniser
    - Heidolph DIAX 900
- Other
    - Applied Biosystems 48-capillary DNA analyser ABI-3730

    - Intavis *In Situ* Pro Robot
- pH-Meter
    - Sentix 81
- Photometer
    - Eppendorf Bio Photometer
    - Nanodrop ND-1000
- Thermoblock
    - Eppendorf Thermomixer Comfort
- Thermo Cycler
    - ABI Prims 7900HT Sequence Detection System
    - BioRAD ALS 1296
    - MJ Research PTC 200
    - Robocycler Gradient 96

6. Results

6.1 *cis*- mediated *Dll1* gene regulation

6.1.1 Generation of MSD alleles

The targeting vector for the MSD replacement allele was constructed, including two homologous arms 3964 bp and 1909 bp in length of the MSD flanking regions (Figure 4 A). In the targeting vector the 1.6 kb MSD enhancer was replaced by a hygromycin resistance cassette, flanked by LoxP sites. Following homologous recombination in mouse ES cells, the endogenous MSD enhancer was replaced with the hygromycin selection cassette (Figure 4 B).

Southern blot analysis was used to identify ES cell colonies with homologous integration of the targeting vector (not shown). ES cells carrying a homologous integration of the targeting vector were used for injection into blastocysts. One cell line successfully contributed to the germ line of a chimeric mouse, generating the *Dll1*^{tm1leg} founder mouse line. In order to generate the *Dll1*$^{tm1.1leg}$ MSD deletion allele, homozygous *Dll1*^{tm1leg} mice were crossed to a heterozygous C57BL/6$^{rosa26(SA\text{-}CrepA)ARTE}$ general deleter strain, to remove the hygromycin resistance cassette. In this *Dll1*$^{tm1.1leg}$ allele the ~1.6 kb MSD *cis*-regulatory element is replaced by a LoxP site (Figure 4 C). To further confirm correct integration of the targeting vector in both homozygous *Dll1*^{tm1leg} and *Dll1*$^{tm1.1leg}$ mouse lines we used long range PCR and primers F1, R1 and F2, R2 (Figure 4 A, B, C). F1 binds in the HI domain in wild type, as well as in the HI domain of *Dll1*^{tm1leg} and *Dll1*$^{tm1.1leg}$ alleles in the left arm of the targeting vector (Figure 4 A, C). F2 binds a DNA sequence in *Dll1*^{tm1leg} and *Dll1*$^{tm1.1leg}$ alleles upstream of the hygromycin resistance cassette. This particular DNA sequence is exclusive for both targeted alleles (Figure 4 B). R1 and R2 bind outside the right arm of the targeting vector in the *Dll1* coding region of wild type as well as of

Dll1^{tm1leg} and *Dll1*$^{tm1.1leg}$ alleles (Figure 4 A, B, C). Consequently, amplification using primers F2 and R2 alleles produces no fragment in wild type mice, a 5.1 kb fragment in homozygous *Dll1*^{tm1leg} mice and a 2.8 kb fragment in homozygous *Dll1*$^{tm1.1leg}$ mice (Figure 4 D, indicated by F2 R2). Amplification using primers F1 and R1 produces a 4.1 kb fragment in wild type mice, a 5.0 kb fragment in homozygous *Dll1*^{tm1leg} mice and a 2.7 kb fragment in homozygous *Dll1*$^{tm1.1leg}$ mice (Figure 4 D, indicated by F1 R1). To further confirm correct insertion of the targeting vector and deletion of the hygromycin selection cassette, all PCR fragments of wild type, homozygous *Dll1*^{tm1leg} and *Dll1*$^{tm1.1leg}$ mice were sequenced from both 5´ and 3´ ends (not shown), thus proofing correct identity of obtained PCR fragments. To simplify further genotype characterization of generated alleles, *Dll1*^{tm1leg} and *Dll1*$^{tm1.1leg}$ mice were routinely analyzed using two different duplex PCR reactions (Figure 4 E, F) and forward primers, which bind either in wild type (Figure 4 A (Msd2; Flox2)) or newly integrated DNA sequence (Figure 4 B, C (Msd3; Flox3)) and reverse primers which bind in both wild type and targeted alleles (Figure 4 A, B, C (Msd1; Flox1)).

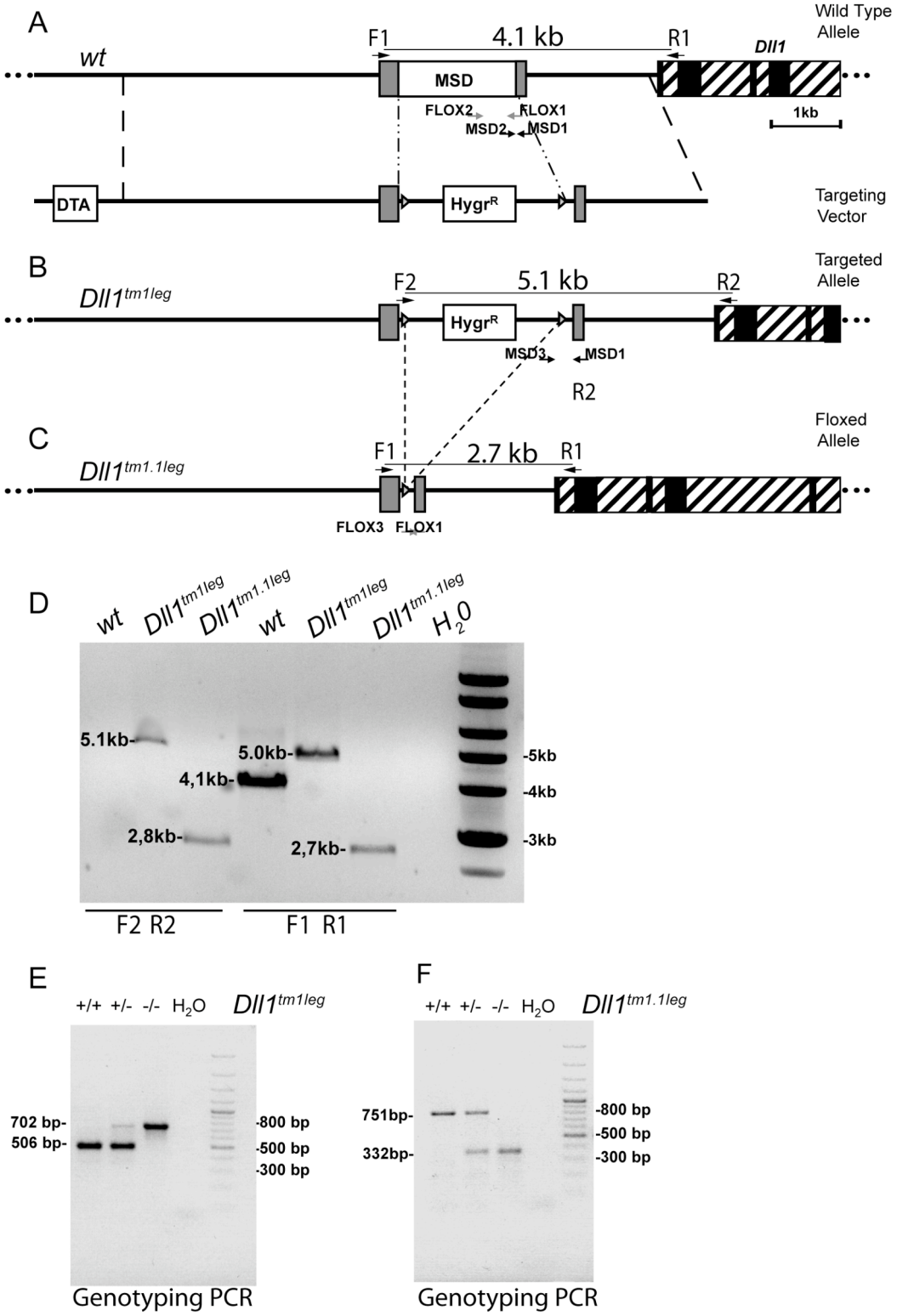

Figure 4: Generation of *Dll1*^{tm1leg} and *Dll1*$^{tm1.1leg}$ alleles.

(**A, B**) Targeting strategy for the generation of the *Dll1*^{tm1leg} allele (MSD replacement) and (**C**) the generation of the *Dll1*$^{tm1.1leg}$ deletion allele (MSD deletion). Black Boxes

indicate *Dll1* exons, grey boxes indicate *Dll1* neural enhancers and grey striped boxes indicate *Dll1* introns. Beyond, targeting vector used for homologous recombination. (**B**) In the *Dll1*^{tm1leg} allele the MSD enhancer is replaced with a hygromycin resistance cassette flanked by LoxP sites (grey triangles). (**C**) In the *Dll1*$^{tm1.1leg}$ allele the hygromycin resistance cassette was deleted through LoxP mediated excision. **(D)** Confirmation of recombination events for homozygous *Dll1*^{tm1leg} and *Dll1*$^{tm1.1leg}$ mice (**F**) Duplex PCR analysis of wild type, heterozygous and homozygous *Dll1*^{tm1leg} mouse tails using primers MSD1, MSD2 and MSD3. Amplification of wild type alleles produces a 506 bp fragment, while amplification of mutated alleles gives a 702 bp fragment. (**G**) Duplex PCR analysis of wild type, heterozygous and homozygous *Dll1*$^{tm1.1leg}$ mouse tails using primers Flox1, Flox2 and Flox3. Amplification of wild type alleles produces a 751 bp fragment, while amplification of mutated alleles gives a 353 bp fragment.

6.1.2 Inheritance of MSD Alleles

Heterozygous and homozygous *Dll1*^{tm1leg} and *Dll1*$^{tm1.1leg}$ mice are viable and fertile. To ascertain, that mutant mice are born according to Mendelian ratios, offspring from nine heterozygous crosses were genotyped by PCR at the age of 1 to 7 days post partum. Numbers of born *Dll1*^{tm1leg} and *Dll1*$^{tm1.1leg}$ animals were close to expected ratios of 1:2:1 for *Dll1*$^{+/+}$: *Dll1*$^{tm1leg/+}$: *Dll1*$^{tm1leg/tm1leg}$ and *Dll1*$^{+/+}$: *Dll1*$^{tm1.1leg/+}$: *Dll1*$^{tm1.1leg/tm1.1leg}$, respectively (Table 1).

Dll1$^{tm1leg/+}$ X *Dll1*$^{tm1leg/+}$	*Dll1*$^{+/+}$		*Dll1*$^{tm1leg/+}$		*Dll1*$^{tm1leg/tm1leg}$	
Expected Mendelian ratio	1	25%	2	50%	1	25%
Ratios calculated	19	25,3%	41	54,6%	15	20%
Dll1$^{tm1.1leg/+}$ X *Dll1*$^{tm1.1leg/+}$	*Dll1*$^{+/+}$		*Dll1*$^{tm1.1leg/+}$		*Dll1*$^{tm1.1leg/tm1.1leg}$	
Expected Mendelian ratio	1	25%	2	50%	1	25%
Ratios calculated	19	29,2%	30	46,1%	16	24,6%

Table 1: Expected and observed numbers for newborn mice of heterozygous intercrosses of *Dll1*$^{tm1leg/+}$ and *Dll1*$^{tm1.1leg/+}$ mice, respectively.

6.1.3 Expression analysis of *Dll1* and *Hes5* by whole mount *in situ* hybridisation

MSD was able to direct reporter gene expression in the paraxial mesoderm of transgenic mice, indicating a *cis*-regulatory function for MSD as a *Dll1* regulatory element (Beckers et al., 2000). Thus, we first characterized the *Dll1* expression by whole mount *in situ* hybridisation in wild type, heterozygous and homozygous *Dll1*^{tm1leg} mutant embryos. Despite the ability of MSD to direct reporter gene expression in the paraxial mesoderm of transgenic mice, *Dll1* expression was not eliminated in heterozygous and homozygous *Dll1*^{tm1leg} embryos and appeared largely normal in the head (Figure 5 E, F, asterisks), neural tube (Figure 5 A - F, white arrows), dermomyotome (Figure 5 A – F, yellow arrows), somites (Figure 5 A - H, red arrows), PSM and tailbud (Figure 5 A - H (blue arrows) and not shown). However, staining for *Dll1* in the PSM and tailbud of all heterozygous and homozygous *Dll1*^{tm1leg} embryos developed slower than in wild type littermates, when the colour reaction was checked early during the staining procedure (shown for 9.5 dpc embryos in Figure 5 I - K (indicated by brackets)). In the PSM of homozygous 8.5 dpc *Dll1*^{tm1leg} embryos we could sometimes detect a *Dll1* down-regulation even when the staining reaction was complete (Figure 5 G, H). To substantiate this potential down-regulation of *Dll1* in the PSM, we analyzed the expression of the Notch target gene *Hes5,* which has been shown to be down-regulated in the PSM of mice after over-expression of a dominant negative Dll1 form in the PSM (Figure 5 L – N) (Cordes et al., 2004). *Hes5* expression is diminished in the PSMs of heterozygous embryos (Figure 5 M, red arrow) (n=9) and is missing in PSMs of homozygous *Dll1*^{tm1leg} embryos (Figure 5 N) (n=4), but appeared normal in the neural tube (Figure 5 L – N, white arrows). Taken together, these data suggest a reduction of *Dll1* expression in the PSM of heterozygous and homozygous *Dll1*^{tm1leg} embryos.

To ascertain that the observed *Hes5* down-regulation is also present in the PSM, after Cre-mediated excision of the hygromycin resistance cassette in *Dll1*$^{tm1.1leg}$ embryos, we analyzed *Hes5* expression in wild type, hetero and homozygous *Dll1*$^{tm1.1leg}$ 9.5 dpc embryos (Figure 5 O - Q). In contrast to *Dll1*^{tm1leg} embryos, heterozygous (n=4) and homozygous (n=4) *Dll1*$^{tm1.1leg}$ embryos showed no down-regulation of *Hes5* expression in the PSM (Figure 5 P, Q, red arrows).

These data indicates, that MSD is not essential for *Dll1* expression in the PSM, tailbud and somites from 8.5 dpc to 11.5 dpc. However, the insertion of a hygromycin selection cassette in the endogenous MSD position leads to a down-regulation of *Dll1* expression and the Notch effector *Hes5* in the PSM. This is not the case after the excision of the hygromycin selection cassette.

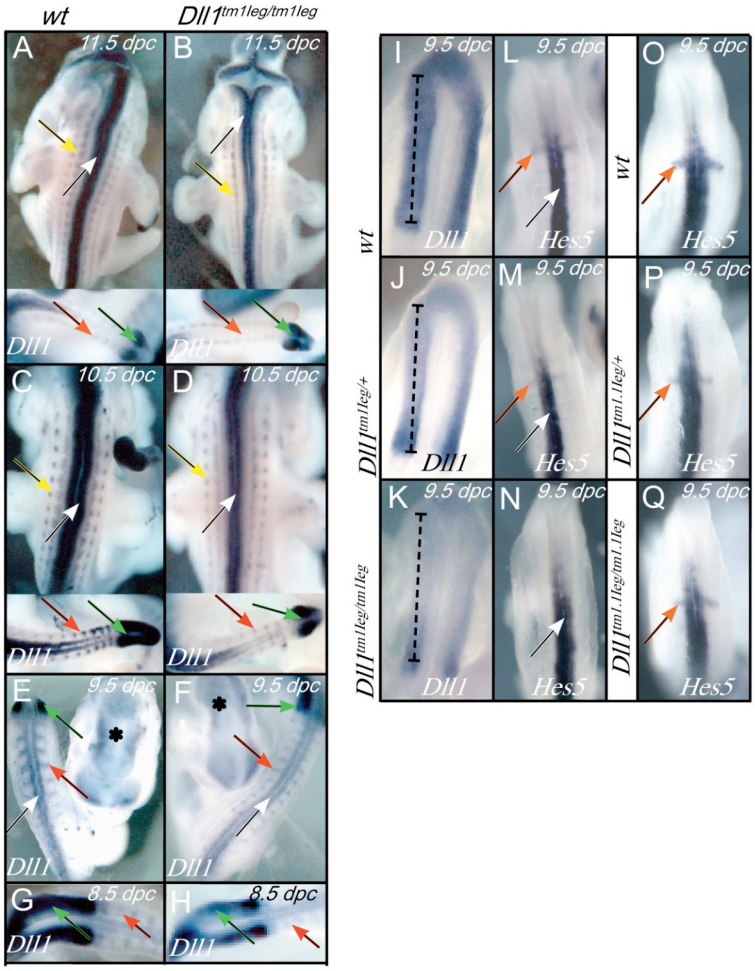

Figure 5: Whole mount *in situ* hybridisation for *Dll1* and *Hes5* mRNA in wild type, hetero and homozygous *Dll1*^{tm1leg} embryos as well as for *Hes5* mRNA in wild type, hetero and homozygous *Dll1*$^{tm1.1leg}$ embryos. (**A, B**) Expression of *Dll1* appeared normal in the dermomytome (yellow arrows) neural tube (white arrows) tail bud (blue arrows) and somites (red arrows). (**C, D**) Expression of *Dll1* appeared normal in dermomytome (yellow arrows) neural tube (white arrows) tail bud (blue arrows) and somites (red arrows). (**E, F**) Expression of *Dll1* appeared normal in neural tube (white arrows), head (asterisks) PSM (blue arrows) and somites (red arrows). (**G, H**) Expression of *Dll1* appeared normal PSM (blue arrows) and somites (red arrows). (**I - Q**) *Dll1* (indicated by brackets) and *Hes5* expression (red arrows) in the PSMs of wild type, heterozygous and homozygous *Dll1*^{tm1leg} and *Dll1*$^{tm1.1leg}$ 9.5 dpc embryos. **(I - K)** By short staining a reduced expression of *Dll1* was observed in the PSMs of heterozygous and homozygous *Dll1*^{tm1leg} embryos. (**L - N**) *Hes5* expression is reduced in the PSM of heterozygous *Dll1*^{tm1leg} embryos (red arrow) and missing in homozygous *Dll1*^{tm1leg} embryos. (**O - Q**) No differences in the *Hes5* expression (red arrows) are detected in PSMs of heterozygous and homozygous *Dll1*$^{tm1.1leg}$ embryos, compared to wild type littermates.

6.1.4 Skeletal alterations of *Dll1*^{tm1leg} newborn mice

The organization of the axial skeleton reflects the preceding organisation of somites (Brent and Tabin, 2002). We therefore examined the morphology of the axial skeleton of *Dll1*^{tm1leg} newborn mice between 1-7 days using skeletal Alizarin Red and Alcian Blue staining. Animals were obtained from mixed crosses of heterozygous and homozygous *Dll1*^{tm1leg} mice.

An ectopic rib was observed in heterozygous ($p<0.001$) and homozygous *Dll1*^{tm1leg} ($p<0.001$) newborn mice located to the left, right or to both sides of the 7th cervical vertebra and fused ventrally to the first thoracic rib (Figure 6 B, C (arrows and data not shown)).

In lumbar segments split vertebral bodies, two centres of ossification, individually surrounded by cartilage were detected in homozygous *Dll1*^{tm1leg} newborns ($p<0.001$)

(Figure 6 G (white arrow)) and in one heterozygous *Dll1*^{tm1leg} animal (not shown).

Bony fusions between vertebral bodies in lumbar segments were observed only in homozygous *Dll1*^{tm1leg} mice ($p<0.001$) (Figure 6 H (white arrow)).

Fused neural arches were detected in cervical and thoracic regions of homozygous *Dll1*^{tm1leg} mice ($p<0.001$) (Figure 6 K (white arrow and data not shown)). In addition some adult homozygous *Dll1*^{tm1leg} mice showed a kinked tail phenotype (data not shown).

6.1.5 Skeletal alterations of *Dll1*$^{tm1.1leg}$ newborn mice

To determine if the excision of the hygromycin resistance cassette has a similar effect for malformations of the axial skeleton, we next examined the skeletal morphology of the axial skeleton of heterozygous and homozygous *Dll1*$^{tm1.1leg}$ newborn mice obtained from heterozygous crosses.

Similar to *Dll1*^{tm1leg} newborn mice, ectopic ribs on the 7th cervical vertebra were detected in heterozygous ($p<0.05$) and homozygous ($p<0.001$) *Dll1*$^{tm1.1leg}$ mice (Figure 6 D, E (arrows)). Split vertebral bodies were occasionally detected in heterozygous ($p>0.05$ (not significant)) and homozygous ($p>0.05$ (not significant)) *Dll1*$^{tm1.1leg}$ animals (Figure 6 I (white arrow) and data not shown). The split vertebral bodies detected in *Dll1*$^{tm1.1leg}$ animals appeared also less severe compared to *Dll1*^{tm1leg} animals, as the two centres of ossification were, in every case, not individually surrounded by cartilage (compare Figure 6 I (white arrow) Figure 6 G (white arrow)). Fused neural arches were occasionally detected in cervical regions of heterozygous ($p>0.05$ (not significant)) and homozygous ($p>0.05$ (not significant)) *Dll1*$^{tm1.1leg}$ animals (data not shown). Adult homozygous *Dll1*$^{tm1.1leg}$ mice did not show a kinked tail phenotype (data not shown).

Taken together deficiency of MSD affects morphology of vertebra predominantly in

the cervical region, since the ectopic rib on the 7th cervical vertebra is the only skeletal malformation, which can be significantly detected in heterozygous and homozygous newborn animals of both alleles. This skeletal malformation thus most likely reflects the endogenous function of MSD.

Since split and fused vertebral bodies are significantly detected only in *Dll1*^{tm1leg} animals, it is unlikely, that these skeletal malformations reflect an endogenous function of MSD. They rather reflect a potential reduction of Delta Notch signalling in the PSM, as observed during whole mount *in situ* hybridisation. Here we observed differences in *Hes5* expression between *Dll1*^{tm1leg} and *Dll1*$^{tm1.1leg}$ 9.5 dpc embryos, which could be causative for the split and fused vertebral bodies in lumbar regions of homozygous *Dll1*^{tm1leg} newborn mice. Alterations in other parts of the skeleton (limbs, skull) could not be detected for both alleles.

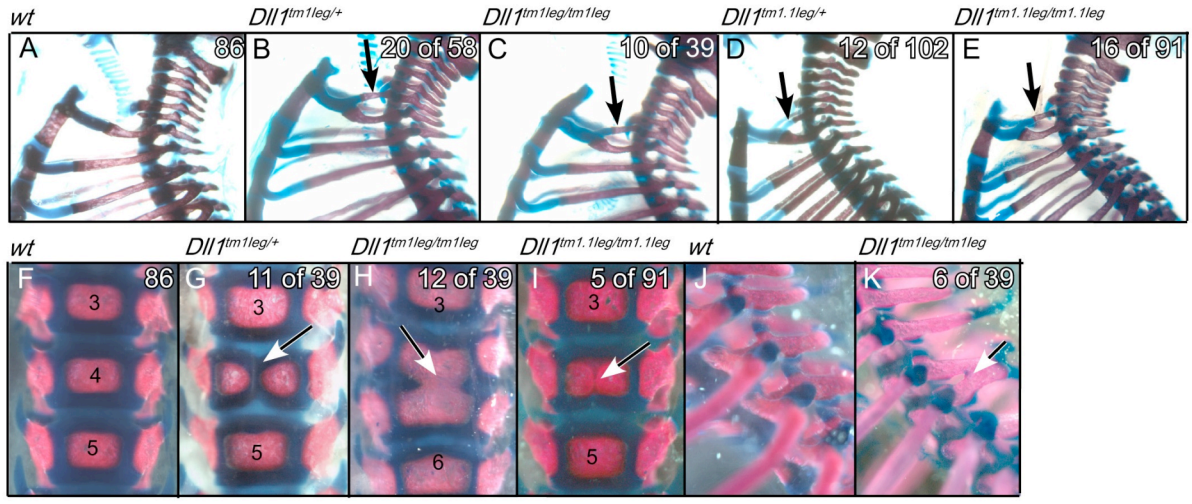

Figure 6: Skeletal preparations of wild type, heterozygous and homozygous *Dll1*^{tm1leg} or *Dll1*$^{tm1.1leg}$ newborn mice, respectively. (**A - E**) Heterozygous and homozygous newborn mice of both alleles show ectopic ribs on the 7th cervical segment (black arrows **B - E**) (**F - H**) Homozygous *Dll1*^{tm1leg} newborn mice showed split (**G**, white arrow) and fused (**H**, white arrow) vertebral bodies in lumbar segments. (**I**) In rare cases homozygous *Dll1*$^{tm1.1leg}$ also showed split vertebral bodies (white arrow) in lumbar segments, which were less severe as they were not individually surrounded

by cartilage. (**J, K**) Homozygous *Dll1*^{tm1leg} showed fused neural arches in cervical (not shown) and thoracic (**K**, white arrow) segments.

6.1.6 Morphology of single vertebra of *Dll1*$^{tm1.1leg}$ newborn mice

The subsequent analysis is thus exclusively focused on *Dll1*$^{tm1.1leg}$ mice. Since in heterozygous and homozygous *Dll1*$^{tm1.1leg}$ mice the external ectopic ribs on the 7th cervical vertebra were reminiscent of an anterior shift of segment and vertebrate identities, the morphology of single vertebrae of these mice was inspected in more detail. For this, vertebral columns of Alizarin Red and Alcian Blue stained wild type, heterozygous and homozygous *Dll1*$^{tm1.1leg}$ newborn mice were dissected to single vertebra and all cervical segments as well as parts of thoracic segments were inspected (Figure 7 A, B). Some dissected 7th cervical vertebra of heterozygous and homozygous *Dll1*$^{tm1.1leg}$ newborn mice were clearly distinguishable from wild type controls by the presence of ectopic ribs (Figure 7 A (red arrows)). In addition, dissection revealed that in some heterozygous and homozygous *Dll1*$^{tm1.1leg}$ newborn mice, which did not show fully developed ribs on the 7th cervical vertebra, rudimentary ribs were sometimes present on this segment (Figure 7 B (red arrows) (*Dll1*$^{tm1.1leg/+}$($p>0.05$ (not significant)) *Dll1*$^{tm1.1leg/tm1.1leg}$ ($p<0.05$)). This indicates that there is a difference in the expressivity of this phenotype. In rare cases fully developed ribs were further sustained on the dorsal part of the 1st thoracic rib (Figure 7 A (black arrows)) and fused to the sternum. One homozygous animal had 14 real thoracic ribs in total, but only 6 cervical vertebrae and thus showed a full transformation of the 7th cervical to the identity of the 1st thoracic segment (not shown).

In addition, occasional changes in segment morphology were detected in further anterior segments. In one heterozygous *Dll1*$^{tm1.1leg}$ animal the anterior tuberculum,

which is normally located on C6 in wild type controls, was located on C5 (Figure 7 A (green arrows)). Another heterozygous animal missed the anterior tuberculum on C6 (not shown).

These combined data suggest a possible homeotic shift through MSD deletion, which results in a partial morphological transformation of C7 to a T1 identity. Furthermore, different occasional alterations of skeletal morphology are detected more anterior, up to fifth cervical vertebra in *Dll1*$^{tm1.1leg}$ mice but never more posterior, further strengthening that MSD deletion leads to an anterior shift of vertebrate identities

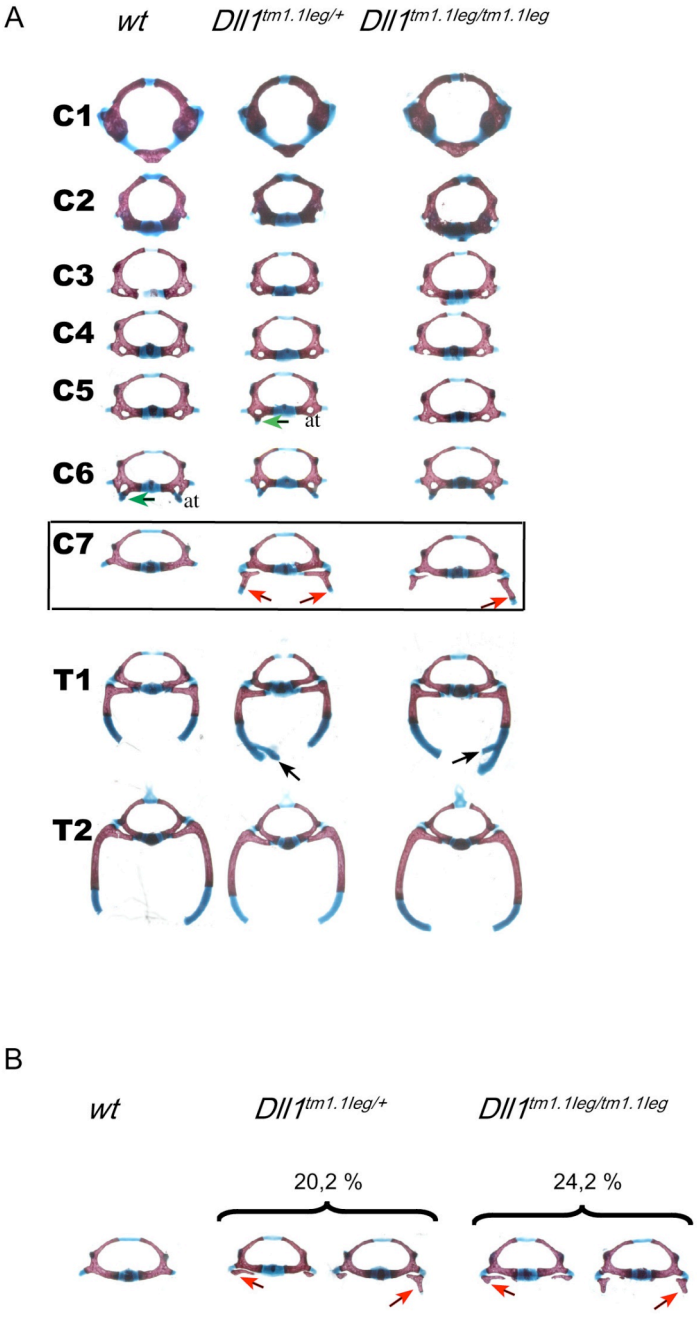

Figure 7: Analysis of single vertebrae of cervical and parts of thoracic segments of wild type, heterozygous and homozygous *Dll1*$^{tm1.1leg}$ newborn mice **(A)** Ectopic ribs were observed on the 7th cervical segment of heterozygous *Dll1*$^{tm1.1leg}$ and homozygous *Dll1*$^{tm1.1leg}$ newborn mice (red arrows). Rare skeletal alterations as a shift of the anterior tuberculum from C6 to C5 can also be detected (green arrows). In some cases, ectopic ribs in hetero and homozygous *Dll1*$^{tm1.1leg}$ animals were sustained on the dorsal part of the 1st thoracic rib (black arrows) and subsequently fused to the sternum (not shown) **(B)** In some heterozygous *Dll1*$^{tm1.1leg}$ and

homozygous *Dll1*$^{tm1.1leg}$, which did not show additional ectopic ribs on the 7th cervical segment rudimentary ribs could sometimes be detected on that segment.

6.1.7 Skeletal alterations of heterozygous *Tbx6*^{tm1Pa} and compound mutant *Tbx6*$^{tm1Pa/+}$ *Dll1*$^{tm1.1leg/+}$ and *Tbx6*$^{tm1Pa/+}$ *Dll1*$^{tm1.1leg/tm1.1leg}$ newborn mice

Tbx6 is a transcription factor, which is placed upstream of the Delta Notch signalling pathway *in vivo* as *Dll1* expression is reduced in embryos deficient for *Tbx6* (White and Chapman, 2005). Most of this regulatory function of *Tbx6* on *Dll1* expression appears to be mediated by MSD, as it contains multiple potential Tbx6 transcription factor binding sites (Hofmann et al., 2004). To determine whether Tbx6 can mediate *Dll1* function via MSD *in vivo*, we first examined the morphology of axial skeletons of newborn mice for a loss-of-function allele for *Tbx6* (Chapman and Papaioannou, 1998). We focused our analysis exclusively on heterozygous *Tbx6*^{tm1Pa} newborn mice, since homozygous *Tbx6*^{tm1Pa} mice are embryonically lethal (Chapman and Papaioannou, 1998).

In contrast to previously published data (White et al., 2003), we detected skeletal malformations in heterozygous *Tbx6*^{tm1Pa} newborn mice. In particular, split vertebral bodies in lumbar segments (Figure 8 K (white arrow)) ($p<0.001$), ectopic ribs on the 7th cervical segment (Figure 8 B (black arrow)) ($p<0.001$) and fused neural arches (Figure 8 F (yellow arrow)) ($p<0.001$) in cervical regions could be detected. Heterozygous *Tbx6*^{tm1Pa} mice thus copy most phenotypic aspects of heterozygous and homozygous *Dll1*^{tm1leg} and *Dll1*$^{tm1.1leg}$ mice (except fused vertebral bodies and kinked tails, which were exclusively detected in newborn homozygous *Dll1*^{tm1leg} mice). It is thus likely that Tbx6 meditates at least parts of the function of MSD *in vivo*.

To determine whether *Tbx6*^{tm1Pa} and *Dll1*$^{tm1.1leg}$ alleles genetically interact, we next

analyzed skeletal malformations of newborn mice, which carry combinations of these alleles (*Tbx6*$^{tm1Pa/+}$ *Dll1*$^{tm1.1leg/+}$ and *Tbx6*$^{tm1Pa/+}$ *Dll1*$^{tm1.1leg/tm1.1leg}$, respectively).

Ectopic ribs on the 7th cervical segment ($p<0.001$) (Figure 8 C, D (black arrows)) and fused neural arches in the cervical region ($p<0.001$) (Figure 8 G, H (yellow arrows)) appeared with a similar penetrance and appearance in compound mutants in comparison to heterozygous *Tbx6*^{tm1Pa} newborn mice. Ectopic ribs on the 7th cervical segment also appeared at a similar penetrance in compound *Tbx6*^{tm1Pa} and *Dll1*$^{tm1.1leg}$ mutants in comparison to heterozygous and homozygous *Dll1*$^{tm1.1leg}$ newborn mice.

There was, however, an synergistic effect by genetically combing *Tbx6*^{tm1Pa} and *Dll1*$^{tm1.1leg}$ alleles, since the number of split vertebral bodies in lumbar segments of *Tbx6*$^{tm1Pa/+}$ *Dll1*$^{tm1.1leg/tm1.1leg}$ newborn was significantly increased, compared to combined numbers of split vertebral bodies detected for heterozygous *Tbx6*^{tm1Pa} and homozygous *Dll1*$^{tm1.1leg}$ newborn mice (Figure 8 M, white arrows, and indicated total number of split vertebral bodies).

These combined data suggest that most function of MSD during the formation of the cervical vertebrae is mediated by Tbx6. Interestingly, compound *Tbx6*^{tm1Pa} and *Dll1*$^{tm1.1leg}$ mutants do show an synergistic effect for malformations in the lumbar region, but not for malformations in other parts of the axial skeleton.

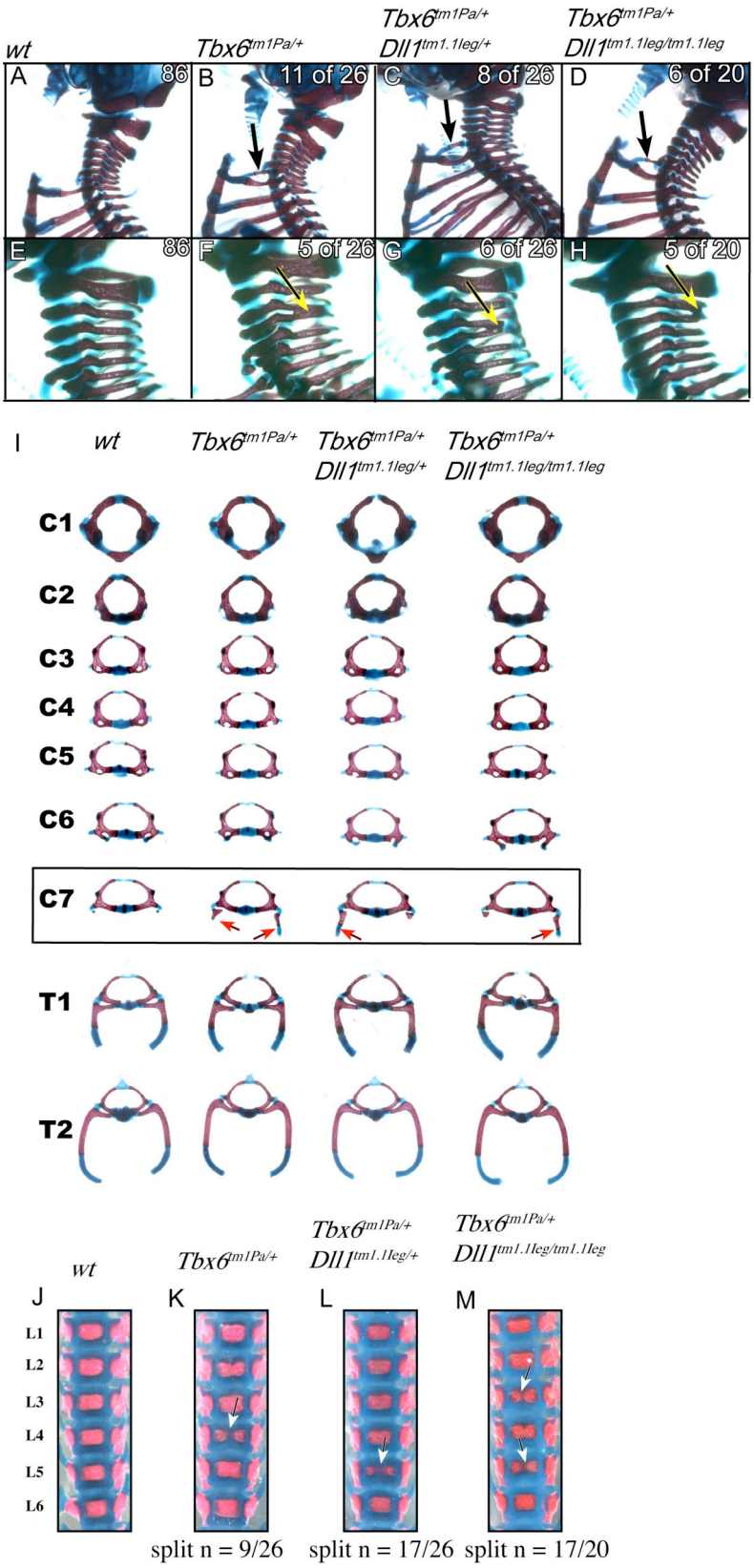

Figure 8: Skeletal preparations of wild type, heterozygous *Tbx6*^{tm1Pa} as well as of compound *Tbx6* and MSD mutant (*Tbx6*$^{tm1Pa/+}$ *Dll1*$^{tm1.1leg/+}$ and *Tbx6*$^{tm1Pa/+}$ *Dll1*$^{tm1.1leg/tm1.1leg}$) newborn mice, respectively. (**A** - **D**) Ectopic ribs on the 7th cervical

segment can be observed in heterozygous *Tbx6*^{tm1Pa}, *Tbx6*$^{tm1Pa/+}$ *Dll1*$^{tm1.1leg/+}$ and *Tbx6*$^{tm1Pa/+}$ *Dll1*$^{tm1.1leg/tm1.1leg}$ newborn mice (black arrows in **B, C, D**). (**E** – **H**) Fused neural arches can be observed in heterozygous *Tbx6*^{tm1Pa}, *Tbx6*$^{tm1Pa/+}$ *Dll1*$^{tm1.1leg/+}$ and *Tbx6*$^{tm1Pa/+}$ *Dll1*$^{tm1.1leg/tm1.1leg}$ newborn mice (yellow arrows in **F**, **G**, **H**) (**I**) Analysis of single vertebrae of cervical and parts of thoracic segments of wild type, heterozygous *Tbx6*^{tm1Pa}, *Tbx6*$^{tm1Pa/+}$ *Dll1*$^{tm1.1leg/+}$ and *Tbx6*$^{tm1Pa/+}$ *Dll1*$^{tm1.1leg/tm1.1leg}$ newborn mice. Ectopic ribs can be observed on the 7th cervical segment for heterozygous *Tbx6*^{tm1Pa} as well as for compound *Tbx6*$^{tm1Pa/+}$ *Dll1*$^{tm1.1leg/+}$ and *Tbx6*$^{tm1Pa/+}$ *Dll1*$^{tm1.1leg/tm1.1leg}$ mutant mice (red arrows). (**J - M**) Representative images of lumbar regions of wild type, heterozygous *Tbx6*^{tm1Pa}, compound *Tbx6*$^{tm1Pa/+}$ *Dll1*$^{tm1.1leg/+}$ and *Tbx6*$^{tm1Pa/+}$ *Dll1*$^{tm1.1leg/tm1.1leg}$ newborn mice (anterior is to the top). White arrows indicate split vertebral bodies. Incidences of split vertebral bodies are indicated as total number of split vertebral bodies per total number of newborn mice. Note that the total numbers of split vertebral bodies increase in lumbar segments L2 - L6 in wild type, heterozygous *Tbx6*^{tm1Pa}, *Tbx6*$^{tm1Pa/+}$ *Dll1*$^{tm1.1leg/+}$ and *Tbx6*$^{tm1Pa/+}$ *Dll1*$^{tm1.1leg/tm1.1leg}$ newborn mice.

6.1.8 Analysis of *Hoxb6* mRNA expression on sagittal histological sections

In a previous study additional ribs on the 7th cervical segment were detected in heterozygous *Dll1*^{tm1Gos} mice and did there coincide with an anterior shift of *Hoxb6* gene expression at 12.5 dpc (Cordes et al., 2004). In order to assess whether a change in *Hoxb6* expression is detectable in our mutant mice, we first performed whole mount *in situ* hybridisations at 8.5 dpc, 9.5 dpc and 10.5 dpc to characterize *Hoxb6* expression in wild type and homozygous *Dll1*$^{tm1.1leg}$ mice at these stages. No differences in the anterior *Hoxb6* expression domain could be detected in homozygous *Dll1*$^{tm1.1leg}$ compared to wild type embryos at the stages analyzed (Figure 9 A, B). We next analyzed *Hoxb6* expression in wild type (n=17), heterozygous *Tbx6*^{tm1Pa} (n=13), homozygous *Dll1*$^{tm1.1leg}$ (n=13), *Tbx6*$^{tm1Pa/+}$ *Dll1*$^{tm1.1leg/tm1.1leg}$ (n=7) and heterozygous *Dll1*^{tm1Gos} (n=6) 12.5 dpc embryos by *in situ*

hybridisation on sagittal sections. In heterozygous *Dll1*^{tm1Gos} 12.5 dpc embryos we could confirm an anterior shift of the *Hoxb6* expression domain from prevertebra 7 to prevertebra 6 in one out of six 12.5 dpc embryos (Figure 10 E, red arrow), which is in accordance with previously published data (Cordes et al., 2004). In four out of thirteen heterozygous *Tbx6*^{tm1Pa} and four out of thirteen homozygous *Dll1*$^{tm1.1leg}$ 12.5 dpc embryos we could detect an anterior shift of the *Hoxb6* expression domain from prevertebra 7 to prevertebra 6 (Figure 10 B, C, red arrows, respectively). In two out of seven *Tbx6*$^{tm1Pa/+}$ *Dll1*$^{tm1.1leg/tm1.1leg}$ (Figure 10 D) 12.5 dpc embryos, *Hoxb6* mRNA expression was also shifted anterior from prevertebra 7 to prevertebra 6, reminiscent of the anterior *Hoxb6* expression shift as detected for heterozygous *Tbx6*^{tm1Pa}, *Dll1*^{tm1Gos} and homozygous *Dll1*$^{tm1.1leg}$ 12.5 dpc embryos (compare to Figure 10 B, C). In conclusion, the *Dll1* MSD enhancer is required for correct formation of the 7th cervical vertebra and for correct positioning of the anterior *Hoxb6* expression border. This data suggests that MSD mediates correct segment identity.

The T-Box transcription factor Tbx6 is an additional factor necessary for correct formation of the 7th cervical vertebra and for correct positioning of the anterior *Hoxb6* expression border. Combining Tbx6 and MSD alleles does not significantly change neither the penetrance of the ectopic ribs on the 7th cervical segment, nor the anterior *Hoxb6* expression border in compound *Tbx6*$^{tm1Pa/+}$ *Dll1*$^{tm1.1leg/tm1.1leg}$ mutants. It is thus likely that Tbx6 function in this context is directly and exclusively mediated through MSD.

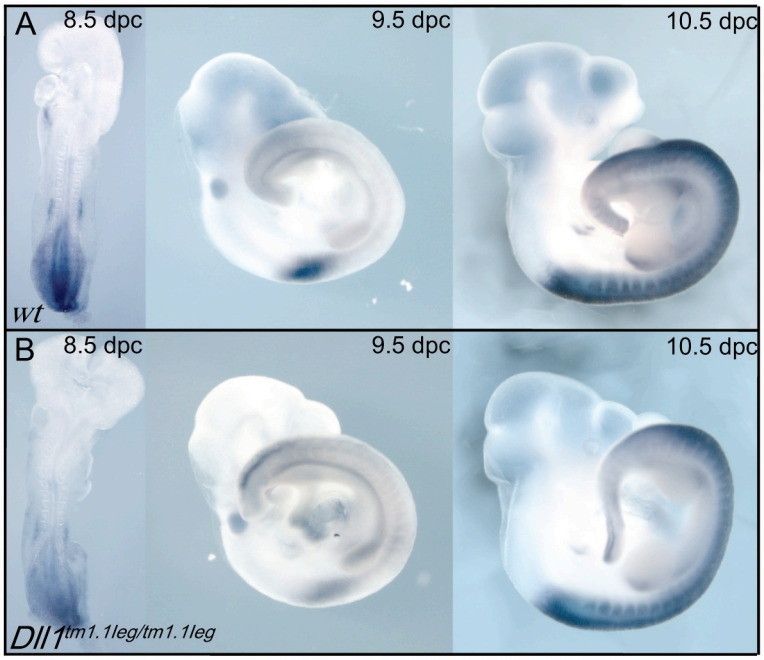

Figure 9: (**A**, **B**) Representative images of whole mount *in situ* hybridisations for *Hoxb6* mRNA expression at 8.5 dpc, 9.5 dpc and 10.5 dpc in wild type and homozygous *Dll1*$^{tm1.1leg}$ mutant mice. No difference in *Hoxb6* expression could be detected.

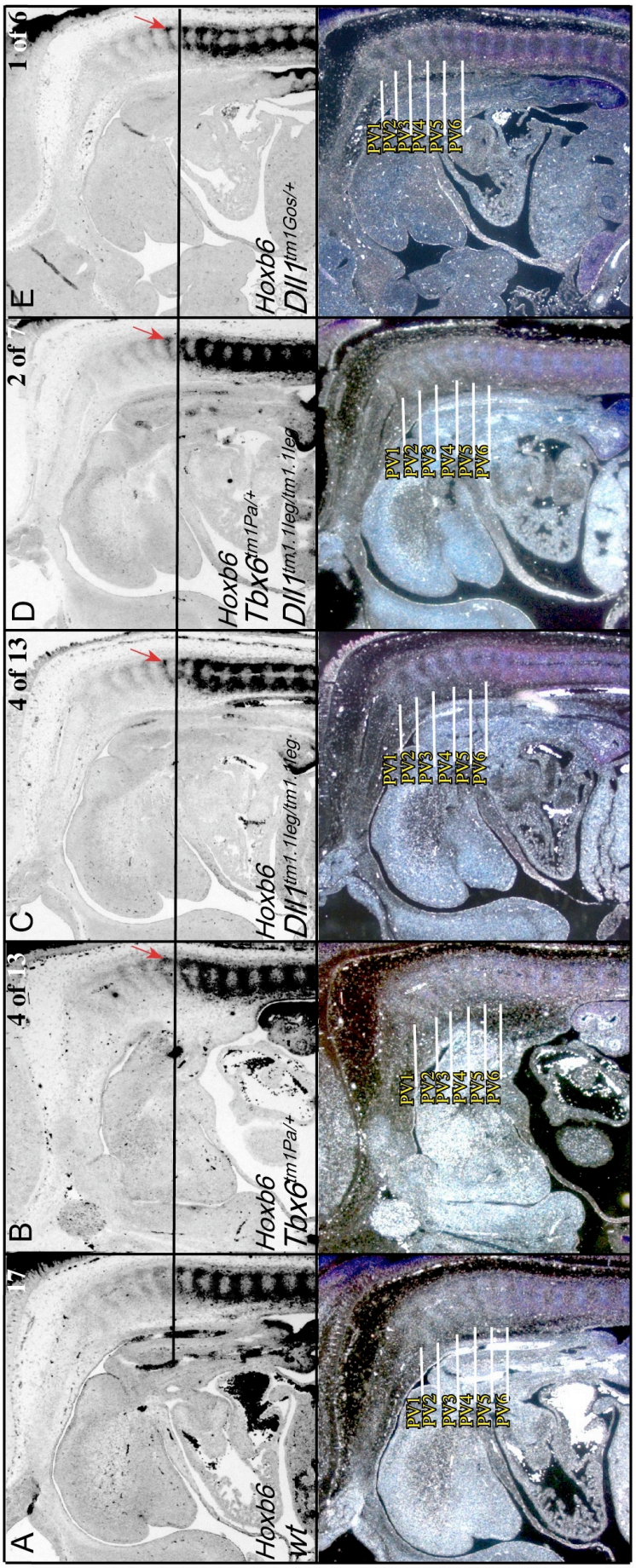

Figure 10: (A – E, top) Representative images of *in situ* hybridisations for *Hoxb6* mRNA expression on sagittal histological sections of wild type, heterozygous *Tbx6*^{tm1Pa}, homozygous *Dll1*$^{tm1.1leg}$, compound *Tbx6*$^{tm1Pa/+}$ *Dll1*$^{tm1.1leg/tm1.1leg}$ and heterozygous *Dll1*^{tm1Gos} 12.5 dpc embryos. The black line indicates the border between prevertebral segment six and seven (**A – E, bottom**) Corresponding dark field images used for determination of prevertebral identity (**B**, **C**, **E**) In four out of thirteen heterozygous *Tbx6*^{tm1Pa} and homozygous *Dll1*$^{tm1.1leg}$ as well as in one heterozygous *Dll1*^{tm1Gos} 12.5 dpc embryo, *Hoxb6* mRNA expression was shifted from prevertebra 7 to prevertebra 6 (red arrows). (**D**) The anterior *Hoxb6* expression domain in compound *Tbx6*$^{tm1Pa/+}$ *Dll1*$^{tm1.1leg/tm1.1leg}$ 12.5 dpc embryos was shifted from prevertebra 7 to prevertebra 6 in one out of seven 12.5 dpc embryos (red arrow).

6.1.9 MSD has a regulatory function for *Dll1* expression in the PSM at 8.5 dpc

Since heterozygous and homozygous *Dll1*$^{tm1.1leg}$ newborn mice showed skeletal malformations mainly in the cervical region, we focused our analysis on *Dll1* expression in 8.5 dpc embryos, since this corresponds to the developmental stage, when the somites, contributing to the vertebrae of cervical to thoracic region, bud off from the PSM. From a first whole mount *in situ* hybridisation experiment on wild type and homozygous *Dll1*$^{tm1.1leg}$ embryos it appeared that *Dll1* mRNA is down-regulated in the posterior PSM of homozygous *Dll1*$^{tm1.1leg}$ embryos (Figure 11 B (red arrows)). This down-regulation of *Dll1* is thus reminiscent as detected for homozygous *Dll1*^{tm1leg} 8.5 dpc embryos (Figure 5 G, H). It has been previously reported that *Dll1* is dynamically expressed in the PSM (Maruhashi et al., 2005). We thus further characterized the *Dll1* expression in wild type and homozygous *Dll1*$^{tm1.1leg}$ 8.5 dpc embryos by additional whole mount *in situ* hybridisations and could confirm dynamic *Dll1* expression at 8.5 dpc in wild type and homozygous *Dll1*$^{tm1.1leg}$ embryos (Figure 11 C – H). We further compared corresponding dynamic *Dll1* stages of wild type and homozygous *Dll1*$^{tm1.1leg}$ embryos with each other. Using this approach we could detect a down-regulation of *Dll1* expression levels in the posterior PSM of homozygous *Dll1*$^{tm1.1leg}$ embryos during some dynamic stages in comparison to wild type (Figure 11 F, indicated by brackets). To determine whether the expression of *Hes5* is altered in homozygous *Dll1*$^{tm1.1leg}$ mice, we analyzed *Hes5* expression by whole mount *in situ* hybridisation on wild type and homozygous *Dll1*$^{tm1.1leg}$ 8.5 dpc embryos. Dynamic *Hes5* expression appeared unchanged in homozygous 8.5 dpc *Dll1*$^{tm1.1leg}$ embryos in comparison to wild type (Figure 11 J - P). We could, however, sometimes detect blurred or diminished *Hes5* expression stripes in the posterior PSM (Figure 11 L, indicated by brackets) in homozygous *Dll1*$^{tm1.1leg}$ embryos. This

indicates that besides the observed *Dll1* down-regulation, *Hes5* is also down-regulated in the posterior PSM in homozygous *Dll1*$^{tm1.1leg}$ embryos. To provide a more quantitative analysis of *Dll1* expression than with *in situ* methods we assessed *Dll1* expression using qRT-PCR on wild type (n=13) and homozygous *Dll1*$^{tm1.1leg}$ (n=14) PSMs of 8.5 dpc embryos. We could detect high variability of *Dll1* expression levels in both wild type and homozygous *Dll1*$^{tm1.1leg}$ PSMs, which is in accordance with a dynamic *Dll1* expression at this stage, as detected during whole mount *in situ* hybridisations (Figure 11 Q blue and red bars, respectively). After the calculation of the mean expression levels from this experiment, we could detect a slight down-regulation of *Dll1* expression levels in PSMs of *Dll1*$^{tm1.1leg}$ embryos (Figure 11 S). To assess whether reduced *Dll1* expression might result in reduced *Tbx6* expression levels in these embryos, we additionally assessed *Tbx6* expression levels by qRT-PCR in both wild type and homozygous *Dll1*$^{tm1.1leg}$ 8.5 dpc embryos. *Tbx6* expression was, however, unaltered in homozygous *Dll1*$^{tm1.1leg}$ embryos in comparison to wild type (Figure 11 T, yellow bars). We next did determine *Dll1* expression levels in the PSM of wild type (n=12) and heterozygous 8.5 dpc *Tbx6*^{tm1Pa} (n=15) embryos using qRT-PCR. We were especially interested whether we can detect an enhanced down-regulation of *Dll1* expression levels in PSMs of heterozygous *Tbx6*^{tm1Pa} mutant embryos compared to homozygous *Dll1*$^{tm1.1leg}$ embryos. Principally, in wild type and heterozygous *Tbx6*^{tm1Pa} PSMs we could again detect a high variability of *Dll1* expression levels (Figure 11 R, blue and red bars). After the calculation of the mean expression levels from this experiment, we could detect a significant reduction of *Dll1* expression levels in the PSMs of heterozygous *Tbx6*^{tm1Pa} embryos compared to wild type. The extent of the reduction of *Dll1* expression levels was not enhanced compared to homozygous *Dll1*$^{tm1.1leg}$ embryos (Figure 11 S).

This combined data indicates that MSD is not essential for dynamic *Dll1* expression and cyclic Notch activity based on the *Hes5* expression data. MSD does, however, have a function for fine-tuning *Dll1* expression levels at this stage. This function appears to be mediated by Tbx6, since an enhanced down-regulation of *Dll1* expression levels was not detectable in heterozygous *Tbx6*^{tm1Pa} embryos compared to homozygous *Dll1*$^{tm1.1leg}$ embryos. Furthermore, reduced *Dll1* expression levels in PSMs of homozygous *Dll1*$^{tm1.1leg}$ embryos did not influence *Tbx6* expression levels.

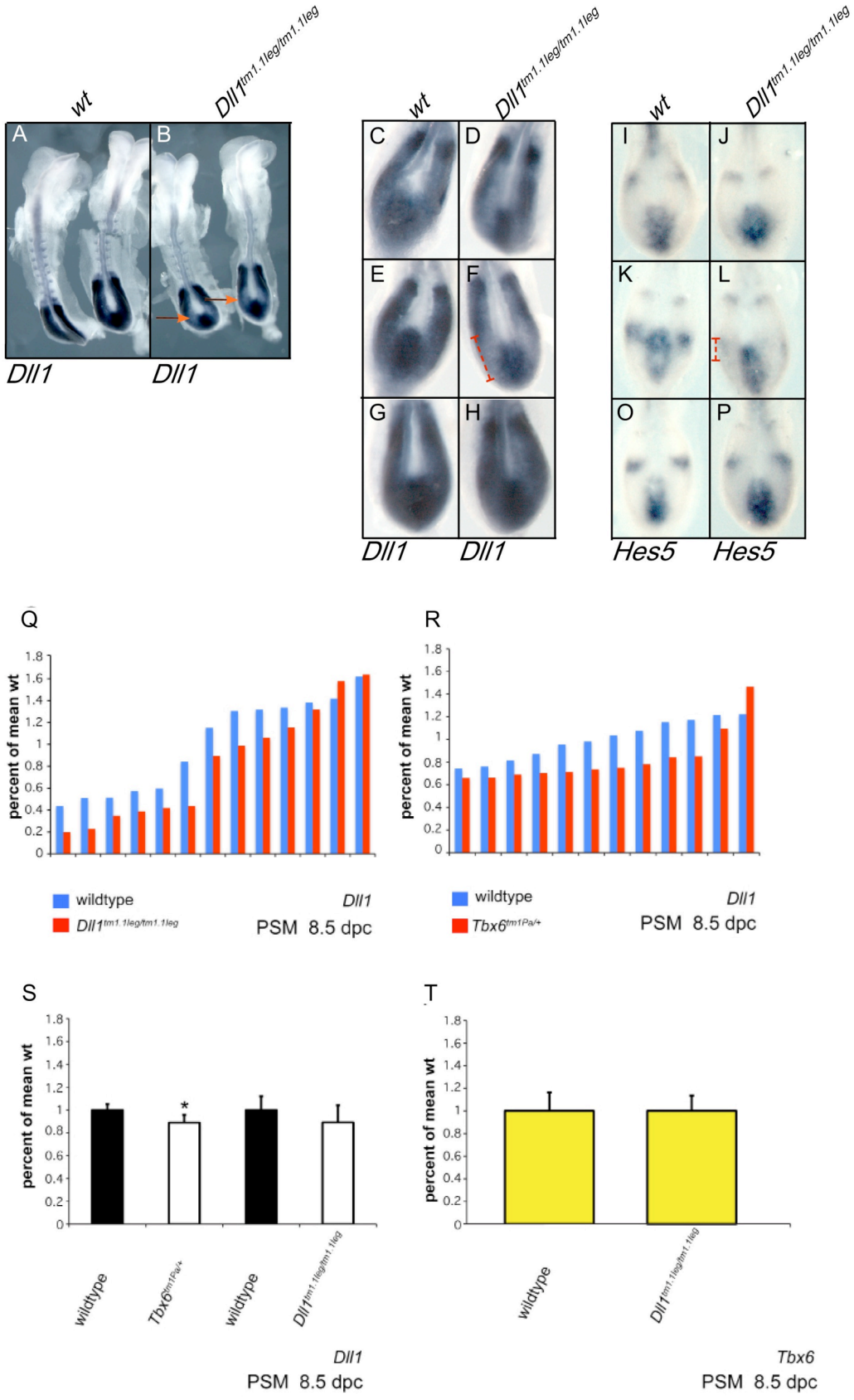

Figure 11: Whole mount *in situ* hybridisations for *Dll1* and *Hes5* and qRT-PCR for *Dll1* and *Tbx6* in wild type, homozygous *Dll1*$^{tm1.1leg}$ and heterozygous *Tbx6*^{tm1Pa} 8.5

dpc embryos. Error bars are depicted in SEM. (**A, B**) *Dll1* mRNA is down-regulated in the posterior PSM of homozygous *Dll1*$^{tm1.1leg}$ embryos. (**B**, red arrows) (**C - P**) *Dll1* and *Hes5* expression at 8.5 dpc in wild type and homozygous *Dll1*$^{tm1.1leg}$ embryos. Corresponding *Dll1* and *Hes*5 dynamic expression patterns are displayed (**Q**) qRT-PCR on single dissected PSMs of wild type (blue bars) and homozygous *Dll1*$^{tm1.1leg}$ (red bars) embryos showing dynamic *Dll1* expression in the PSM. (**R**) qRT-PCR on single dissected PSMs of wild type (blue bars) and heterozygous *Tbx6*^{tm1Pa} (red bars) embryos showing dynamic *Dll1* expression in the PSM. (**S**) Calculated means from the dataset shown in Q, R. *Dll1* expression is significantly reduced in PSMs of heterozygous *Tbx6*^{tm1Pa} embryos and similarly reduced in PSMs of homozygous *Dll1*$^{tm1.1leg}$ embryos. (**T**) *Tbx6* expression is unaltered in homozygous *Dll1*$^{tm1.1leg}$ embryos in comparison to wild type.

6.1.10 qPCR for *Dll1*, *Tbx6* and *Notch1* on single dissected PSMs

Genetically combining Tbx6 and MSD alleles resulted in an increase of split vertebral bodies in the lumbar region, which could potentially be explained by reduced *Dll1* expression levels in compound *Tbx6*$^{tm1Pa/+}$ *Dll1*$^{tm1.1leg/+}$ and *Tbx6*$^{tm1Pa/+}$ *Dll1*$^{tm1.1leg/tm1.1leg}$ mutant mice compared to heterozygous Tbx6 loss-of-function mice alone. This potential reduction of *Dll1* expression levels must take place in the PSM during development, since *Tbx6* is exclusively expressed in that tissue (White and Chapman, 2005).

In order to determine whether we can detect an enhanced down-regulation of *Dll1* in embryos carrying combinations of Tbx6 and MSD alleles, we performed qRT-PCRs for *Dll1* on single dissected PSMs of wild type (n= 30), *Tbx6*$^{tm1Pa/+}$ (n= 10), *Tbx6*$^{tm1Pa/+}$ *Dll1*$^{tm1.1leg/+}$ (n= 10) and *Tbx6*$^{tm1Pa/+}$ *Dll1*$^{tm1.1leg/tm1.1leg}$ (n= 8) embryos at 9.5 dpc (Figure 12 A), because this is the time point when the somites, corresponding to lumbar segments, are generated. We additionally included *Tbx6* in our analysis, since it was postulated earlier that *Tbx6* expression could be directly dependent on Dll1 (Shifley and Cole, 2007; White et al., 2005). We further included *Notch1* in our

expression analysis. As expected, we can detect a significant decrease of *Dll1* expression levels in PSMs of *Tbx6*$^{tm1Pa/+}$, *Tbx6*$^{tm1Pa/+}$ *Dll1*$^{tm1.1leg/+}$ and *Tbx6*$^{tm1Pa/+}$ *Dll1*$^{tm1.1leg/tm1.1leg}$ animals compared to wild type controls (Figure 12 A, blue bars). Furthermore, the *Dll1* expression in the PSM of *Tbx6*$^{tm1Pa/+}$ *Dll1*$^{tm1.1leg/tm1.1leg}$ was significantly reduced compared to *Dll1* expression in the PSM of *Tbx6*$^{tm1Pa/+}$ animals. The extent of the *Dll1* down-regulation is thus correlated with the increase of numbers in split vertebral bodies. *Tbx6* expression levels were significantly down-regulated in the PSMs of *Tbx6*$^{tm1Pa/+}$, *Tbx6*$^{tm1Pa/+}$ *Dll1*$^{tm1.1leg/+}$ and *Tbx6*$^{tm1Pa/+}$ *Dll1*$^{tm1.1leg/tm1.1leg}$ embryos compared to wild type controls (Figure 12 A, red bars). Interestingly, *Tbx6* expression levels in the PSM of *Tbx6*$^{tm1Pa/+}$ *Dll1*$^{tm1.1leg/tm1.1leg}$ were significantly reduced compared to *Tbx6* expression levels in the PSM of heterozygous *Tbx6*^{tm1Pa} animals. To further evaluate, whether *Tbx6* expression depends on *Dll1* in the PSM, we measured *Tbx6* and *Dll1* expression levels in PSMs of heterozygous (n=13) and homozygous (n=8) *Dll1*^{tm1Gos} embryos at 9.5 dpc (Figure 12 B). In heterozygous *Dll1*^{tm1Gos} animals we could detect, a significant down-regulation of *Dll1* expression levels (Figure 12 B, blue bars), but no significant alteration of *Tbx6* expression levels (Figure 12 B, red bars). In PSMs of homozygous *Dll1*^{tm1Gos} embryos we could detect a significant down-regulation of *Dll1* (Figure 12 B) and *Tbx6* (Figure 12 B) expression levels.

To fit the *Dll1*$^{tm1.1leg}$ allele into the context we next analyzed expression levels of *Dll1, Notch1* and *Tbx6* in PSMs of heterozygous (n=4) and homozygous (n=6) *Dll1*$^{tm1.1leg}$ mice by qRT-PCR (Figure 12 C). As expected *Dll1* expression levels were not strongly down-regulated in PSMs of heterozygous and homozygous *Dll1*$^{tm1.1leg}$ embryos. However, *Dll1* expression levels were slightly down-regulated in these animals (Figure 12 C, blue bars). Interestingly *Tbx6* expression levels were

significantly down-regulated in PSMs of homozygous *Dll1*$^{tm1.1leg}$ embryos (Figure 12 C, red bars). This combined data thus favours the possibility of a feedback loop between *Tbx6,* MSD and *Dll1*, during the development of lumbar vertebrae, respectively.

To determine, whether *Hoxb6* expression is directly dependent on functional *Dll1* and *Tbx6* alleles in the PSM (Figure 12 D, yellow bars) we subsequently assessed *Hoxb6* expression in homozygous *Dll1*^{tm1Gos} and homozygous *Tbx6*^{tm1Pa} 9.5 dpc embryos using qRT-PCR. We could, however, not detect a significant alteration of *Hoxb6* expression in PSMs of homozygous *Dll1*^{tm1Gos} and homozygous *Tbx6*^{tm1Pa} embryos. A slight down-regulation of *Hoxb6* expression levels in homozygous *Dll1*^{tm1Gos} and homozygous *Tbx6*^{tm1Pa} 9.5 dpc embryos was, however, detected.

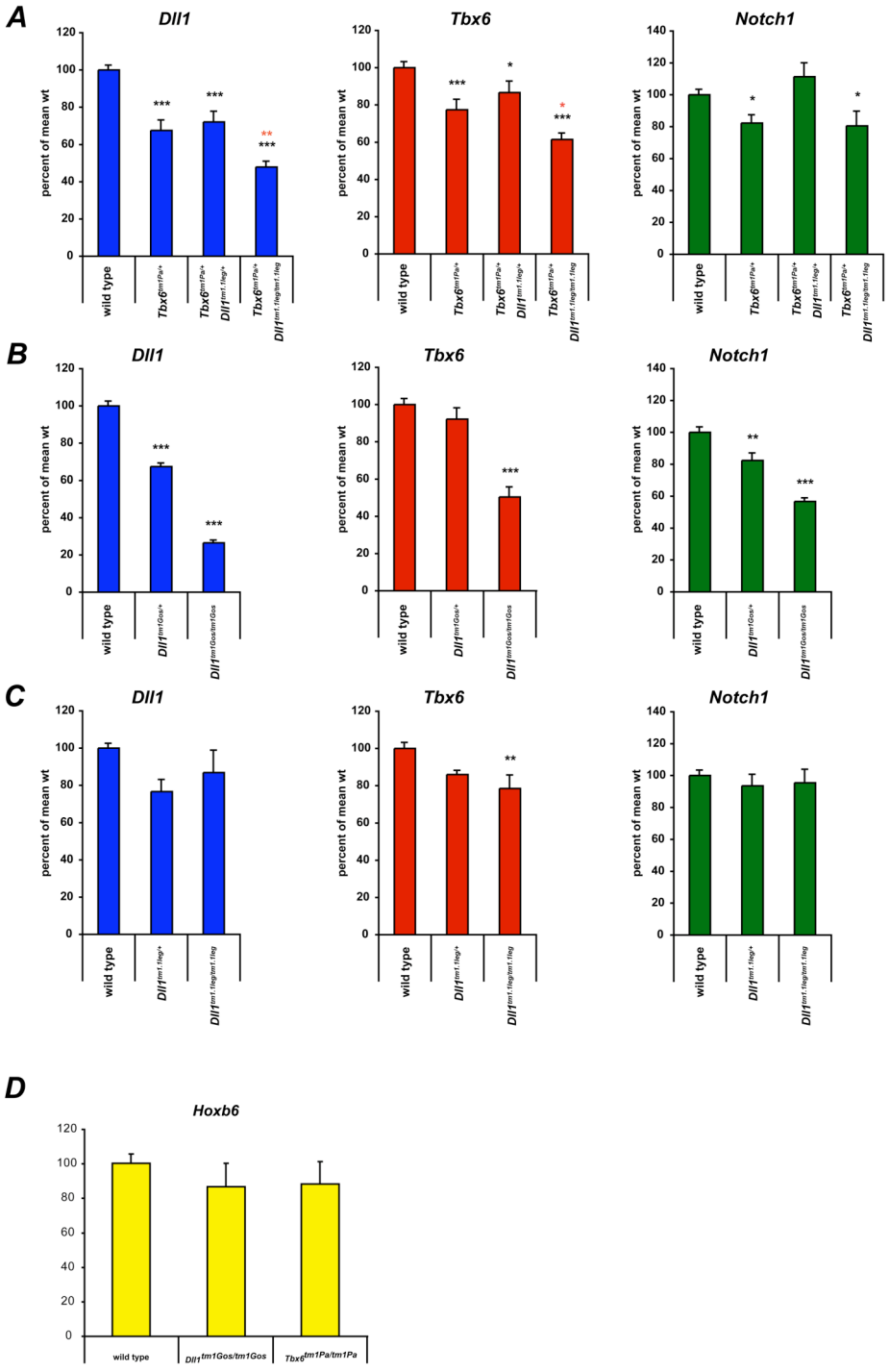

Figure 12: (**A** - **D**) qPCRs for *Dll1* (blue bars), *Tbx6* (red bars), *Notch1* (green bars) and *Hoxb6* (yellow bars) on dissected PSMs of 9.5 dpc embryos with indicated genotypes. Error bars are depicted in SEM. Black asterisks indicate significant regulation compared to wild type. Red asterisks indicate significant regulation compared to heterozygous *Tbx6*^{tm1Pa} embryos. (**A**) *Dll1* expression is significantly down-regulated in PSMs of *Tbx6*$^{tm1Pa/+}$ *Tbx6*$^{tm1Pa/+}$ *Dll1*$^{tm1.1leg/+}$ and *Tbx6*$^{tm1Pa/+}$

Dll1$^{tm1.1leg/tm1.1leg}$ embryos. *Dll1* expression is significantly down-regulated in PSMs of *Tbx6*$^{tm1Pa/+}$ *Dll1*$^{tm1.1leg/tm1.1leg}$ mice compared to *Tbx6*$^{tm1Pa/+}$ embryos. *Tbx6* expression is significantly down-regulated in PSMs of *Tbx6*$^{tm1Pa/+}$, *Tbx6*$^{tm1Pa/+}$ *Dll1*$^{tm1.1leg/+}$ and *Tbx6*$^{tm1Pa/+}$ *Dll1*$^{tm1.1leg/tm1.1leg}$ embryos. Interestingly, *Tbx6* expression is significantly down-regulated in PSMs of *Tbx6*$^{tm1Pa/+}$ *Dll1*$^{tm1.1leg/tm1.1leg}$ embryos in comparison to *Tbx6*$^{tm1Pa/+}$ embryos. (**B**) *Dll1* expression is significantly down-regulated in PSMs of heterozygous and homozygous *Dll1*^{tm1Gos} embryos. *Tbx6* expression is significantly down-regulated in PSMs of homozygous *Dll1*^{tm1Gos} embryos. (**C**) *Dll1* expression is slightly down-regulated in PSMs of heterozygous and homozygous *Dll1*$^{tm1.1leg}$ embryos. *Tbx6* expression is significantly down-regulated in PSMs of homozygous *Dll1*$^{tm1.1leg}$ embryos. (**D**) *Hoxb6* expression is slightly down-regulated in PSMs of homozygous *Dll1*$^{tm1.1leg}$ and heterozygous *Tbx6*^{tm1Pa} embryos.

6.1.11 Hoxb6 protein expression in wild type embryos

As we could detect an anterior shift for the *Hoxb6* mRNA in MSD deletion and heterozygous *Tbx6* loss-of-function mice, we wanted to determine whether the Hoxb6 protein expression domain is altered in a similar manner. For that we first tested two different commercially available antibodies for the Hoxb6 protein on sagittal cryosections of 12.5 dpc wild type embryos. The first antibody (Abcam, ab26077) we tested did not show any specific staining on sagittal sections of 12.5 dpc embryos (not shown). The second antibody (Santa Cruz, SC-17171), which was previously shown to work on adult lung tissue in mice (Volpe et al., 2008), showed reproducible staining patterns. Using horseradish peroxidase (HRP) as a detecting enzyme, we could observe a specific reproducible Hoxb6 protein pattern in the neural tube and in the lung (Figure 12 B, C, brackets and white arrow, respectively). We could, however, not detect Hoxb6 protein expression in the prevertebral condensations of wild type embryos (Figure 12 D). We considered the possibility that HRP might be not sensitive enough to detect Hoxb6 protein expression in the prevertebral condensations, as also during RNA *in situ* hybridisations, the *Hoxb6* mRNA expression was quite low in

this tissue. We thus tried alkaline phosphatase (AP) (not shown), or a fluorescently labelled secondary antibody for detection (Figure 13 and Figure 14). Using either AP or a fluorescent labelled secondary antibody, we detected strong expression domains comparable to the previously observed expression patterns (Figure 12) in the neural tube (Figure 13 A - F) and the lung (not shown). Using immunofluoresence we could additionally observe a slight positive staining in prevertebral condensations (Figure 14 F), but the signal observed was ubiquitously distributed in all prevertebral condensations (no clear anterior boundary of the Hoxb6 expression domain was observed at prevertebra 7, as it would be expected also for the protein distribution) and the signal detected is thus most likely due to antibody trapped in blood cells or autofluorescence.

This data indicates that Hoxb6 mRNA is either not yet translated into protein at this stage or, more likely, that Hoxb6 protein concentration in the prevertebral condensation is under the threshold detection limit for Immunohistochemistry.

Generally, there is one positive report about detection of Hox protein expression in prevertebral condensations using immunohistochemistry. The Hox protein expression was here, however, also barely detectable (Awgulewitsch and Jacobs, 1990). Most other reported data for *Hox* gene expression in prevertebral condensations is *in situ* hybridisation data (Cordes et al., 2004; Galliot et al., 1989; Williams et al., 2006). It is thus evident that the detection of Hox protein expression in prevertebral condensations is not well established.

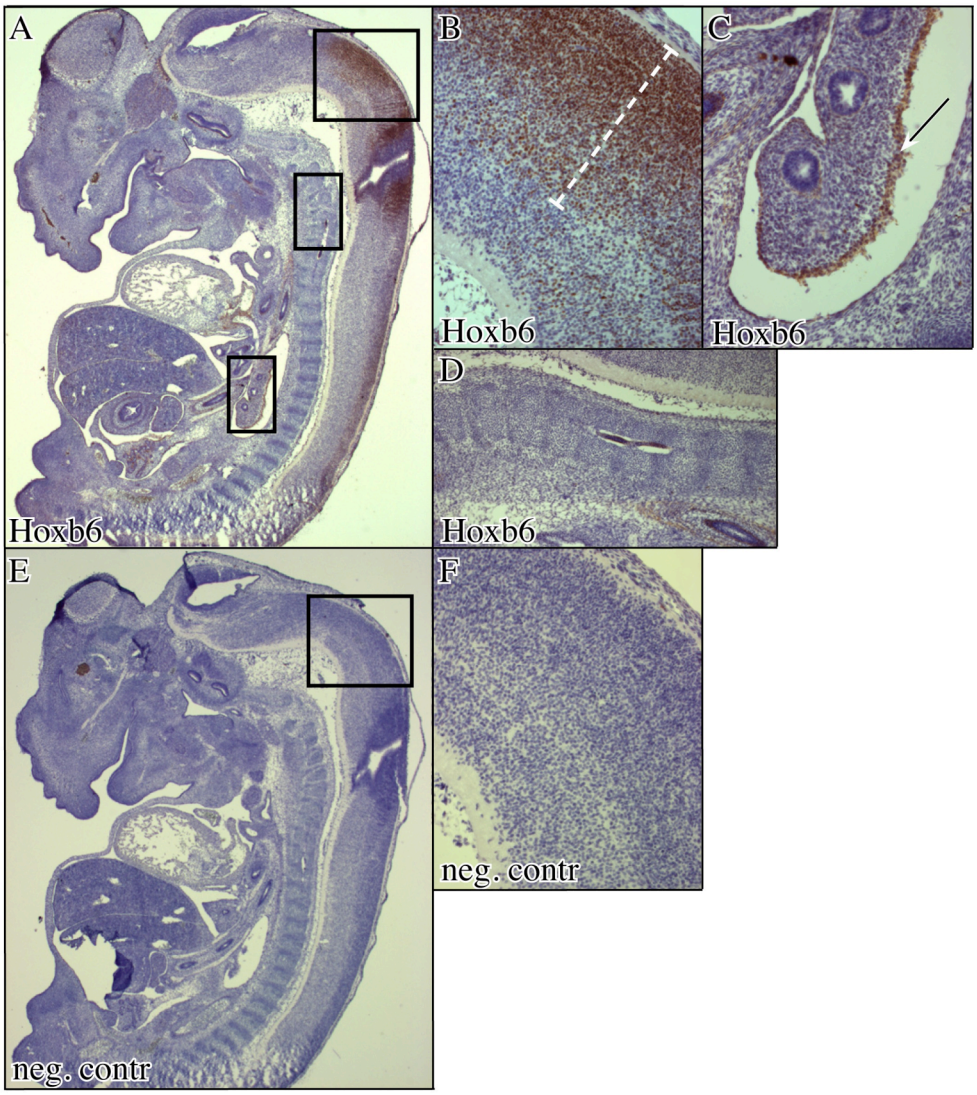

Figure 13: Immunohistochemistry on sagittal cryosections of 12.5 dpc wild type embryos for Hoxb6 protein (**A - D**) and negative control using no primary antibody (**E, F**). (**A - D**) Hoxb6 protein can be detected in the neural tube (**B**, indicated by brackets) and in the lung (**C**, white arrow) but not in the prevertebral condensations of wild type embryos (**D**).

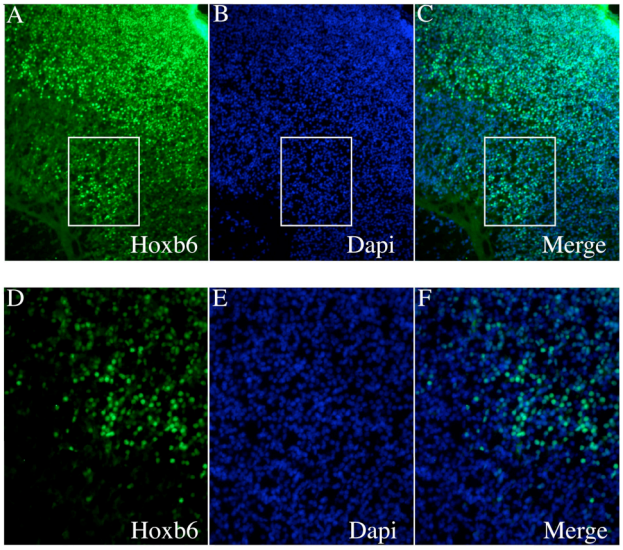

Figure 14: Immunohistochemistry on sagittal cryosections of wild type 12.5 dpc embryos in the neural tube for Hoxb6 protein using immunofluorescence **(A - F)**. (**A – C**) Hoxb6 protein is expressed in the neural tube of wild type 12.5 dpc embryos and the pattern is comparable to the staining pattern observed during HRP staining (compare to Figure 12 A, B). (**D** - **E**) Higher magnification of the section as shown in (**A –C**).

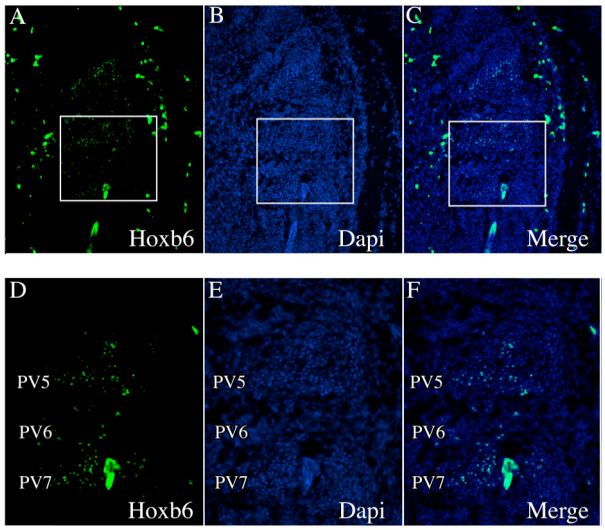

Figure 15: Immunohistochemistry on sagittal cryosections of wild type 12.5 dpc embryos in prevertebral condensations of wild type embryos for Hoxb6 protein using immunofluorescence **(A - F)**. (**A – C**) Hoxb6 protein is not detected in prevertebral condensations of wild type embryos. (**D - E**) Higher magnification of sections as shown in (**A –C**). No Hoxb6 protein can be detected. The slight staining observed

was ubiquitously distributed in all prevertebral condensations and is most lightly due to signal trapped in blood cells or autofluorescence.

6.2 miRNA mediated *Dll1* gene regulation

6.2.1 *In silico* prediction and conservation of *Dll1* miRNA binding sites

To identify miRNAs which possibly regulate the *Dll1* gene, we performed an *in silico* interspecies comparison of the human, mouse and chicken *Dll1* 3´UTRs, using the public miRBase Targets Database (Version 5.1) (Griffiths-Jones et al., 2008), to identify evolutionary conserved miRNA binding sites. With this strategy we expected a higher chance for choosing relevant miRNAs due to a selective pressure on the respective sites that could be indicative for a potential function. For the selection of miRNA binding sites we took it as a requirement that the corresponding miRNA exists in the respective species.

The human *DLL1* 3´UTR is 674 bases long and contains 20 predicted sites for 51 distinct and described miRNAs. The mouse *Dll1* 3´UTR is 678 bases long and contains 18 predicted sites for 24 distinct and described mouse miRNAs, whereas the chicken *Dll1* 3´UTR is 486 base pairs long and contains 16 predicted sites for 13 miRNAs. We analyzed the human, mouse and chicken *Dll1* 3´UTRs for miRNA binding sites, which are conserved among these three species. Using this approach we identified 16 candidate miRNAs (miR-15a, miR-15b, miR-34a, miR-34c, miR-103, miR-107, miR-130a, miR-130b, miR-301a, miR-301b, miR-363, miR-362-5p, miR-369-3p, miR-449a, miR-449c and miR-497), which are either conserved in all three species (Figure 15 A) or between man and mouse only (Figure 16 B). Also, the relative position of miRNA target sites in the *Dll1* 3' UTRs was largely conserved between the three species (Figure 16 A and 16 B).

Sites for most of these miRNAs were not predicted *in silico* for the 3' UTRs of the mouse *Dll3* and *Dll4* genes. One site for miR-449a/b/c was predicted in the 3' UTR of

the mouse *Jag2* gene and one site for miR-34c was predicted in the 3´UTR of the *Jag1* gene (not shown). We take these observations as evidence that the combination of miRNAs sites predicted *in silico* for the mouse and human *Dll1* 3' UTRs are not generic Notch ligand signatures, but are rather specific for the *Dll1* gene.

In turn, we analyzed which other genes possess predicted sites for miRNAs that we identified as conserved in the 3' UTRs of human and mouse *Dll1*. We find that several genes involved in Delta/Notch, such as *Wnt3a* (Dunty et al., 2008), *Pax9* (Mansouri et al., 2000), *Neurogenin1* (Ma et al., 1998), *Fgf18* (Hajihosseini and Heath, 2002) and *Jagged2* (Lan et al., 1997), carry predicted miRNA sites that are also present in the *Dll1* 3´UTR (Appendix, Table 4).

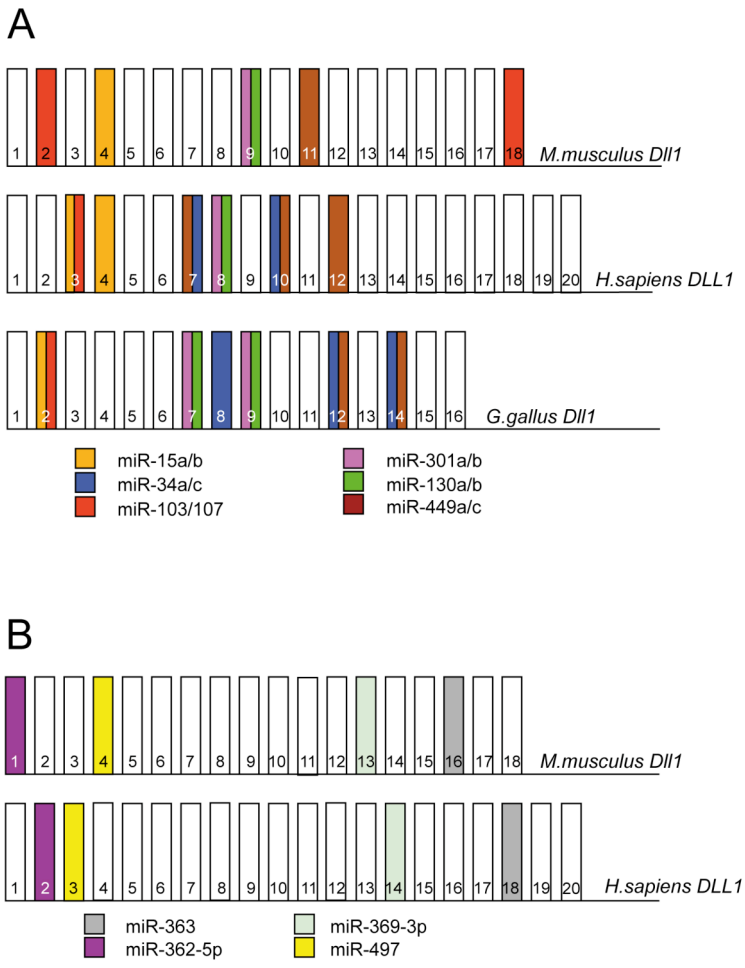

Figure 16: (**A**) Alignment of the mouse (top) and human (middle) and chicken (bottom) *Dll1* 3´UTRs, showing conserved miRNA binding sites indicated by coloured boxes. The relative order of the miRNA binding sites is highly conserved between the three species. (**B**) Alignment of the mouse (top) and human (bottom) *Dll1* 3´UTRs showing conserved miRNA-binding sites, which are conserved between man and mouse, but not in chicken.

6.2.2 Expression patterns of candidate miRNAs in mouse embryos

To identify miRNAs, which are spatially and temporally co-expressed with the *Dll1* mRNA in the same embryonic tissues at 9.5 dpc and 10.5 dpc (Figure 17 C, 18 E, respectively), we performed a systematic whole mount *in situ* hybridisation screen using single (SL) and/or double (DL) DIG labelled and LNA modified DNA probes for the respective miRNAs.

The published sequence of the miR-1 *in situ* probe was used as positive control and shows expression in the heart and myotomes of 9.5 and 10.5 dpc mouse embryos (Figures 17 A, 17 B, 18 A, and 18 B, respectively). A scrambled probe was used as negative control and showed no expression except a weak staining in the neural tube of 9.5 dpc embryos (Figure 16 D, and 16 E, SL and DL probes, dashed arrows, respectively). This weak staining in the neural tube was present in all 9.5 dpc embryos (but not in older embryos) hybridised with any LNA modified probe (Figure 17 A, and 17 B, SL and DL probes, dashed arrows and data not shown) and was thus considered as background staining and not indicative of genuine miRNA expression. In addition, similar background staining in neural tubes has been reported by others, for example, in chicken embryos also using LNA modified DNA probes (Sweetman et al., 2006).

6.2.3 miRNA whole mount *in situ* hybridisations at 9.5 dpc

The SL and/or DL probes for miR-15a, miR-15b, miR-34c, miR-301a, miR-301b, miR-362-5p, miR-369-3p, miR-363, miR-449a, miR-449c and miR-497 showed no detectable expression in whole mount *in situ* hybridisations at 9.5 dpc except the unspecific staining in the neural tube (Appendix, Table 4 and data not shown). In contrast, expression for miR-103, miR-130a and miR-130b was reproducibly detected for both SL and DL probes (Figure 17 H, I, N, O, P, R)). Expression of miR-34a and miR-107 was reproducibly detected only using the DL probes (Figure 17 F, G, J, K). Remarkably, the patterns of staining obtained with these five positive miRNA probes at 9.5 dpc were very similar and hardly distinguishable (Figure 17 G, I, K, O, R). Using the DL probes, some weak staining for miR-34a, miR-103, miR-107, miR-130a and miR-130b was present throughout the developing embryo. Only the looping tubes of the developing heart were always without staining for any of the five miRNA probes at 9.5 dpc (Figure 17 G, I, R, red arrows). At this developmental stage, there was significantly stronger staining in the base of the allantois (Figure 17 M, blue arrow), in the presomitic mesoderm (Figure 17 M, brackets), in all somites along the entire anterior-posterior axis (Figure 17 G, H, K, M, O, R, dotted arrow), in the lateral plate mesoderm (Figure 17 L, arrow), the forebrain (Figure 17 L, dotted arrow), in the first and second branchial arches (Figure 19 A - E), and the otic vesicle (Figure 19 A - E, yellow arrows). In the head, staining obtained with SL probes for miR-103, miR-130a and miR-130b was particularly strong in the trigeminal (V) and facial /auditory (VII/VIII) ganglia (Figure 19 A, B, C, arrows).

Histological cryosections of whole mount *in situ* embryos hybridised with DL probes revealed stronger staining for miR-103/107 and miR-130a/130b in the developing brain, neural tube and cephalic mesenchyme compared to the positive control miR-1

(expressed in heart and myotomes) and the negative control scramble miR (not shown).

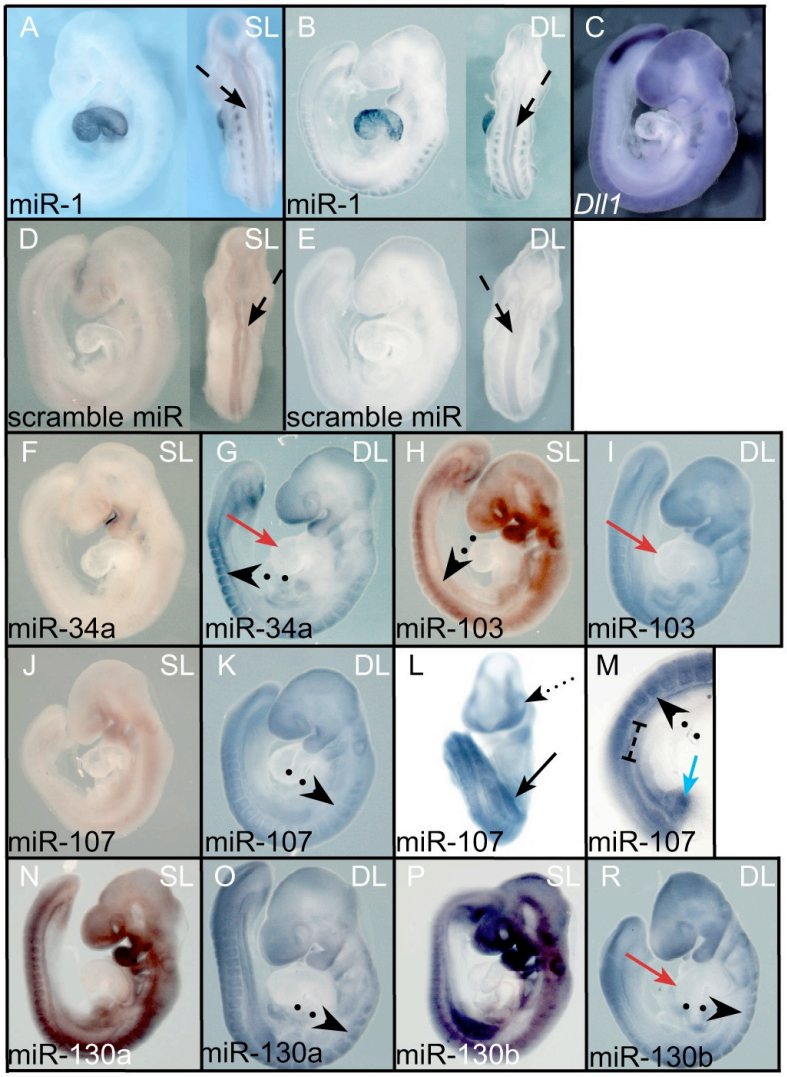

Figure 17: *In situ* hybridisations of candidate miRNAs with detectable expression at 9.5 dpc with single DIG labelled (**SL**) and double DIG labelled (**DL**) LNA modified probes. Positive control (**A, B**) and negative control (**D, E**) for *in situ* hybridisation showing unspecific staining in the neural tube (dashed arrow) and **(C)** *Dll1* mRNA expression at 9.5 dpc. (**F, G**) miR-34a, (**H, I**) miR-103, (**J, K, L, M**) miR-107, (**N, O**) miR-130a, (**P, R**) miR-130b all showed similar patterns of staining. Staining was detected in all somites along the posterior anterior axis (**G, H, K, M, O, R,** dotted arrows), the head region (**L**, dotted arrow), the lateral plate mesoderm (**L,** arrow), the base of the allantois (**M,** blue arrow), and the PSM (**M,** brackets). All positive DL probes developed some weak staining throughout the developing embryo (**G, I, K, O,**

R). Only the tubes of the developing heart were always without staining (**G, I, R,** red arrows).

6.2.4 miRNA whole mount *in situ* hybridisations at 10.5 dpc

The SL and/or DL probes for miR-15a, miR-15b, miR-34c, miR-301a, miR-301b, miR-362-5p, miR-369-3p, miR-363 and miR-497 again either showed no staining or no reproducible pattern in mouse embryos at 10.5 dpc (Appendix, Table 4 and data not shown). Generally stainings of whole mount *in situ* hybridisations using DL probes developed much faster but showed increased background staining as compared to SL probes. Using SL and DL probes, specific and reproducible expression patterns of miR-103, miR-130a, miR-130b, miR-449a, and miR-449c were detected in 10.5 dpc mouse embryos (Figure 18 F, G, H, I, J, K, L, Figure 19 F - I and 19 J, K). The SL probes for miR-34a, miR-107 and miR-301a only developed weak and non-reproducible signals (not shown). The specific staining obtained with the SL probe for miR-107 was clearly enhanced at 10.5 dpc, using the respective DL probe (Figure 18 H). However, the signals observed for miR-34a and miR-301a still remained below detection levels or were not reproducible in 10.5 dpc embryos even when DL probes were used.

Comparable to the expression at 9.5 dpc, the observed patterns for the probes of miR-103, miR-107, miR-130a, and miR-130b at 10.5 dpc were again very similar. They each were detected in the developing fore- and hind limbs (Figure 18 F, H, I, J, L, yellow arrows) and in the neural tube (Figure 18 F, I, L, dashed arrows). In the older, more anterior somites (approximately somites 7 to 20 as counted from the presomitic mesoderm (PSM)) of 10.5 dpc embryos expression was strongest in the posterior compartment of each somite (Figure 18 F, H, I, J, L, dotted arrows). In the caudal, recently formed somites (somites 1 to 7) of 10.5 dpc embryos, expression of

these miRNAs was detected at the inner epithelial walls without restriction to the posterior compartments (Figure 18 F, I, L, arrows). In the head the four miRNA probes showed staining in the cranial nerves, in the trigeminal (V) and facial /auditory (VII/VIII) ganglia, in the 1st and 2nd branchial arch (Figure 19 F - I, arrows, respectively) and the otic vesicle (Figure 19 F - I, yellow arrows, respectively). The expression domains of these four miRNAs were thus reminiscent of the earlier expression at 9.5 dpc. In the developing brains of 10.5 dpc embryos we observed staining in the forebrain and the midbrain using the probes for miR-103, miR-107, miR-130a and miR-130b, which we did not observe, for example, in embryos hybridised with the negative control scrambled probe and in the *in situ* hybridisations with the miR-449 probes.

Whole mount *in situ* hybridisations at 10.5 dpc with probes for miR-449a and miR-449c showed expression patterns that were distinct from the patterns obtained with other positive probes. They both were expressed in a sharp V shaped domain in the dorsal aspect of the rhombic lip at 10.5 dpc (Figure 19). The caudal limit of the expression domain is at the hindbrain - spinal cord junction (Figure 19 J, arrow) and the domain extends approximately towards the posterior boundary of rhombomere 1. Expression appeared to be in single cells, in a salt and pepper pattern that is reminiscent of the expression of the Delta and Notch ligands and receptors in neural tissues (Figure 19 K, arrow). 10.5 dpc embryos hybridised with the probes for miR-449a and miR-449c did not show any staining outside the rhombencephalon. Expression domains of the 449 miRNAs were consistent with recently published data (Redshaw et al., 2009).

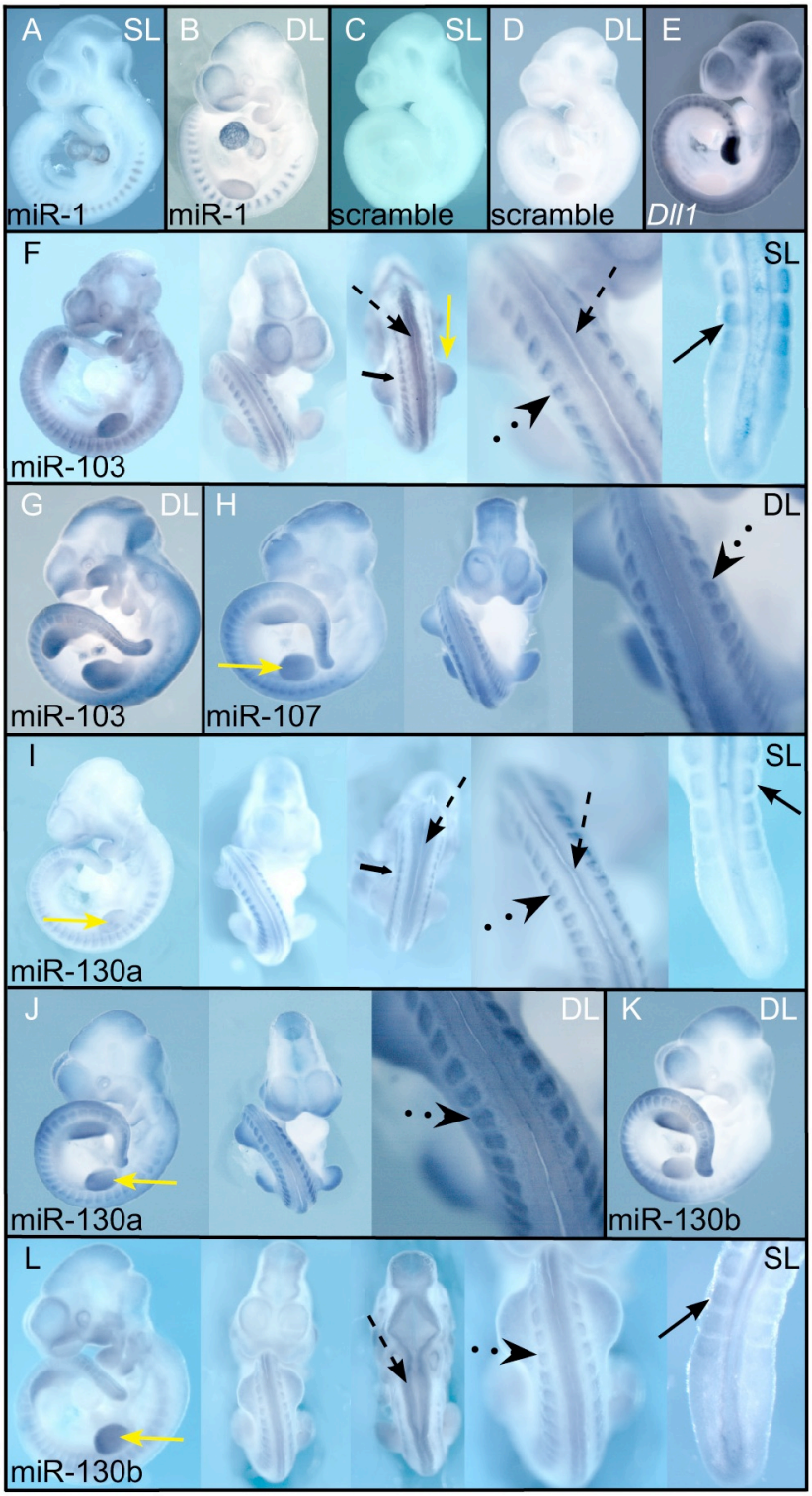

Figure 18: *In situ* hybridisation for candidate miRNAs with detectable expression using single DIG labelled (**SL**) and double DIG labelled **(DL)** LNA modified probes at 10.5 dpc. Positive control (**A, B**) and negative control (**C, D**) for *in situ* hybridisations and (**E**) *Dll1* mRNA expression at 10.5 dpc. (**F, G, H**) miR-103/107 can be detected in the limbs (yellow arrows) and in the neural tube (dashed arrow). In older somites miR-103/107 expression is strongest in the posterior part of a somite (dotted arrow).

In the five most posterior somites miR-103/107 is present in the whole somite close to the epithelial wall (arrow). They are also detected in the dermomyotome (small arrow). (**H, I, J, K, L**) Expression of miR-130a/130b appeared quite similar to expression of miR-103/107 and can be detected in the limbs (yellow arrows) and in the neural tube (dashed arrow). In older somites miR-130a/130b are strongest in posterior somite compartments (dotted arrow). In the most posterior somites miR-130a/130b are present in the whole somite (arrow). They can also be detected in the dermomyotome (small arrow).

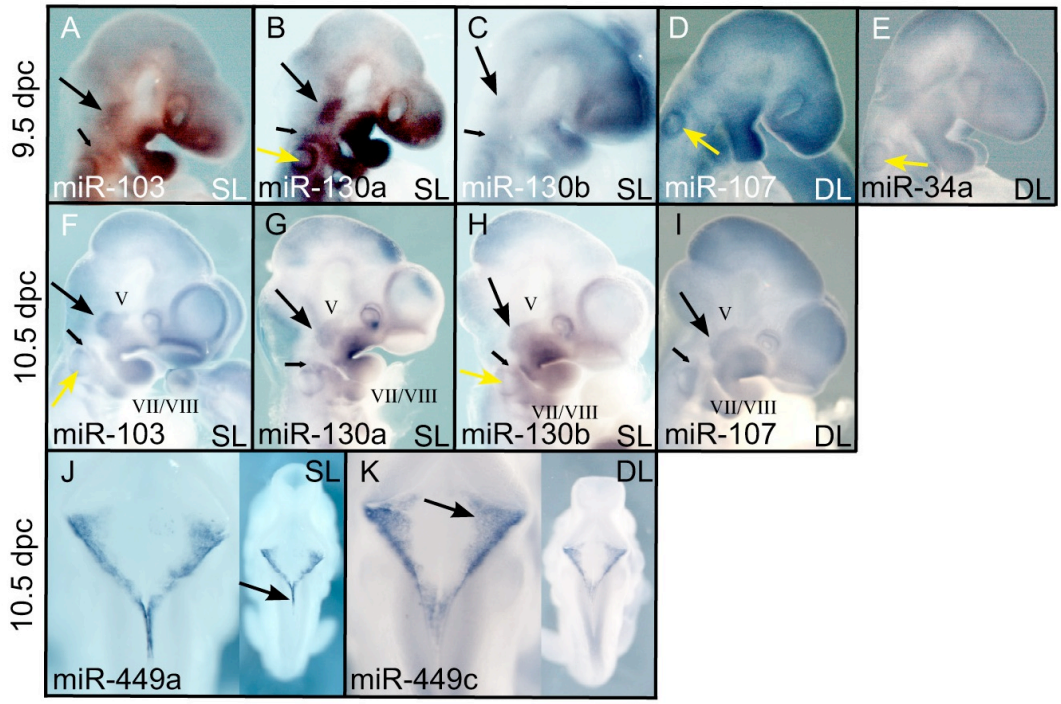

Figure 19: miRNAs with expression during neurogenesis. (**A - I**) miR-103, miR-130a and miR-130b are expressed in the V (large arrows) and VII/VIII (small arrows) cranial ganglia at 9.5 and 10.5 dpc, which correspond to the trigeminal placode and facial/auditory cranial ganglia, respectively. miR-34a**,** miR-103, miR-107, miR-130a and miR-130b are expressed in the 1st and 2nd branchial arches and the otic vesicle (yellow arrows). (**J, K**) miR-449a/c are expressed in a V shaped domain in the dorsal most aspect of the rhombencephalon. Expression starts at the hindbrain spinal cord junction (**J**, large arrow) and is detected in the rhombic lip and appeared to be in a salt and pepper pattern (**K**, small arrow).

6.2.5 miRNA 103, 130a and 130b expression in epithelial somites

To describe the expression patterns of miR-103, miR-130a and miR-130b in the recently formed somites at 10.5 dpc in more detail, we inspected histological sections of *in situ* hybridised embryos. We dissected posterior regions containing approximately the 5 youngest somites and the PSM for histological analysis. MiR-103 was strongly expressed throughout the anterior and posterior compartments of recently formed somites within the somitic epithelia with strongest expression towards the lumen of the somite (Figure 20 B, arrow). In transverse sections of posterior neural tubes at 10.5 dpc strongest staining with the miR-103 probe was found in the neuroepithelium towards the lumen of the tube (Figure 20 A, arrow). The patterns of staining obtained with the probes for miR-130a and miR-130b in posterior somites and neural tubes at 10.5 dpc was comparable to the pattern observed in sections of embryos hybridised with the miR-103 probe (Figure 20 D, E and 20 F, G, respectively).

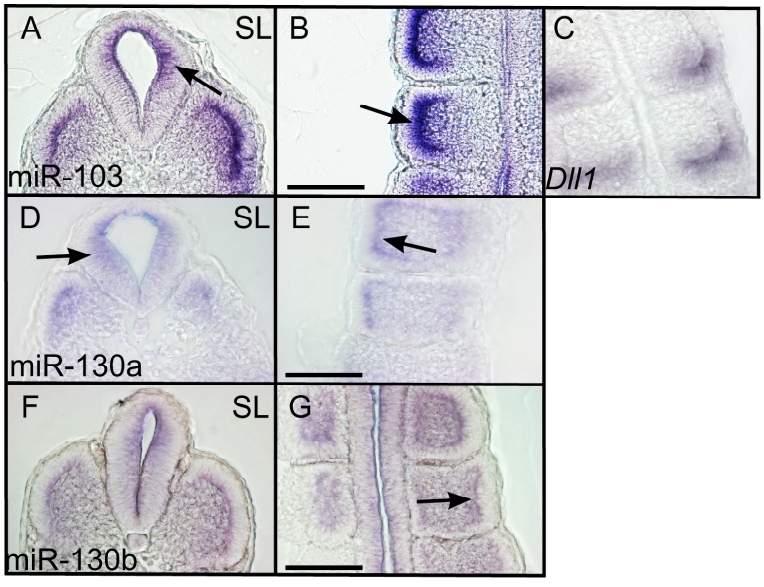

Figure 20: Cryosections of dissected posterior trunk regions containing the posterior 4-5 most recently formed somites at 10.5 dpc. Bars are 100 μm. (**A**) Transversal section showing miR-103 expression in the neural tube (arrow) and in the epithelia of somites towards the somitocoel. (**B**) Anterior is to the top. Coronal section showing

miR-103 expression in the second (arrow) and third most posterior somite. (**C**) *Dll1* expression in epithelial somites at 10.5 dpc, with anterior to the top of the panel. (**D**) Transversal section showing miR-130a expression in the neural tube (arrow), in the ventricular surface and again in the epithelia of somites. (**E**) Anterior is to the top. Coronal section showing miR-130a expression in the first two newly formed somites (arrow). (**F**) Transversal section showing miR-130b expression in the neural tube and close to the epithelial border of a somite. (**G**) Anterior is to the top. Coronal section showing miR-130b expression in the second (arrow) and third most posterior somite.

6.2.6 Radioactive *in situ* hybridisations on histological sections at 12.5 dpc

Since expression of the *Dll1* gene continues throughout development and organogenesis (Beckers et al., 1999) we also performed *in situ* hybridisations on histological sections of 12.5 dpc embryos, for the 7 miRNAs, we identified as positive in our whole mount *in situ* study at 9.5 dpc and 10.5 dpc (miR-34a, miR-103, miR-107- miR-130a, miR-130b, miR-449a and miR-449c). For *in situ* hybridisation on histological sections we used radioactively labelled LNA modified probes. The published sequence of miR-124, which is expressed in the nervous system at 12.5 dpc (Figure 21 A), was used as positive control (Deo et al., 2006). A scrambled miR was used as a negative control (Figure 21 B) and showed no detectable expression.

miR-449a and miR-449c were specifically expressed in the choroid plexus of the fourth and the lateral ventricle at 12.5 dpc (Figure 21 E, F, G, H). Additional sites of expression could not be detected for these miRNAs at this developmental stage (not shown). This suggests highly restricted expression domains of the miR-449 family during the analysed developmental stages.

In situ hybridisation on sections using the miR-103 and miR-107 probes showed more background staining (signal trapped in blood cells) than miR-124 and miR-449a/c, but a strong signal was seen in the central nervous system in the forebrain,

midbrain and hindbrain (Figure 21 C, D, respectively and not shown). Interestingly expression was mostly confined to the mantle zone of the neural tube. Expression was also confirmed for the ganglia of the facial nerves and the otic vesicle (data not shown). Expression in other developing organs (such as heart, lung, liver, kidney) could not be detected in section *in situ* hybridisations (Fig. 21 C, D and data not shown). MiR-34a, miR-130a and miR-130b were not detectable using radioactive *in situ* hybridisation at this stage (not shown).

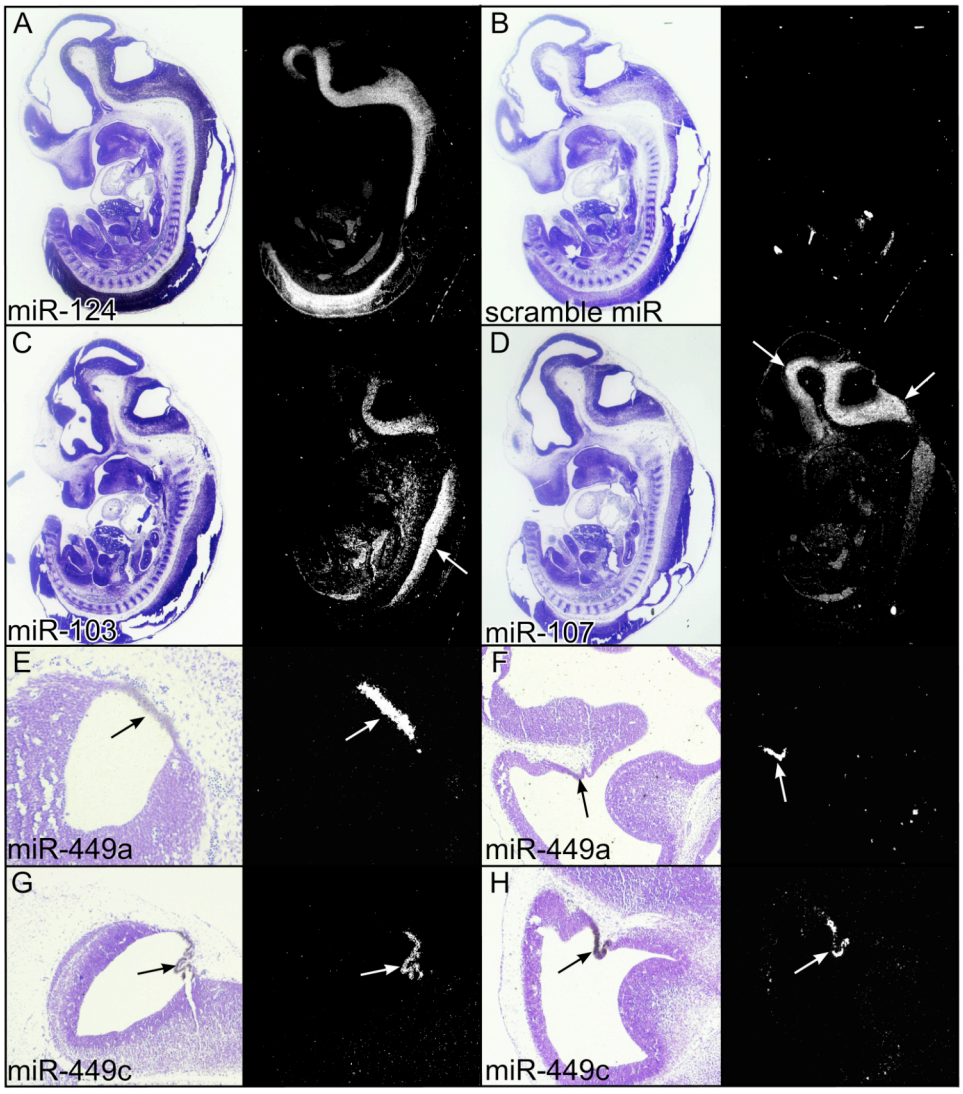

Figure 21: Radioactive *in situ* hybridisation on sections of 12.5 dpc embryos for positive miRNAs identified in the whole mount *in situ* hybridisation study. Positive (**A**) and negative (**B**) control for *in situ* hybridisations. (**C, D**) miR-103 and miR-107 expression is enriched in the central nervous system, in the forebrain (not shown),

the midbrain and the hindbrain as well as in the spinal cord (arrows)**.** Expression in other developing organs could not be detected (not shown). (**E, F, G, H**) miR-449a and miR-449c are specifically expressed in the roofplate of the fourth ventricle (**E, G,** arrows) and the choroid plexus of the lateral ventricle (**F, H,** arrows).

7. Discussion

7.1 *cis*- mediated *Dll1* gene regulation

7.1.1 MSD function

To summarize, we generated two different alleles by replacing (*Dll1*^{tm1leg}) and by deleting (*Dll1*$^{tm1.1leg}$) the endogenous *Dll1 cis*-regulatory element (MSD), to evaluate its function at its endogenous genomic position. Heterozygous and homozygous newborn mice of both alleles are viable and fertile. Heterozygous and homozygous *Dll1*^{tm1leg} and *Dll1*$^{tm1.1leg}$ newborn mice show one common skeletal malformation, an additional ectopic rib on the 7th cervical segment. In addition, homozygous *Dll1*^{tm1leg} and *Dll1*$^{tm1.1leg}$ 8.5 dpc embryos do show a down-regulation of *Dll1* expression levels in the PSM, as detected during whole mount *in situ* hybridisations. These particular effects are thus likely to reflect the endogenous function of MSD, since they appear in mutant mice of both alleles. The additional ectopic rib on the 7th cervical vertebra is reminiscent of a posterior homeotic transformation, since it co-insides with anterior shifts of the *Hoxb6* expression domain.

Besides, heterozygous and homozygous *Dll1*^{tm1leg} and *Dll1*$^{tm1.1leg}$ mice do show additional phenotypic differences. In heterozygous and homozygous *Dll1*^{tm1leg} mice we observe a down-regulation of *Dll1* and *Hes5* expression in the PSM at 9.5 dpc and skeletal malformations in most parts of the axial skeleton, like fused neural arches in cervical and thoracic regions, fused and split vertebral bodies in lumbar regions and additionally kinked tails. The down-regulation of *Hes5* at 9.5 dpc was not detectable and most malformations of skeletal morphology were diminished after the excision of the hygromycin resistance cassette in *Dll1*$^{tm1.1leg}$ mice (except the additional ectopic ribs on the 7th cervical segment).

This supports the possibility that the insertion of the hygromycin resistance cassette

is the cause for the majority of skeletal malformations in the axial skeleton of *Dll1*^{tm1leg} mice, especially for skeletal malformations in the lumbar region. Fused and split vertebral bodies in lumbar regions have been previously associated with reduced Delta-Notch signalling in the PSM (Cordes et al., 2004; Geffers et al., 2007). Further, it has been demonstrated earlier that the insertion of a selection cassette can lead to a down-regulation of adjacent genes (Olson et al., 1996). It is thus likely that the down-regulation of *Dll1* and *Hes5* expression in the PSM, as detected during whole mount *in situ* hybridizations in heterozygous and homozygous *Dll1*^{tm1leg} embryos is directly caused by the insertion of the hygromycin resistance cassette. This down-regulation in turn could lead to most skeletal malformations in heterozygous and homozygous *Dll1*^{tm1leg} newborn mice. Furthermore, most skeletal malformations are more frequently detected in homozygous *Dll1*^{tm1leg} newborn mice and appear more severe than in heterozygous *Dll1*^{tm1leg} newborn mice, which thus might directly reflect differences in *Dll1* expression levels. The *Dll1*^{tm1leg} allele could thus be a hypomorphic *Dll1* allele.

7.1.2 Transgenic and endogenous MSD

Previous results indicated an requirement for MSD in controlling *Dll1* expression during somitogenesis, as it was able to direct reporter gene expression in the presomitic and somitic mesoderm of transgenic mice (Beckers et al., 2000). Our results show that MSD has a function for controlling *Dll1* expression during somitogenesis especially in the PSM, but the contribution of MSD for *Dll1* expression is specific and restricted. These functional results are unexpected, since MSD does contain multiple Lef1 and Tbx6 binding sites, *Dll1* is severely down-regulated when these genes are mutated and most of their regulatory function is considered to be mediated via MSD (Galceran et al., 2004; Hofmann et al., 2004). Our results do,

however, demonstrate that besides transgenic reporter gene experiments, endogenous deletion of potential enhancer elements is absolutely necessary for a full functional characterization of the respective element.

Another possibility, which might explain the minor changes of *Dll1* expression in MSD deficient mice, is the redundancy of MSD function. In other words, there could be additional elements with a similar function as MSD, which are able to overtake MSD function in its absence. This theory is also supported by our *in silico* analysis using Genomatix MatInspector software (Outlook 8.1). In addition, the MSD sequence is not evolutionary conserved between zebrafish, mouse and human, further arguing against an exclusive role for MSD in controlling *Dll1* expression in the paraxial mesoderm (Beckers et al., 2000; Hans and Campos-Ortega, 2002).

7.1.3 Heterozygous *Tbx6*^{tm1Pa} loss-of-function mutants phenocopy most aspects of *Dll1*^{tm1leg} and *Dll1*$^{tm1.1leg}$ mice

Tbx6 is considered as an important factor, which binds to MSD and mediates *Dll1* expression *in vivo*. In agreement with this, most phenotypic aspects of heterozygous and homozygous *Dll1*^{tm1leg} and *Dll1*$^{tm1.1leg}$ MSD deficient mice are phenocopied by heterozygous *Tbx6*^{tm1Pa} loss-of-function mutants, indicating that Tbx6 indeed mediates most of MSD function *in vivo*. It has so far, been demonstrated that Tbx6 can bind to MSD *in vitro*, but direct evidence that Tbx6 binds to MSD *in vivo* is still lacking (White and Chapman, 2005). Interestingly, the skeletal malformations detected for heterozygous *Tbx6*^{tm1Pa} mutant mice are more reminiscent of skeletal malformations observed for homozygous *Dll1*^{tm1leg} mice, indicating a similar down-regulation of *Dll1* expression levels in heterozygous *Tbx6*^{tm1Pa} mutant mice compared to homozygous *Dll1*^{tm1leg} mutant mice.

The additional ectopic rib on the 7th cervical vertebra, however, appeared with a

similar penetrance and appearance in heterozygous *Tbx6*^{tm1Pa} newborn mice, compared to heterozygous and homozygous *Dll1*^{tm1leg} and *Dll1*$^{tm1.1leg}$ newborn mice. Genetically combining *Tbx6*^{tm1Pa} and *Dll1*$^{tm1.1leg}$ alleles does not lead to an enhancement or alteration of this particular phenotype. It is thus likely that a direct signalling cascade mediated by *Tbx6*, MSD and *Dll1* exists, which is essential for the correct identity of the 7th cervical segment.

Besides that, our data indicates that the functional interaction of *Tbx6*, MSD and *Dll1* must take place in the PSM, since *Tbx6* is exclusively expressed in this tissue during development (Chapman and Papaioannou, 1998). This also further indicates that MSD has its functional role in controlling *Dll1* expression in the PSM. Another gene expressed mainly in the PSM, which has been associated with the development of additional ribs on the 7th cervical segment and is thought to control Tbx6 protein distribution in the PSM, is *ripply 1* (Takahashi et al., 2010). It is thus likely that *ripply 1* can be added to this signalling cascade, probably by modulating Tbx6 protein levels.

7.1.4 MSD as a *cis*- regulatory element for *Dll1*

Whole mount *in situ* hybridisations and qRT-PCR data suggest that replacement and deletion of MSD does not dramatically change *Dll1* expression in heterozygous and homozygous *Dll1*^{tm1leg} and *Dll1*$^{tm1.1leg}$ MSD deficient mice. Generally, MSD appears to have its major role in controlling *Dll1* expression in the PSM of 8.5 embryos. This is underpinned by the fact that we observe a common down-regulation of *Dll1* in the PSM at 8.5 dpc of homozygous *Dll1*$^{tm1.1leg}$ and *Dll1*^{tm1leg} MSD deficient embryos. A more precise analysis of the contribution of MSD to *Dll1* expression in homozygous *Dll1*$^{tm1.1leg}$ 8.5 dpc embryos was, however, complicated by the fact that the *Dll1* and *Hes5* mRNAs are dynamically expressed at that stage. Unfortunately, there is so far

no direct Delta-Notch target gene known, which is constantly expressed in the PSM. Moreover, *Dll1* and *Hes5* expression are not altered in their dynamic expression pattern nor altered at all dynamic stages in homozygous *Dll1*$^{tm1.1leg}$ mutant embryos. Nevertheless, we observe significant differences in *Dll1* and *Hes5* gene expression, using whole mount *in situ* hybridisation in *Dll1*$^{tm1.1leg}$ embryos compared to wild type, during some dynamic *Dll1* and *Hes5* stages. Furthermore, *Dll1* mRNA expression level was slightly down-regulated in PSMs of homozygous *Dll1*$^{tm1.1leg}$ mutants in qRT-PCR experiments compared to wild type controls. We could also not detect an enhanced down-regulation of *Dll1* expression levels in the PSM of heterozygous *Tbx6*^{tm1Pa} embryos, compared to homozygous *Dll1*$^{tm1.1leg}$ 8.5 dpc embryos, indicating that Tbx6 mediates the function of MSD at this respective time point.

In contrast, in the PSM of 9.5 dpc embryos, we observe an enhanced down-regulation of *Dll1* expression levels in heterozygous *Tbx6*^{tm1Pa} mutants compared to homozygous *Dll1*$^{tm1.1leg}$ mutants. Split vertebral bodies are detected in heterozygous *Tbx6*^{tm1Pa} newborn mice at a high in heterozygous and homozygous *Dll1*$^{tm1.1leg}$ newborn mice at a really low frequency. Furthermore, we observe the highest number of split vertebral bodies in the lumbar region of *Tbx6*$^{tm1Pa/+}$ *Dll1*$^{tm1.1leg/tm1.1leg}$ newborn mice, which show the lowest *Dll1* expression levels in the PSM. The incidences of split vertebral bodies thus directly correspond to the obtained differences in *Dll1* expression levels, as detected during qRT-PCR experiments in the PSM of 9.5 dpc embryos (high incidences of split vertebral bodies thus appear to be directly corresponding to low *Dll1* expression in the PSM).

It is thus possible that the expression levels of *Dll1* in PSM at 8.5 dpc could in turn reflect incidences for malformations of the 7th cervical vertebra. We cannot formally prove this hypothesis, as strong differences of penetrances for malformations of the

7th cervical segment are not observed between heterozygous *Tbx6*^{tm1Pa} and heterozygous and homozygous *Dll1*^{tm11leg} and *Dll1*$^{tm.1.1leg}$ mutants. Nevertheless, our data thus also suggests that there might be additional enhancer elements, which mediate Tbx6 function at 9.5 dpc.

7.1.5 *Tbx6*, MSD and *Dll1* act during the development of lumbar vertebrae probably via a feedback loop

There was, however, an synergistic effect by genetically combing *Tbx6*^{tm1Pa} and *Dll1*$^{tm.1.1leg}$ alleles, since the number of split vertebral bodies in lumbar segments of *Tbx6*$^{tm1Pa/+}$ *Dll1*$^{tm.1.1leg/tm.1.1leg}$ newborn was significantly increased, compared to combined numbers of split vertebral bodies detected for heterozygous *Tbx6*^{tm1Pa} and homozygous *Dll1*$^{tm.1.1leg}$ newborn mice.

This effect is most likely due to a feedback loop of *Dll1* and *Tbx6,* which was postulated earlier also by others (Shifley and Cole, 2007; White et al., 2005), since we observe a significant down-regulation of *Tbx6* and *Dll1* expression levels in PSMs of 9.5 dpc *Tbx6*$^{tm1Pa/+}$ *Dll1*$^{tm.1.1leg/tm.1.1leg}$ embryos compared to heterozygous *Tbx6*^{tm1Pa} embryos. Furthermore, additional qRT-PCR experiments in heterozygous and homozygous 9.5 dpc *Dll1*^{tm1Gos} mice suggest that *Tbx6* expression is dependent on *Dll1* expression. We further observe a significant reduction of *Tbx6* expression levels in PSMs of homozygous *Dll1*$^{tm.1.1leg}$ embryos compared to wild type. The effect appears to be restricted to lumbar segments, as we could not detect other additive effects for skeletal malformations in other parts of the axial skeleton by combining MSD deletion and *Tbx6* loss-of function alleles.

7.1.6 Wnt, Delta-Notch and the establishment of vertebrate identities

Our data indicates that a connection between the Wnt, the Delta-Notch and the

establishment of vertebrate identities exists. In this postulated cascade, MSD exists as potential link between the Wnt and the Delta-Notch pathway. However, we did not completely characterize the link between the Delta-Notch signalling pathway and the establishment of vertebral identities. A link by directly mediating *Hox* expression is unlikely, since we could not observe major changes of *Hoxb6* expression levels in PSMs of homozygous *Dll1*^{tm1Gos} and *Tbx6*^{tm1Pa} 9.5 dpc embryos in qRT-PCR experiments compared to wild type controls. Nevertheless, our data indicates that the Wnt and the Delta-Notch signalling are likely to be interconnected within the PSM in regards to the regionalization process. *Hox* genes, in turn, are not only expressed in the PSM but also in somites and their derivatives (Gridley 2003). It has, however, been shown before that a linkage between the segmentation clock and Hox genes takes place mainly in the PSM and not in the somites (Dubrulle et al., 2001; Zákány et al., 2001).

Theoretically, common enhanced cell death or diminished proliferation of PSM cells of heterozygous *Tbx6*^{tm1Pa} as well as of heterozygous and homozygous *Dll1*^{tm1leg} and *Dll1*$^{tm1.1leg}$ embryos could lead to a fastened migration of *Hox* expressing cells through the presomitic mesoderm and result in an anteriorly shifted Hox expression domain in the somites. We could, however, not detect anteriorly shifted *Hox* expression domains in the somites throughout embryonic development in homozygous *Dll1*$^{tm1.1leg}$ embryos compared to wild type controls. This could be due to technical problems as slight changes of the anterior *Hox* gene expression boundary might not be detectable by whole mount *in situ* hybridizations. In addition, it is known that *Hox* gene expression levels increase until 12.5 dpc, which might thus potentially facilitate detection of subtle spatial changes of *Hox* gene expression by *in situ* hybridization on sections at 12.5 dpc (Wellik, 2007). However, whole mount TUNEL

and histone H3 staining in homozygous *Tbx6*^{tm1Pa} mutant embryos did not reveal apparent changes neither in cell death nor of the mitotic index in the PSM and tailbud of homozygous *Tbx6*^{tm1Pa} mutant embryos compared to wild type (Chapman et al., 2003).

Alternatively, a decelerated clock period in heterozygous *Tbx6*^{tm1Pa} as well as in heterozygous and homozygous *Dll1*^{tm1leg} and *Dll1*$^{tm1.1leg}$ embryos could lead to delayed somitogenesis, which consequently could lead to an anterior shifted *Hox* expression domain in heterozygous *Tbx6*^{tm1Pa} as well as in heterozygous and homozygous *Dll1*^{tm1leg} and *Dll1*$^{tm1.1leg}$ embryos. Conflictive data for this hypothesis comes from a hypomorphic hes6 zebrafish mutant, which shows delayed somitogenesis, where anterior *Hox* gene boundaries and anatomical markers aligned with lowered segment numbers (Schröter and Oates, 2010). Interspecies differences are, however, possible.

7.2 miRNA mediated *Dll1* regulation

7.2.1 miR-103/107, miR-130a/b and miR-449a/c are candidates for regulating *Dll1* during mouse development

It is noteworthy, that we did not observe significant differences between miR-103/miR-107 and miR-130a/miR-130b expression patterns, respectively. This may be due to the fact that the sequences of processed miR-103/miR-107 on the one hand and miR-130a/miR-130b on the other hand differ only in one, respectively, two nucleotide(s). Thus it cannot be excluded that cross-hybridisation may at least to some extend contribute to the observed similarities in expression patterns. However, cross-hybridisation is unlikely to account for the similarity of patterns observed between miR-103/107 and miR-130a/b since the sequences of the two miRNA pairs do not share significant sequence similarities.

miR-103, miR-107, miR-130a, and miR-130b show expression domains, which overlap with sites of *Dll1* expression in 9.5 dpc, 10.5 dpc and 12.5 dpc embryos and suggests a role for the respective miRNAs in regulating the *Dll1* mRNA during somitogenesis and neurogenesis in the mouse. Recent data supports the expression of miR-130a during somitogenesis, as it was detected in chicken somites based on a high throughput sequencing screen (Rathjen et al., 2009). In contrast miR-15b, which was also identified in the latter study, was not expressed during mouse embryogenesis in our analysis. This could either be due to interspecies differences in miRNA expression, or miR-15b expression levels could be below the sensitivity of the *in situ* hybridisation approach in mouse embryos. Further, in a more recent study a *T (Brachury)* Cre line was used to conditionally delete *Dicer1* in most cells of the mesodermal lineage. These mice do not show obvious defects in the expression of segmentation machinery genes, but did show defects in the compartmentalisation of

somites. This co-occurred with spatially elevated expression of the *Dll1* mRNA in recently formed somites (Zhang et al., 2011). This is accordance with a potential repressive function for miR-103/107 and miR-130a/b for *Dll1* during somite compartmentalisation. In addition, we identify miR-34a as a potential candidate for regulating *Dll1* at 9.5 dpc. We did not detect miR-34a expression at 10.5 dpc and 12.5 dpc in contrast to the other expressed miRNAs in our expression analyses. This could again be due to expression levels below the limits of detection in the *in situ* hybridisation approach. Interestingly, miR-34a is known to have a role in cell cycle regulation and apoptosis and was previously shown to target *Dll1, Jag1* and *Wnt1* (Hashimi et al., 2009; Hermeking, 2010).

We also identified miR-449a and miR-449c as potential candidates for *Dll1* regulation during choroid plexus development. These two miRNAs are also temporally and spatially co-expressed with other genes of the Delta-Notch pathway (Kusumi et al., 2001), including *Jagged2* and *Notch1,* which are potential additional targets of the miR-449 family (Appendix, Table 4), suggesting that miR-449a/c might potentially have a role in controlling hindbrain expression of one or more of these genes.

7.2.2 miRNAs, *Dll1* and the development of cranial ganglia

During the development of the cranial ganglia, *Dll1* expression is first detected at 8.5 dpc in the trigeminal placode, but is subsequently repressed during later embryonic stages (Ma et al., 1998). A transgene reporter gene construct, under the *Dll1* promoter, which lacks the *Dll1* 3´UTR, directed lacZ expression in the cranial nerves (Beckers et al., 2000). Besides, it is known that mice, which carry a loss of function allele for *Dll1*, have abnormal cranial ganglia (De Bellard et al., 2002), proofing a functional role for *Dll1* in their development. *Ngn1 (Neurog1)* is expressed shortly before *Dll1* in the cranial ganglia, but the expression persists throughout development

(Ma et al., 1998). *Ngn1* in turn is a potential target of miR-130a/b but not of miR-103/107 (Appendix, Table 4) and is expressed in the same embryonic tissue as these miRNAs at 9.5 dpc and 10.5 dpc in the cranial ganglia, respectively. miR-130a/b and miR-103/107 thus have a potential a role in regulating the expression of *Ngn1* and *Dll1* during the development of the cranial ganglia.

7.2.3 miR-103/107 and epithelial to mesenchymal transition

In recent work up-regulation of miR-103/107 in primary breast cancer tumours was associated with a lowered survival rate in these patients (probably through an elevated potential for metastatic disease in these tumours). Interestingly, this finding was paralleled by the observation that miR-107 over-expression increased cell motility and epithelial to mesenchymal transition in human breast cancer cell lines (Martello et al., 2010). In addition, Delta-Notch mediated signalling was previously shown to be required for a Wnt induced tumorgenic transformation in mouse mammary glands (Ayyanan et al., 2006). It would thus be interesting to investigate whether *Dll1* expression levels are anti-correlated with elevated miR-103/107 in metastatic breast cancers and thus might contribute to the epithelial to mesenchymal transition state of these tumours. It would be further interesting to rule out whether miR-103/107 play a role for the epithelial to mesenchymal transition state during somitogenesis, as for example for the epithelialisation of somites or their de-epithelialisation into the sclerotome.

8. Outlook

8.1 *cis*- mediated *Dll1* regulation

In this work, we determined the endogenous function of MSD as a *cis*-regulatory element for *Dll1*. Remarkably, the endogenous function of MSD appears to be specific and restricted and our data also suggest that there might be additional *cis*-regulatory elements, which could drive *Dll1* expression *in vivo*. It is known that some *cis*-regulatory elements are located tens of kilobases upstream of the transcriptional start site (Wray, 2007). This prompted us to analyze the 5´upstream *Dll1* region *in silico*, using the Genomatix MatInspector software, which detects consensus binding motifs for certain transcription factor families. For our analysis, we specifically concentrated on T/Tbx and Lef1/Tcf consensus binding motifs, as these two transcription factor families are essential for *Dll1* expression in the paraxial mesoderm, as previously mentioned (Galceran et al., 2004; Hofmann et al., 2004). We systematically determined all potential consensus binding sites of these transcription factors up to 20 kb upstream of the MSD enhancer and approx. 22 kb upstream of the *Dll1* transcription start (Figure 21). Using this approach, we could identify two potential additional *Dll1 cis*-regulatory elements, which clearly show an enrichment of T/Tbx and Lef1/Tcf consensus binding motifs in comparison to the rest of the 5´upstream *Dll1* DNA sequence. Interestingly these potential enhancer elements have approximately the same length as the MSD enhancer (1.6 kb) (Figure 21, double-headed arrows) and do show a similar linear distribution for T/Tbx and Lef1/Tcf consensus binding motifs as MSD (Figure 21, indicated by brackets). In addition, the newly identified PE 1, is located at the same distance to the *Dll1* transcription start site as a Delta D enhancer in zebrafish (Hans and Campos-Ortega, 2002). Taken together, this data indicates that the two newly identified enhancer

elements might have a similar function as MSD, and these elements might be able to take over MSD function in its absence. This *in silico* prediction however is only the first step in identifying additional *cis*-regulatory elements for *Dll1*. In a second step, both identified potential enhancers have to be tested in a transgene reporter gene approach. In parallel, *in vitro* binding assays for Tbx6, Lef1 and PE1/2 (EMSA) and *in vivo* tests have to be performed (Chip followed by qPCR), respectively. If one or both of these transcription factors are able to bind the potential elements *in vitro* and *in vivo* and if these potential elements can drive reporter gene expression in transgenic mice, the generation of single and combined endogenous deletions of all of these elements also in combination with MSD could follow.

Figure 21: *In silico* prediction of additional potential Lef1/Tcf (**L**) and Tbx6 (**T**) consensus transcription factor binding sites in the 5´upstream *Dll1* region using Genomatix Matinspector software. Two additional potential *Dll1* enhancers (**PE1** / **PE2** (marked red)) were identified as they clearly show an accumulation of **L** and **T** sites, in comparison to the rest of the *Dll1* 5´upstream DNA sequence. Additionally, both potential enhancer elements have a similar distribution of **L** and **T** sites, which is reminiscent to the distribution of these sites in MSD (indicated by brackets). The potential enhancer regions do have approx. the same length (1.6 kb, double-headed arrows) as MSD, indicating a similar function.

8.2 miRNA mediated *Dll1* regulation

8.2.1 A transgenic approach for miRNA mediated *Dll1* gene regulation

Using a combined *in silico* and *in situ* hybridisation approach we have identified seven miRNAs, which might regulate *Dll1* expression during development, as they are spatially and temporally co-expressed with the *Dll1* mRNA. Since we suggest, that *Dll1* is a potential *in vivo* target for these miRNAs, the next step is to see how these miRNAs regulate *Dll1* mRNA and protein levels and distribution *in vivo* (especially in paraxial and neuronal tissues).

First, Luciferase assays must be performed, to show that the identified miRNAs can target *Dll1* 3´UTR *in vitro*.

Furthermore, the influence of the miRNAs on the endogenous *Dll1* mRNA and protein levels and distribution must be determined. A strategy for analyzing miRNA mediated influence on mRNA and protein distribution *in vivo* was previously published and is adaptable for this purpose (Yoo et al., 2009). Here, two different targeting constructs must be generated, which each consist of the *Dll1* 5´ UTR and the third *Dll1* exon to assure proper homologous recombination (Figure 22 A). In the targeting constructs the first and second *Dll1* exons are replaced with a GFP (Figure 22 A). In the first construct, the GFP is followed by the endogenous *Dll1* 3´UTR, whereas in the second construct the GFP is followed by a simian-virus 40 (*SV40)* 3´UTR. These two targeting constructs are then used for homologous recombination in bacterial artificial chromosomes containing the *Dll1* coding region and approx. 30 - 40 kb of its upstream and downstream genomic sequences. Following homologues recombination, two different BACs are generated (BAC1; BAC2, respectively), where the GFP is fused in frame with the *Dll1* ATG transcriptional start site (Figure 22 B).

8. Outlook

These two BACs are subsequently used for injection into zygotes, to generate two different stable mouse lines. First, it must be determined whether the GFP mRNA and protein distribution of the BAC1 containing the endogenous *Dll1* 3´UTR matches the endogenous *Dll1* mRNA and protein distribution *in vivo*. If this is the case, analyzing GFP mRNA and protein distribution in the BAC2 containing the *SV40* 3´UTR can be used to determine, if there is a general influence on the *Dll1* mRNA and protein distribution, which is normally mediated by its endogenous 3´UTR. Finally, site directed mutagenesis of miRNA binding sites (Figure 22 C) in the *Dll1* 3´UTR of BAC1 could follow. This strategy can be used to determine whether single or combined mutations of these sites influence the *Dll1* mRNA and protein distribution *in vivo*.

Screening a F1 archive of ENU derived mouse mutants for mutations in the seed region of the identified miRNA binding sites could be an alternative method (Beckers et al., 2009). Homologous recombination could also be used to insert mutations in the seed region of the identified sites in *Dll1* 3´UTR.

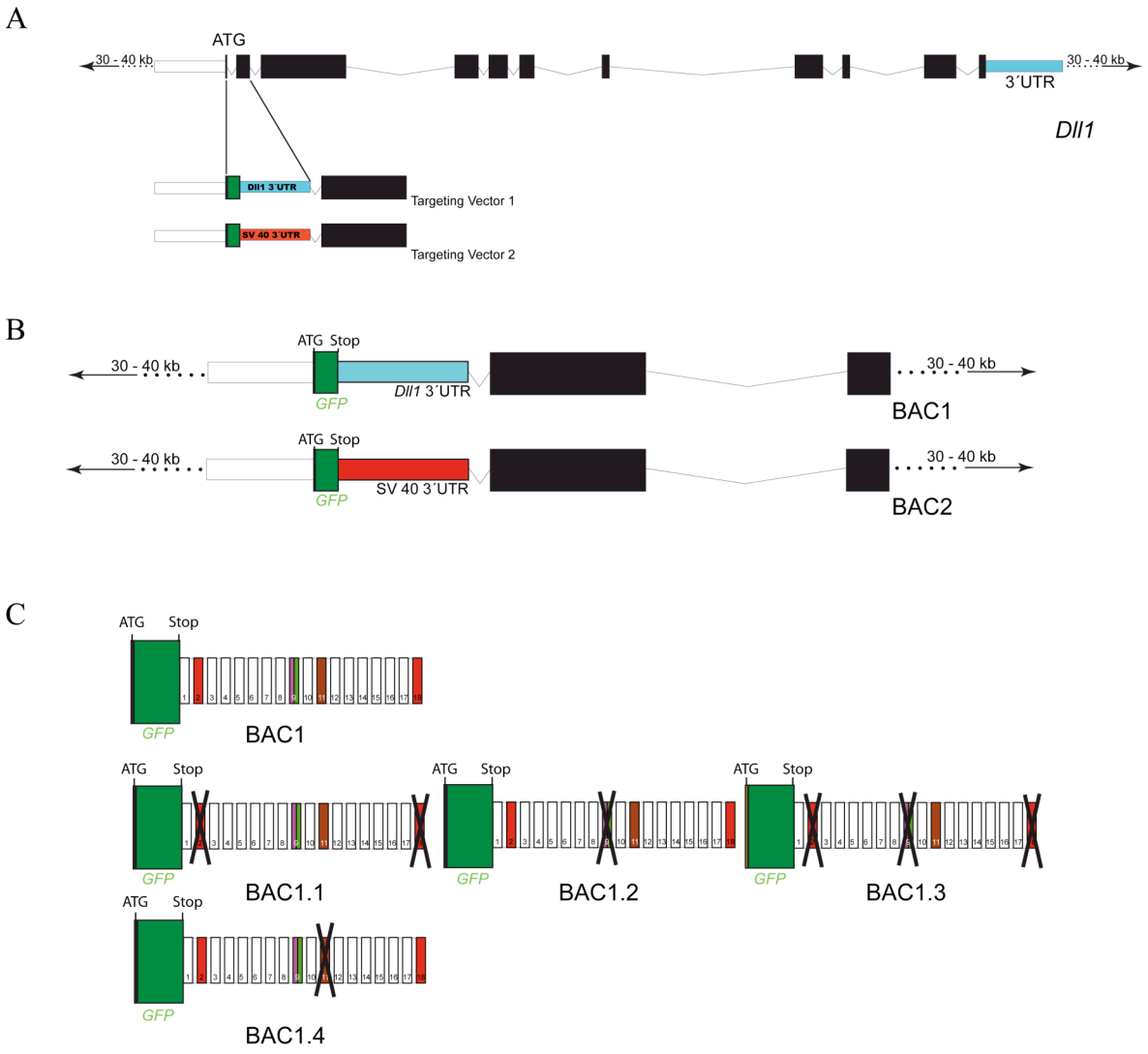

Figure 22: Strategy for functional *in vivo* analysis of the *Dll1* 3´UTR.

(**A**) A BAC containing the endogenous *Dll1* gene (top) and the two different vectors for homologous integration in the endogenous *Dll1* locus (bottom). Following homologous recombination a GFP followed by two different 3´UTR is fused in frame with the *Dll1* coding region. (**B**) This GFP is either followed by the endogenous *Dll1* 3´UTR (BAC1) or a *SV40* 3´UTR (BAC2). Two different BACs are generated, which can be used for injection into zygotes to generate stable mouse lines carrying the construct. (**C**) Site directed mutagenesis can be used two functionally delete single or combinations of miRNA binding sites in the 3´UTR of BAC1 to determine the influence of these sites on GFP mRNA and protein distribution *in vivo*.

8.2.2 Strategies to determine the molecular function of miRNAs during somitogenesis

A more general approach to determine the biological function of miRNAs is, to inactivate the *Dicer1* gene using appropriate Cre- lines and a *Dicer1*$^{fl/fl}$ allele. Conditional deletion of *Dicer1* in both the PSM and somites has already been performed using a *T (Brachury)* Cre line, suggesting a role for miRNAs in somite compartmentalisation, but not for somite formation (Zhang et al., 2011). The next step would be to independently inactivate *Dicer1* in the PSM or in the somites, to separately characterize miRNA function for segmentation and somite compartmentalisation. This approach, however, falls short to determine the function of unique miRNAs during somitogenesis. It has been shown in zebrafish that injection of specific miRNAs can partially rescue the phenotype in a *Dicer1* null background, thus providing functional information about one specific miRNA (Giraldez, 2005). These experiments could principally also be performed in the mouse.

A second possibility is to generate transgenic mice with tissue specific over-expression of miRNAs (which would be especially interesting for miR-103/107 and miR-130a/b). This is complicated by the fact that over-expression of miRNAs might target mRNAs which are normally not targeted in a physiological context, because of spatial differences between the miRNA and its target.

A third possibility is to construct conditional knock out alleles for the identified miRNAs, which would allow complete abrogation or deletion in specific compartments. For the construction of the conditional miRNA alleles, it is essential to retain the normal expression and function of the respective host gene. Another problem is that miRNAs often exists in families of highly related or even identical sequences throughout the genome (Figure 23, miR-103.1/miR-103.2), which puts the construction of conditional alleles to a challenge.

8.2.3 miRNAs and *in silico* modelling of somitogenesis

There exist lots of different computational programs, which model the gene regulatory networks taking place during the somitogenesis process *in silico* (Lewis, 2003; Tiedemann et al., 2007). Our ultimate goal is to integrate miRNA mediated gene regulation in these *in silico* models, especially for the *Dll1* gene, but also for other genes of the Delta-Notch pathway.

To integrate the mediated miRNA influence on *Dll1* (besides the knowledge of additional target mRNAs and how the miRNAs affect *Dll1* expression *in vivo*) it is necessary to know, which transcription factors regulate the expression of the identified miRNAs. miRNAs are generally dispersed throughout the genome. Their genomic location can either be intronic (in exonic or intronic location of protein coding genes) or intergenic (located between transcriptional units). Until recently, it was generally believed, that intronic miRNAs are transcribed directly with their host gene, whereas intergenic miRNAs do have their own *cis*-regulatory regions. Recent work, however, indicated that even some intronic miRNAs can have their own *cis*-regulatory regions. This work also implicated miR-107 as a potential candidate for intronic *cis*-regulation independent of host gene expression (Monteys et al., 2010).

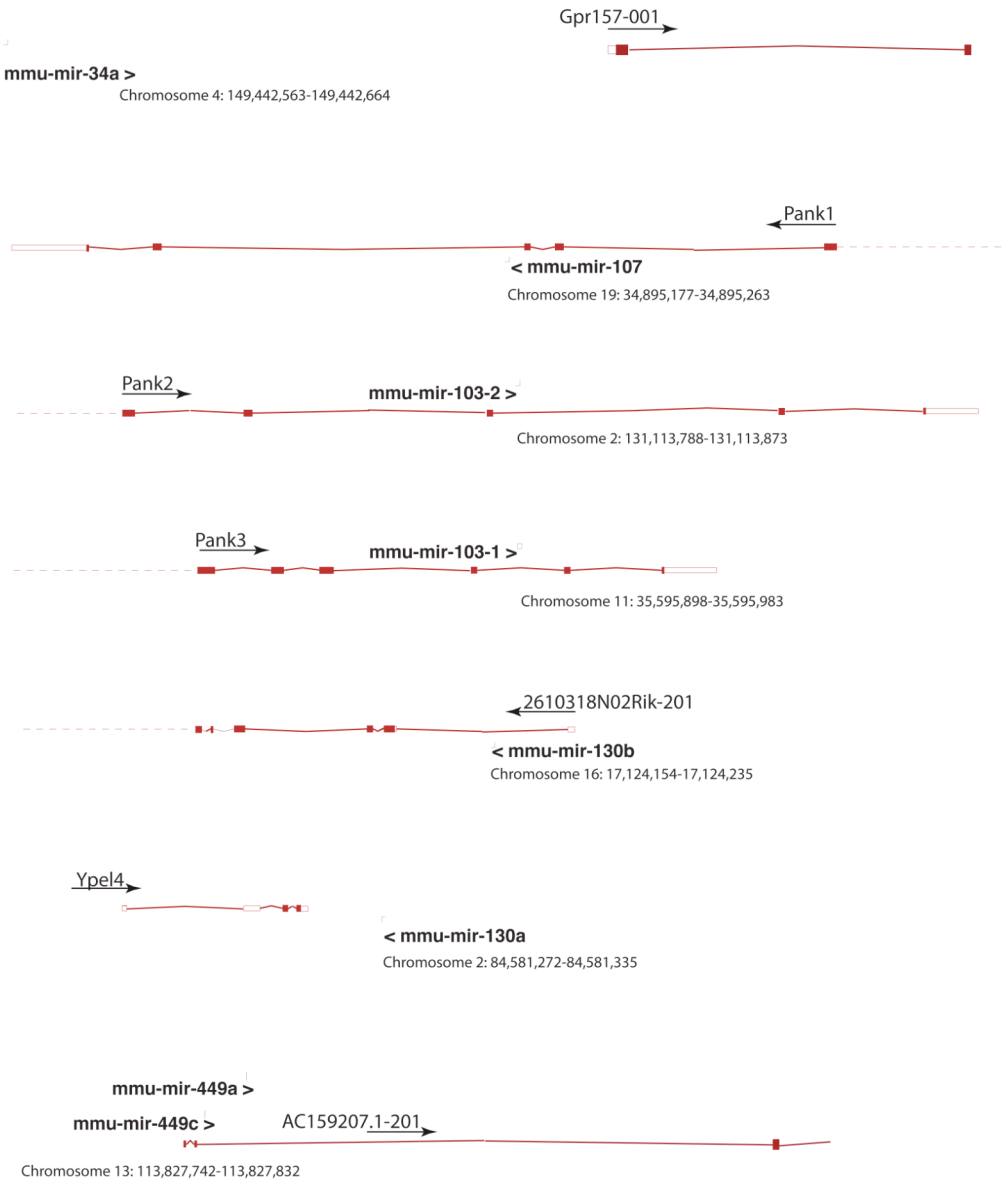

Figure 23: Genomic location of the 7 miRNAs identified in the whole mount *in situ* hybridisation screen (modified from http://www.ensembl.org/). Arrows indicate transcriptional direction of the respective mRNAs and miRNAs. miR-107 (Pank1), miR-103-2 (Pank2), miR-103-1 (Pank3), miR-130b (2610318N02Rik-201) and miR-449a/c (AC159207.2-201) do have an intronic genomic location. miR-34a and miR-130a do have an intergenic genomic location.

Among the miRNAs identified, two are intergenic (miR-34a, miR-130a), whereas five are intronic (miR-107, miR-103-1, miR-103-2, miR-130b) (Figure 23). It is thus now necessary to determine, whether the miRNAs are expressed and excised directly

from their host mRNAs, or if they do have their own *cis*-regulatory regions. It is then necessary to determine, which transcription factors control miRNA and/or host mRNA expression.

8.2.4 Potential approaches to identify cycling miRNAs in the PSM

miRNAs might also play a direct role on the transcriptional rate for cycling genes of all pathways in the PSM as it is known that mRNA half-life of components of the segmentation clock is critical for correct segmentation (Hendrik Tiedemann; personal communication). It is thus likely that miRNAs, which show a dynamic expression profile in the PSM, might tune the mRNA half-lifes of their respective target genes to assure proper segmentation. To identify miRNAs, which show a dynamic expression profile in the PSM, it is possible to modify and expand a strategy, which was previously published to identify cycling mRNAs in the PSM (Dequéant et al., 2006). First PSMs of 9.5 dpc embryos are dissected and separated in two halves. One half is subsequently used for whole mount *in situ* hybridisation for a cycling gene in the PSM e.g. *Lfng* (Figure 24 A, B). These *in situ* hybridised halves are used to determine the respective cycling stage of the PSM. A small lesion of the posterior PSM of the second half is dissected and stored.

After *in situ* staging, these small lesions are used to extract miRNA (Figure 24 A), or mRNA and miRNAs (Figure 24 B).

In the first approach the isolated miRNAs are used for hybridisation on single colour miRNA arrays. After normalization of arrays, cycling miRNAs should be characterized by dynamic expression patterns (Figure 24 A), whereas miRNAs that do not cycle should be constant.

In a second approach miRNA and mRNA expression levels are quantified on qPCR panels containing all murine miRNAs. These panels must additionally contain cycling

control genes of the Delta-Notch, Fgf and Wnt pathway (Figure 24B). Cycling miRNAs in the PSM should here be also characterized by a dynamic expression profile, which follows in phase or in antiphase, the expression pattern of the control cycling genes.

All miRNAs identified are subsequently validated by *in situ* hybridisation on mouse embryos.

All validated miRNAs can then be analyzed *in silico* for potential target genes among known cycling genes in the PSM and their *in vitro* influence on these genes can be determined.

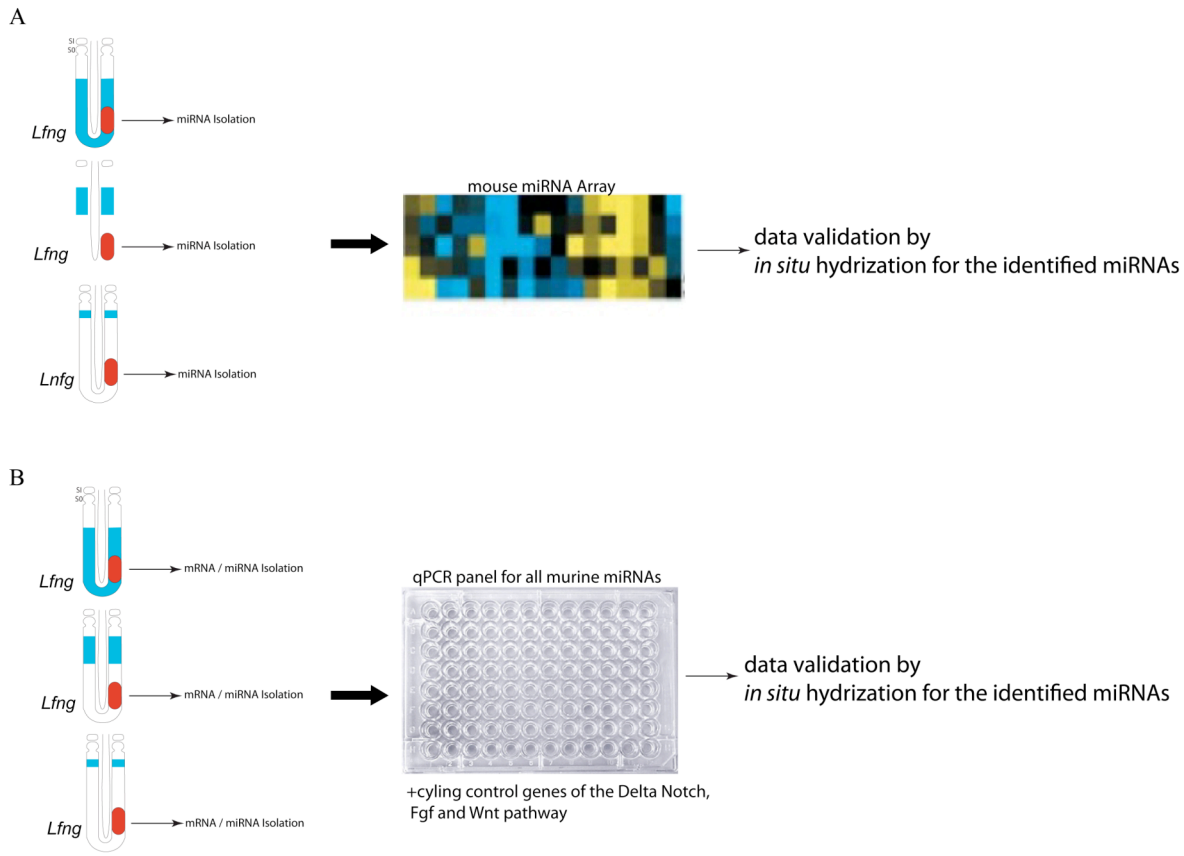

Figure 24: Two different strategies to identify cycling miRNAs in the PSM. (**A, B**) A cycling gene in the PSM e.g. *Lfng* is used for *in situ* staging of dissected PSMs. A small lesion of the posterior PSM is removed (marked red) and used for RNA/miRNA isolation. (**A**) In the first approach the isolated miRNAs are used for hybridisation on single colour miRNA arrays. After normalization cycling miRNAs should be

characterized by dynamic expression patterns on the arrays, corresponding to the respective segmentation clock stages (microarray picture was modified from (Dequéant et al., 2006)) (**B**) In a second approach miRNA and mRNA expression levels are quantified on qRT-PCR panels containing all murine miRNAs. These panels should additionally contain cycling control genes of the Delta-Notch, Fgf and Wnt pathway. Cycling miRNAs should be characterized by dynamic expression levels, which follow in phase or in antiphase the cycling control genes.

9.Abbreviations

°C	degree Celsius
BAC	Bacterial Artificial Chromosome
bp	base pair
cis	on the same chromosome
DL	double labelled DIG probe
DNA	deoxyribonucleic acid
dpc	days post coitum
dpp	days post partum
EMT	epithelial to mesenchymal transition
GFP	green fluorescent protein
Hox	Homeobox-containing
in silico	performed on computer or via computer simulation
in situ	in the place
in vivo	using a whole living organism
kb	kilo base pair
MET	mesenchymal to epithelial transition
miRNA	microRNA
MSD	mesodermal
NICD	Notch intracellular domain
PCR	Polymerase Chain Reaction
PE	Potential Enhancer
PSM	presomitic mesoderm
qPCR	quantitative PCR
RNA	ribonucleic acid

9. Abbreviations

SL	single labelled DIG probe
Tbx6	T-Box transcription factor 6
UTR	untranslated region

10. Appendix

Type of malformation	C7 to T1 transformation		Split vertebral bodies in lumbar segments		Fused neural arches in cervical segments		Fused vertebral bodies		Total
		P %		P %	C	P %		P %	N=
wildtype	2	2.3	3	3.4	0	0	0	0	86
Dll1$^{tm1leg/+}$	20	34.5	1	1.7	0	0	0	0	58
Dll1$^{tm1leg/\ tm1leg}$	10	25.6	11	28.1	6	15.4	12	20.5	39
Dll1$^{tm1.1leg/+}$	12	11.7	5	4.9	2	5.4	0	0	102
Dll1$^{tm1.1leg/\ tm1.1leg}$	16	15.3	5	5.4	1	2.7	0	0	91
Tbx6$^{tm1Pa/+}$	11	42.3	9	34.6	5	19.2	0	0	26
Tbx6$^{tm1Pa/+}$ *Dll1*$^{tm1.1leg/+}$	8	30.7	17	65.3	6	23.0	0	0	26
Tbx6$^{tm1Pa/+}$ *Dll1*$^{tm1.1leg/tm1.1leg}$	6	30.0	17	80.0	4	20.0	0	0	20

Table 1: Complete data of skeletal malformations of newborn mice as observed for wild type, hetero and homozygous *Dll1*^{tm1leg}, hetero and homozygous *Dll1*$^{tm1.1leg}$, heterozygous *Tbx6*^{tm1Pa} and combinations of MSD and Tbx6 alleles (*Tbx6*$^{tm1Pa/+}$ *Dll1*$^{tm1.1leg/+}$ *Tbx6*$^{tm1Pa/+}$ *Dll1*$^{tm1.1leg/tm1.1leg}$). This data set was used to calculate statistical significance.

Type of malformation	C7->T1 (rudimentary ribs)		Total
		P %	N=
wild type	1	3.3	30
Dll1$^{tm1.1leg/+}$	5	11.9	42
Dll1$^{tm1.1leg/\ tm1.1leg}$	10	18.5	54

Table 2: Complete data of rudimentary ribs of newborn mice as observed for wild type, hetero and homozygous *Dll1*$^{tm1.1leg}$ mice.

miRNA	PSM	Somites	CNS	cranial/dorsal root ganglia	limbs	lateral plate mesoderm	heart	branchial arches	otic vesicle	allantois	choroid plexus
miR-1	-	√	-	-	-	-	√	-	-	-	-
miR-34a	√	√	-	-	-	√	-	√	√	√	-
miR-103	√	√	√	√	√	√	-	√	√	√	-
miR-107	√	√	√	√	√	√	-	√	√	√	-
miR-130a	√	√	√	√	√	√	-	√	√	√	-
miR-130b	√	√	√	√	√	√	-	√	√	√	-
miR-449a	-	-	-	-	-	-	-	-	-	-	√
miR-449c	-	-	-	-	-	-	-	-	-	-	√
Dll1	√	√	√	-	-	-	-	-	√	-	√

Table 3: Summarizing overview of overlapping miRNA and *Dll1* expression domains.

miRNA ID	Expression detected in single DIG labeling approach (SL)	Expression detected in double DIG labeling approach (DL)	Selection of other predicted target genes	
mmu-miR-15a	none	none	Sos2 Fgf8 Ihh	Wnt8a
mmu-miR-15b	none	none	Acvr2a Epha1 Dll1	Clock
mmu-miR-34a	not reproducible	yes	Klhdc3 Pdzk1 Fbxo30	Bmp7 Dll1 Foxg1
mmu-miR-34c	none	none	Ddx17 Pdzk1 Bmp7	Dll1 Gadd45g Jag1
mmu-miR-103	yes	yes	Fgf18 Ihh Dll1	Sall1 Wnt3a Dvl1
mmu-miR-107	yes	yes	Fgf18 Dll1 Sall1	Ihh Ddx39 Dvl1
mmu-miR-130a	yes	yes	Neurog1 Acvr1 Sos2	
mmu-miR-130b	yes	yes	Neurog1 Acvr1 Sos2	
mmu-miR-301a	not reproducible	none	Sos2 Dll1 Wnt1	
mmu-miR-301b	not analysed	none	Lrp2 Dlx5 Dll1	
mmu-miR-362-5	not analysed	none	Lhx4 Apba2 Dll1	
mmu-miR-363	none	none	Smad7 Pax9 Cdh10	Dll1 Klf6 Bmp7
mmu-miR-369-3	not analysed	none	Pnrc1 Cno Sgms2	
mmu-miR-449a	yes	not analysed	Fut8 Lef1 Jag2	Notch1
mmu-miR-449c	not analysed	yes	Fut8 Dll1 Lef1	Jag2 Notch1
mmu-miR-497	not analysed	none	Dll1 Wnt8a Fgf8	

Table 4: Summarizing overview of miRNA IDs and *in situ* hybridisation data and selection of additional genes predicted *in silico* to contain target sites for the respective miRNAs. The selection is biased towards genes that are implicated in Delta/Notch

11. Literature

Alvares, L.E., Schubert, F.R., Thorpe, C., Mootoosamy, R.C., Cheng, L., Parkyn, G., Lumsden, A., Dietrich, S., 2003. Intrinsic, Hox-dependent cues determine the fate of skeletal muscle precursors. Developmental Cell 5, 379-390.

Aoyama, H., Asamoto, K., 1988. Determination of somite cells: independence of cell differentiation and morphogenesis. Development 104, 15-28.

Aoyama, H., Asamoto, K., 2000. The developmental fate of the rostral/caudal half of a somite for vertebra and rib formation: experimental confirmation of the resegmentation theory using chick-quail chimeras. Mechanisms of Development 99, 71-82.

Appel, B., Givan, L.A., Eisen, J.S., 2001. Delta-Notch signaling and lateral inhibition in zebrafish spinal cord development. BMC Dev Biol 1, 13.

Artavanis-Tsakonas, S., Matsuno, K., Fortini, M.E., 1995. Notch signaling. Science 268, 225-232.

Artavanis-Tsakonas, S., Rand, M.D., Lake, R.J., 1999. Notch signaling: cell fate control and signal integration in development. Science 284, 770-776.

Aulehla, A., Johnson, R.L., 1999. Dynamic expression of lunatic fringe suggests a link between notch signaling and an autonomous cellular oscillator driving somite segmentation. Developmental Biology 207, 49-61.

Aulehla, A., Wehrle, C., Brand-Saberi, B., Kemler, R., Gossler, A., Kanzler, B., Herrmann, B.G., 2003. Wnt3a plays a major role in the segmentation clock controlling somitogenesis. Developmental Cell 4, 395-406.

Awgulewitsch, A., Jacobs, D., 1990. Differential expression of Hox 3.1 protein in subregions of the embryonic and adult spinal cord. Development 108, 411-420.

Ayyanan, A., Civenni, G., Ciarloni, L., Morel, C., Mueller, N., Lefort, K., Mandinova, A., Raffoul, W., Fiche, M., Dotto, G.P., Brisken, C., 2006. Increased Wnt signaling triggers oncogenic conversion of human breast epithelial cells by a Notch-dependent mechanism. Proc Natl Acad Sci USA 103, 3799-3804.

Bagnall, K.M., Higgins, S.J., Sanders, E.J., 1988. The contribution made by a single somite to the vertebral column: experimental evidence in support of resegmentation using the chick-quail chimaera model. Development 103, 69-85.

Barrios, A., Poole, R.J., Durbin, L., Brennan, C., Holder, N., Wilson, S.W., 2003. Eph/Ephrin signaling regulates the mesenchymal-to-epithelial transition of the paraxial mesoderm during somite morphogenesis. Curr Biol 13, 1571-1582.

Bartel, D.P., 2004. MicroRNAs: genomics, biogenesis, mechanism, and function. Cell 116, 281-297.

Beckers, J., Clark, A., Wünsch, K., Hrabé de Angelis, M., Gossler, A., 1999. Expression of the mouse Delta1 gene during organogenesis and fetal development. Mechanisms of Development 84, 165-168.

Beckers, J., Schlautmann, N., Gossler, A., 2000. The mouse rib-vertebrae mutation disrupts anterior-posterior somite patterning and genetically interacts with a Delta1 null allele. Mechanisms of Development 95, 35-46.

Beckers, J., Wurst, W., de Angelis, M., 2009. Towards better mouse models: enhanced genotypes, systemic phenotyping and envirotype modelling. Nat Rev Genet.

Berezikov, E., Thuemmler, F., van Laake, L.W., Kondova, I., Bontrop, R., Cuppen, E., Plasterk, R.H.A., 2006. Diversity of microRNAs in human and chimpanzee brain. Nat Genet 38, 1375-1377.

Bernstein, E., Kim, S.Y., Carmell, M.A., Murchison, E.P., Alcorn, H., Li, M.Z., Mills, A.A., Elledge, S.J., Anderson, K.V., Hannon, G.J., 2003. Dicer is essential for mouse development. Nat Genet 35, 215-217.

Bessho, Y., Miyoshi, G., Sakata, R., Kageyama, R., 2001. Hes7: a bHLH-type repressor gene regulated by Notch and expressed in the presomitic mesoderm. Genes Cells 6, 175-185.
Bettenhausen, B., Hrabě de Angelis, M., Simon, D., Guénet, J.L., Gossler, A., 1995. Transient and restricted expression during mouse embryogenesis of Dll1, a murine gene closely related to Drosophila Delta. Development 121, 2407-2418.
Bray, S.J., 2006. Notch signalling: a simple pathway becomes complex. Nat Rev Mol Cell Biol 7, 678-689.
Brent, A.E., Tabin, C.J., 2002. Developmental regulation of somite derivatives: muscle, cartilage and tendon. Current Opinion in Genetics & Development 12, 548-557.
Brody, T., Rasband, W., Baler, K., Kuzin, A., Kundu, M., Odenwald, W.F., 2007. cis-Decoder discovers constellations of conserved DNA sequences shared among tissue-specific enhancers. Genome Biol 8, R75.
Bussen, M., Petry, M., Schuster-Gossler, K., Leitges, M., Gossler, A., Kispert, A., 2004. The T-box transcription factor Tbx18 maintains the separation of anterior and posterior somite compartments. Genes & Development 18, 1209-1221.
Calin, G.A., Croce, C.M., 2006. MicroRNA signatures in human cancers. Nat Rev Cancer 6, 857-866.
Carapuço, M., Nóvoa, A., Bobola, N., Mallo, M., 2005. Hox genes specify vertebral types in the presomitic mesoderm. Genes & Development 19, 2116-2121.
Chalfie, M., Horvitz, H.R., Sulston, J.E., 1981. Mutations that lead to reiterations in the cell lineages of C. elegans. Cell 24, 59-69.
Chapman, D.L., Cooper-Morgan, A., Harrelson, Z., Papaioannou, V.E., 2003. Critical role for Tbx6 in mesoderm specification in the mouse embryo. Mechanisms of Development 120, 837-847.
Chapman, D.L., Papaioannou, V.E., 1998. Three neural tubes in mouse embryos with mutations in the T-box gene Tbx6. Nature 391, 695-697.
Chen, C.Z., Li, L., Lodish, H.F., Bartel, D.P., 2004. MicroRNAs modulate hematopoietic lineage differentiation. Science 303, 83-86.
Chen, J.-F., Mandel, E.M., Thomson, J.M., Wu, Q., Callis, T.E., Hammond, S.M., Conlon, F.L., Wang, D.-Z., 2006. The role of microRNA-1 and microRNA-133 in skeletal muscle proliferation and differentiation. Nat Genet 38, 228-233.
Chitnis, A., Henrique, D., Lewis, J., Ish-Horowicz, D., Kintner, C., 1995. Primary neurogenesis in Xenopus embryos regulated by a homologue of the Drosophila neurogenic gene Delta. Nature 375, 761-766.
Christ, B., Ordahl, C.P., 1995. Early stages of chick somite development. Anat Embryol 191, 381-396.
Christ, B., Wilting, J., 1992. From somites to vertebral column. Ann Anat 174, 23-32.
Conlon, R.A., Reaume, A.G., Rossant, J., 1995. Notch1 is required for the coordinate segmentation of somites. Development 121, 1533-1545.
Cooke, J., Zeeman, E.C., 1976. A clock and wavefront model for control of the number of repeated structures during animal morphogenesis. Journal of Theoretical Biology 58, 455-476.
Cooke, J.E., Kemp, H.A., Moens, C.B., 2005. EphA4 is required for cell adhesion and rhombomere-boundary formation in the zebrafish. Curr Biol 15, 536-542.
Cordes, R., Schuster-Gossler, K., Serth, K., Gossler, A., 2004. Specification of vertebral identity is coupled to Notch signalling and the segmentation clock. Development 131, 1221-1233.
Couly, G.F., Coltey, P.M., Le Douarin, N.M., 1993. The triple origin of skull in higher vertebrates: a study in quail-chick chimeras. Development 117, 409-429.
Dale, J.K., Malapert, P., Chal, J., Vilhais-Neto, G., Maroto, M., Johnson, T., Jayasinghe, S., Trainor, P., Herrmann, B., Pourquié, O., 2006. Oscillations of the snail genes in the

presomitic mesoderm coordinate segmental patterning and morphogenesis in vertebrate somitogenesis. Developmental Cell 10, 355-366.
Darnell, D., Kaur, S., Stanislaw, S., Konieczka, J.H., Konieczka, J., Yatskievych, T., Antin, P., 2006. MicroRNA expression during chick embryo development. Dev Dyn 235, 3156-3165.
De Bellard, M.E., Ching, W., Gossler, A., Bronner-Fraser, M., 2002. Disruption of segmental neural crest migration and ephrin expression in delta-1 null mice. Developmental Biology 249, 121-130.
Delic, S., Streif, S., Deussing, J.M., Weber, P., Ueffing, M., Hölter, S.M., Wurst, W., Kühn, R., 2008. Genetic mouse models for behavioral analysis through transgenic RNAi technology. Genes Brain Behav 7, 821-830.
Deo, M., Yu, J.-Y., Chung, K.-H., Tippens, M., Turner, D.L., 2006. Detection of mammalian microRNA expression by in situ hybridization with RNA oligonucleotides. Dev Dyn 235, 2538-2548.
Dequéant, M.-L., Glynn, E., Gaudenz, K., Wahl, M., Chen, J., Mushegian, A., Pourquié, O., 2006. A complex oscillating network of signaling genes underlies the mouse segmentation clock. Science 314, 1595-1598.
Dequéant, M.-L., Pourquié, O., 2008. Segmental patterning of the vertebrate embryonic axis. Nat Rev Genet 9, 370-382.
Deschamps, J., van Nes, J., 2005. Developmental regulation of the Hox genes during axial morphogenesis in the mouse. Development 132, 2931-2942.
Dottori, M., Hartley, L., Galea, M., Paxinos, G., Polizzotto, M., Kilpatrick, T., Bartlett, P.F., Murphy, M., Köntgen, F., Boyd, A.W., 1998. EphA4 (Sek1) receptor tyrosine kinase is required for the development of the corticospinal tract. Proc Natl Acad Sci USA 95, 13248-13253.
Duband, J.L., Dufour, S., Hatta, K., Takeichi, M., Edelman, G.M., Thiery, J.P., 1987. Adhesion molecules during somitogenesis in the avian embryo. The Journal of Cell Biology 104, 1361-1374.
Duboule, D., 2007. The rise and fall of Hox gene clusters. Development 134, 2549-2560.
Duboule, D., Morata, G., 1994. Colinearity and functional hierarchy among genes of the homeotic complexes. Trends Genet 10, 358-364.
Dubrulle, J., McGrew, M.J., Pourquié, O., 2001. FGF signaling controls somite boundary position and regulates segmentation clock control of spatiotemporal Hox gene activation. Cell 106, 219-232.
Dunty, W., Biris, K., Chalamalasetty, R.B., Taketo, M.M., Lewandoski, M., Yamaguchi, T., 2008. Wnt3a/beta-catenin signaling controls posterior body development by coordinating mesoderm formation and segmentation. Development 135, 85-94.
Dunwoodie, S.L., Henrique, D., Harrison, S.M., Beddington, R.S., 1997. Mouse Dll3: a novel divergent Delta gene which may complement the function of other Delta homologues during early pattern formation in the mouse embryo. Development 124, 3065-3076.
Durbin, L., Brennan, C., Shiomi, K., Cooke, J., Barrios, A., Shanmugalingam, S., Guthrie, B., Lindberg, R., Holder, N., 1998. Eph signaling is required for segmentation and differentiation of the somites. Genes & Development 12, 3096-3109.
Ellisen, L.W., Bird, J., West, D.C., Soreng, A.L., Reynolds, T.C., Smith, S.D., Sklar, J., 1991. TAN-1, the human homolog of the Drosophila notch gene, is broken by chromosomal translocations in T lymphoblastic neoplasms. Cell 66, 649-661.
Evrard, Y.A., Lun, Y., Aulehla, A., Gan, L., Johnson, R.L., 1998. lunatic fringe is an essential mediator of somite segmentation and patterning. Nature 394, 377-381.
Fischer, A., Gessler, M., 2007. Delta-Notch--and then? Protein interactions and proposed modes of repression by Hes and Hey bHLH factors. Nucleic Acids Research 35, 4583-4596.

Forlani, S., Lawson, K.A., Deschamps, J., 2003. Acquisition of Hox codes during gastrulation and axial elongation in the mouse embryo. Development 130, 3807-3819.
Forsberg, H., Crozet, F., Brown, N.A., 1998. Waves of mouse Lunatic fringe expression, in four-hour cycles at two-hour intervals, precede somite boundary formation. Curr Biol 8, 1027-1030.
Funayama, N., Sato, Y., Matsumoto, K., Ogura, T., Takahashi, Y., 1999. Coelom formation: binary decision of the lateral plate mesoderm is controlled by the ectoderm. Development 126, 4129-4138.
Galceran, J., Sustmann, C., Hsu, S.-C., Folberth, S., Grosschedl, R., 2004. LEF1-mediated regulation of Delta-like1 links Wnt and Notch signaling in somitogenesis. Genes & Development 18, 2718-2723.
Gale, N.W., Dominguez, M.G., Noguera, I., Pan, L., Hughes, V., Valenzuela, D.M., Murphy, A.J., Adams, N.C., Lin, H.C., Holash, J., Thurston, G., Yancopoulos, G.D., 2004. Haploinsufficiency of delta-like 4 ligand results in embryonic lethality due to major defects in arterial and vascular development. Proc Natl Acad Sci USA 101, 15949-15954.
Galliot, B., Dollé, P., Vigneron, M., Featherstone, M.S., Baron, A., Duboule, D., 1989. The mouse Hox-1.4 gene: primary structure, evidence for promoter activity and expression during development. Development 107, 343-359.
Geffers, I., Serth, K., Chapman, G., Jaekel, R., Schuster-Gossler, K., Cordes, R., Sparrow, D.B., Kremmer, E., Dunwoodie, S.L., Klein, T., Gossler, A., 2007. Divergent functions and distinct localization of the Notch ligands DLL1 and DLL3 in vivo. The Journal of Cell Biology 178, 465-476.
Gomez, C., Ozbudak, E.M., Wunderlich, J., Baumann, D., Lewis, J., Pourquié, O., 2008. Control of segment number in vertebrate embryos. Nature 454, 335-339.
Gregory, P.A., Bert, A.G., Paterson, E.L., Barry, S.C., Tsykin, A., Farshid, G., Vadas, M.A., Khew-Goodall, Y., Goodall, G.J., 2008. The miR-200 family and miR-205 regulate epithelial to mesenchymal transition by targeting ZEB1 and SIP1. Nat Cell Biol 10, 593-601.
Griffiths-Jones, S., Saini, H.K., van Dongen, S., Enright, A.J., 2008. miRBase: tools for microRNA genomics. Nucleic Acids Research 36, D154-158.
Guo, H., Ingolia, N.T., Weissman, J.S., Bartel, D.P., 2010. Mammalian microRNAs predominantly act to decrease target mRNA levels. Nature 466, 835-840.
Hajihosseini, M.K., Heath, J.K., 2002. Expression patterns of fibroblast growth factors-18 and -20 in mouse embryos is suggestive of novel roles in calvarial and limb development. Mechanisms of Development 113, 79-83.
Hans, S., Campos-Ortega, J.A., 2002. On the organisation of the regulatory region of the zebrafish deltaD gene. Development 129, 4773-4784.
Harris, K.S., Zhang, Z., McManus, M.T., Harfe, B.D., Sun, X., 2006. Dicer function is essential for lung epithelium morphogenesis. Proc Natl Acad Sci USA 103, 2208-2213.
Harrison, S.M., Houzelstein, D., Dunwoodie, S.L., Beddington, R.S., 2000. Sp5, a new member of the Sp1 family, is dynamically expressed during development and genetically interacts with Brachyury. Developmental Biology 227, 358-372.
Hashimi, S.T., Fulcher, J.A., Chang, M.H., Gov, L., Wang, S., Lee, B., 2009. MicroRNA profiling identifies miR-34a and miR-21 and their target genes JAG1 and WNT1 in the coordinate regulation of dendritic cell differentiation. Blood 114, 404-414.
Hermeking, H., 2010. The miR-34 family in cancer and apoptosis. Cell Death and Differentiation 17, 193-199.
Hirata, H., Bessho, Y., Kokubu, H., Masamizu, Y., Yamada, S., Lewis, J., Kageyama, R., 2004. Instability of Hes7 protein is crucial for the somite segmentation clock. Nat Genet 36, 750-754.
Hoesel, B., Bhujabal, Z., Przemeck, G.K.H., Kurz-Drexler, A., Weisenhorn, D.M.V., de Angelis, M.H., Beckers, J., 2010. Combination of in silico and in situ hybridisation

approaches to identify potential Dll1 associated miRNAs during mouse embryogenesis. Gene Expr Patterns.
Hofmann, M., Schuster-Gossler, K., Watabe-Rudolph, M., Aulehla, A., Herrmann, B.G., Gossler, A., 2004. WNT signaling, in synergy with T/TBX6, controls Notch signaling by regulating Dll1 expression in the presomitic mesoderm of mouse embryos. Genes & Development 18, 2712-2717.
Horan, G.S., Wu, K., Wolgemuth, D.J., Behringer, R.R., 1994. Homeotic transformation of cervical vertebrae in Hoxa-4 mutant mice. Proc Natl Acad Sci USA 91, 12644-12648.
Horsch, M., Schädler, S., Gailus-Durner, V., Fuchs, H., Meyer, H., de Angelis, M.H., Beckers, J., 2008. Systematic gene expression profiling of mouse model series reveals coexpressed genes. Proteomics 8, 1248-1256.
Hrabe de Angelis, M., McIntyre, J., 2nd, Gossler, A., 1997. Maintenance of somite borders in mice requires the Delta homologue DII1. Nature 386, 717-721.
Hrabě de Angelis, M., McIntyre, J., Gossler, A., 1997. Maintenance of somite borders in mice requires the Delta homologue DII1. Nature 386, 717-721.
Iimura, T., Denans, N., Pourquié, O., 2009. Establishment of Hox vertebral identities in the embryonic spine precursors. Curr Top Dev Biol 88, 201-234.
Iimura, T., Pourquié, O., 2006. Collinear activation of Hoxb genes during gastrulation is linked to mesoderm cell ingression. Nature 442, 568-571.
Ivey, K.N., Muth, A., Arnold, J., King, F.W., Yeh, R.F., Fish, J.E., Hsiao, E.C., Schwartz, R.J., Conklin, B.R., Bernstein, H.S., Srivastava, D., 2008. MicroRNA regulation of cell lineages in mouse and human embryonic stem cells. Cell Stem Cell 2, 219-229.
JACOB, F., PERRIN, D., SANCHEZ, C., MONOD, J., 1960. [Operon: a group of genes with the expression coordinated by an operator.]. C R Hebd Seances Acad Sci 250, 1727-1729.
Jouve, C., Iimura, T., Pourquie, O., 2002. Onset of the segmentation clock in the chick embryo: evidence for oscillations in the somite precursors in the primitive streak. Development 129, 1107-1117.
Jouve, C., Palmeirim, I., Henrique, D., Beckers, J., Gossler, A., Ish-Horowicz, D., Pourquié, O., 2000. Notch signalling is required for cyclic expression of the hairy-like gene HES1 in the presomitic mesoderm. Development 127, 1421-1429.
Juan, A.H., Ruddle, F.H., 2003. Enhancer timing of Hox gene expression: deletion of the endogenous Hoxc8 early enhancer. Development 130, 4823-4834.
Kessel, M., Balling, R., Gruss, P., 1990. Variations of cervical vertebrae after expression of a Hox-1.1 transgene in mice. Cell 61, 301-308.
Kessel, M., Gruss, P., 1991. Homeotic transformations of murine vertebrae and concomitant alteration of Hox codes induced by retinoic acid. Cell 67, 89-104.
Kloosterman, W.P., Wienholds, E., De Bruijn, E., Kauppinen, S., Plasterk, R.H.A., 2006. In situ detection of miRNAs in animal embryos using LNA-modified oligonucleotide probes. Nat Meth 3, 27-29.
Kullander, K., Mather, N.K., Diella, F., Dottori, M., Boyd, A.W., Klein, R., 2001. Kinase-dependent and kinase-independent functions of EphA4 receptors in major axon tract formation in vivo. Neuron 29, 73-84.
Kusumi, K., Dunwoodie, S.L., Krumlauf, R., 2001. Dynamic expression patterns of the pudgy/spondylocostal dysostosis gene Dll3 in the developing nervous system. Mechanisms of Development 100, 141-144.
Kusumi, K., Sun, E.S., Kerrebrock, A.W., Bronson, R.T., Chi, D.C., Bulotsky, M.S., Spencer, J.B., Birren, B.W., Frankel, W.N., Lander, E.S., 1998. The mouse pudgy mutation disrupts Delta homologue Dll3 and initiation of early somite boundaries. Nat Genet 19, 274-278.
Kwon, C., Han, Z., Olson, E.N., Srivastava, D., 2005. MicroRNA1 influences cardiac differentiation in Drosophila and regulates Notch signaling. Proc Natl Acad Sci USA 102, 18986-18991.

Lan, Y., Jiang, R., Shawber, C., Weinmaster, G., Gridley, T., 1997. The Jagged2 gene maps to chromosome 12 and is a candidate for the lgl and sm mutations. Mamm Genome 8, 875-876.
Lardelli, M., Dahlstrand, J., Lendahl, U., 1994. The novel Notch homologue mouse Notch 3 lacks specific epidermal growth factor-repeats and is expressed in proliferating neuroepithelium. Mechanisms of Development 46, 123-136.
Leimeister, C., Dale, K., Fischer, A., Klamt, B., Hrabe de Angelis, M., Radtke, F., McGrew, M.J., Pourquié, O., Gessler, M., 2000. Oscillating expression of c-Hey2 in the presomitic mesoderm suggests that the segmentation clock may use combinatorial signaling through multiple interacting bHLH factors. Developmental Biology 227, 91-103.
Lewis, B.P., Burge, C.B., Bartel, D.P., 2005. Conserved seed pairing, often flanked by adenosines, indicates that thousands of human genes are microRNA targets. Cell 120, 15-20.
Lewis, J., 2003. Autoinhibition with transcriptional delay: a simple mechanism for the zebrafish somitogenesis oscillator. Curr Biol 13, 1398-1408.
Lindsell, C.E., Shawber, C.J., Boulter, J., Weinmaster, G., 1995. Jagged: a mammalian ligand that activates Notch1. Cell 80, 909-917.
Liu, N., Williams, A.H., Kim, Y., McAnally, J., Bezprozvannaya, S., Sutherland, L.B., Richardson, J.A., Bassel-Duby, R., Olson, E.N., 2007. An intragenic MEF2-dependent enhancer directs muscle-specific expression of microRNAs 1 and 133. Proc Natl Acad Sci USA 104, 20844-20849.
Livak, K.J., Schmittgen, T.D., 2001. Analysis of relative gene expression data using real-time quantitative PCR and the 2(-Delta Delta C(T)) Method. Methods 25, 402-408.
Lufkin, T., Mark, M., Hart, C.P., Dollé, P., LeMeur, M., Chambon, P., 1992. Homeotic transformation of the occipital bones of the skull by ectopic expression of a homeobox gene. Nature 359, 835-841.
Ma, Q., Chen, Z., del Barco Barrantes, I., de la Pompa, J.L., Anderson, D.J., 1998. neurogenin1 is essential for the determination of neuronal precursors for proximal cranial sensory ganglia. Neuron 20, 469-482.
MacDonald, B.T., Adamska, M., Meisler, M.H., 2004. Hypomorphic expression of Dkk1 in the doubleridge mouse: dose dependence and compensatory interactions with Lrp6. Development 131, 2543-2552.
Mansouri, A., Voss, A.K., Thomas, T., Yokota, Y., Gruss, P., 2000. Uncx4.1 is required for the formation of the pedicles and proximal ribs and acts upstream of Pax9. Development 127, 2251-2258.
Marklund, U., Hansson, E.M., Sundström, E., de Angelis, M.H., Przemeck, G.K.H., Lendahl, U., Muhr, J., Ericson, J., 2010. Domain-specific control of neurogenesis achieved through patterned regulation of Notch ligand expression. Development 137, 437-445.
Martello, G., Rosato, A., Ferrari, F., Manfrin, A., Cordenonsi, M., Dupont, S., Enzo, E., Guzzardo, V., Rondina, M., Spruce, T., Parenti, A.R., Daidone, M.G., Bicciato, S., Piccolo, S., 2010. A MicroRNA targeting dicer for metastasis control. Cell 141, 1195-1207.
Maruhashi, M., Van De Putte, T., Huylebroeck, D., Kondoh, H., Higashi, Y., 2005. Involvement of SIP1 in positioning of somite boundaries in the mouse embryo. Dev Dyn 234, 332-338.
McGrew, M.J., Dale, J.K., Fraboulet, S., Pourquié, O., 1998. The lunatic fringe gene is a target of the molecular clock linked to somite segmentation in avian embryos. Curr Biol 8, 979-982.
Mittapalli, V.R., Huang, R., Patel, K., Christ, B., Scaal, M., 2005. Arthrotome: a specific joint forming compartment in the avian somite. Dev Dyn 234, 48-53.
Monteys, A.M., Spengler, R.M., Wan, J., Tecedor, L., Lennox, K.A., Xing, Y., Davidson, B.L., 2010. Structure and activity of putative intronic miRNAs promoters. RNA.

Morimoto, M., Takahashi, Y., Endo, M., Saga, Y., 2005. The Mesp2 transcription factor establishes segmental borders by suppressing Notch activity. Nature 435, 354-359.
Morrison, A., Hodgetts, C., Gossler, A., Hrabé de Angelis, M., Lewis, J., 1999. Expression of Delta1 and Serrate1 (Jagged1) in the mouse inner ear. Mechanisms of Development 84, 169-172.
Müller, J., Scheyer, T.M., Head, J.J., Barrett, P.M., Werneburg, I., Ericson, P.G.P., Pol, D., Sánchez-Villagra, M.R., 2010. Homeotic effects, somitogenesis and the evolution of vertebral numbers in recent and fossil amniotes. Proc Natl Acad Sci USA.
Nakajima, Y., Morimoto, M., Takahashi, Y., Koseki, H., Saga, Y., 2006. Identification of Epha4 enhancer required for segmental expression and the regulation by Mesp2. Development 133, 2517-2525.
Nakaya, Y., Kuroda, S., Katagiri, Y.T., Kaibuchi, K., Takahashi, Y., 2004. Mesenchymal-epithelial transition during somitic segmentation is regulated by differential roles of Cdc42 and Rac1. Developmental Cell 7, 425-438.
Oka, C., Nakano, T., Wakeham, A., de la Pompa, J.L., Mori, C., Sakai, T., Okazaki, S., Kawaichi, M., Shiota, K., Mak, T.W., Honjo, T., 1995. Disruption of the mouse RBP-J kappa gene results in early embryonic death. Development 121, 3291-3301.
Olson, E.N., Arnold, H.H., Rigby, P.W., Wold, B.J., 1996. Know your neighbors: three phenotypes in null mutants of the myogenic bHLH gene MRF4. Cell 85, 1-4.
Palmeirim, I., Henrique, D., Ish-Horowicz, D., Pourquié, O., 1997. Avian hairy gene expression identifies a molecular clock linked to vertebrate segmentation and somitogenesis. Cell 91, 639-648.
Pfaffl, M.W., 2001. A new mathematical model for relative quantification in real-time RT-PCR. Nucleic Acids Res 29, e45.
Pourquié, O., 2004. The chick embryo: a leading model in somitogenesis studies. Mechanisms of Development 121, 1069-1079.
Przemeck, G.K.H., Heinzmann, U., Beckers, J., Hrabé de Angelis, M., 2003. Node and midline defects are associated with left-right development in Delta1 mutant embryos. Development 130, 3-13.
Rathjen, T., Pais, H., Sweetman, D., Moulton, V., Munsterberg, A., Dalmay, T., 2009. High throughput sequencing of microRNAs in chicken somites. FEBS Letters 583, 1422-1426.
Redshaw, N., Wheeler, G., Hajihosseini, M.K., Dalmay, T., 2009. microRNA-449 is a putative regulator of choroid plexus development and function. Brain Res 1250, 20-26.
Richardson, M.K., Allen, S.P., Wright, G.M., Raynaud, A., Hanken, J., 1998. Somite number and vertebrate evolution. Development 125, 151-160.
Riley, M., 2010. Post-transcriptional Regulation of Lfng by miR-125a is Crucial for Vertebrate Segmentation. kb.osu.edu.
Rubio-Aliaga, I., Soewarto, D., Wagner, S., Klaften, M., Fuchs, H., Kalaydjiev, S., Busch, D.H., Klempt, M., Rathkolb, B., Wolf, E., Abe, K., Zeiser, S., Przemeck, G.K., Beckers, J., de Angelis, M.H., 2007. A genetic screen for modifiers of the delta1-dependent notch signaling function in the mouse. Genetics 175, 1451-1463.
Saga, Y., Hata, N., Koseki, H., Taketo, M.M., 1997. Mesp2: a novel mouse gene expressed in the presegmented mesoderm and essential for segmentation initiation. Genes & Development 11, 1827-1839.
Schröter, C., Oates, A.C., 2010. Segment Number and Axial Identity in a Segmentation Clock Period Mutant. Curr Biol.
Serth, K., Schuster-Gossler, K., Cordes, R., Gossler, A., 2003. Transcriptional oscillation of lunatic fringe is essential for somitogenesis. Genes & Development 17, 912-925.
Shifley, E.T., Cole, S.E., 2007. The vertebrate segmentation clock and its role in skeletal birth defects. Birth Defects Res C Embryo Today 81, 121-133.

Stern, C.D., Fraser, S.E., Keynes, R.J., Primmett, D.R., 1988. A cell lineage analysis of segmentation in the chick embryo. Development 104 Suppl, 231-244.
Struhl, G., 1983. Role of the esc+ gene product in ensuring the selective expression of segment-specific homeotic genes in Drosophila. Journal of embryology and experimental morphology 76, 297-331.
Sweetman, D., Goljanek, K., Rathjen, T., Oustanina, S., Braun, T., Dalmay, T., Münsterberg, A., 2008. Specific requirements of MRFs for the expression of muscle specific microRNAs, miR-1, miR-206 and miR-133. Developmental Biology 321, 491-499.
Sweetman, D., Rathjen, T., Jefferson, M., Wheeler, G., Smith, T.G., Wheeler, G.N., Münsterberg, A., Dalmay, T., 2006. FGF-4 signaling is involved in mir-206 expression in developing somites of chicken embryos. Dev Dyn 235, 2185-2191.
Takada, S., Stark, K.L., Shea, M.J., Vassileva, G., McMahon, J.A., McMahon, A.P., 1994. Wnt-3a regulates somite and tailbud formation in the mouse embryo. Genes & Development 8, 174-189.
Takahashi, J., Ohbayashi, A., Oginuma, M., Saito, D., Mochizuki, A., Saga, Y., Takada, S., 2010. Analysis of Ripply1/2-deficient mouse embryos reveals a mechanism underlying the rostro-caudal patterning within a somite. Developmental Biology.
Takahashi, Y., Koizumi, K., Takagi, A., Kitajima, S., Inoue, T., Koseki, H., Saga, Y., 2000. Mesp2 initiates somite segmentation through the Notch signalling pathway. Nat Genet 25, 390-396.
Takahashi, Y., Yasuhiko, Y., Kitajima, S., Kanno, J., Saga, Y., 2007. Appropriate suppression of Notch signaling by Mesp factors is essential for stripe pattern formation leading to segment boundary formation. Developmental Biology 304, 593-603.
Tam, P.P., 1981. The control of somitogenesis in mouse embryos. Journal of embryology and experimental morphology 65 Suppl, 103-128.
Tam, P.P., Trainor, P.A., 1994. Specification and segmentation of the paraxial mesoderm. Anat Embryol 189, 275-305.
Teppner, I., Becker, S., de Angelis, M.H., Gossler, A., Beckers, J., 2007. Compartmentalised expression of Delta-like 1 in epithelial somites is required for the formation of intervertebral joints. BMC Dev Biol 7, 68.
Thomsen, R., Nielsen, P.S., Jensen, T.H., 2005. Dramatically improved RNA in situ hybridization signals using LNA-modified probes. RNA 11, 1745-1748.
Tiedemann, H.B., Schneltzer, E., Zeiser, S., Rubio-Aliaga, I., Wurst, W., Beckers, J., Przemeck, G.K.H., Hrabé de Angelis, M., 2007. Cell-based simulation of dynamic expression patterns in the presomitic mesoderm. Journal of Theoretical Biology 248, 120-129.
Uyttendaele, H., Marazzi, G., Wu, G., Yan, Q., Sassoon, D., Kitajewski, J., 1996. Notch4/int-3, a mammary proto-oncogene, is an endothelial cell-specific mammalian Notch gene. Development 122, 2251-2259.
van den Akker, E., Fromental-Ramain, C., de Graaff, W., Le Mouellic, H., Brûlet, P., Chambon, P., Deschamps, J., 2001. Axial skeletal patterning in mice lacking all paralogous group 8 Hox genes. Development 128, 1911-1921.
Volpe, M.V., Wang, K.T.W., Nielsen, H.C., Chinoy, M.R., 2008. Unique spatial and cellular expression patterns of Hoxa5, Hoxb4, and Hoxb6 proteins in normal developing murine lung are modified in pulmonary hypoplasia. Birth Defects Res Part A Clin Mol Teratol 82, 571-584.
Watabe-Rudolph, M., Schlautmann, N., Papaioannou, V.E., Gossler, A., 2002. The mouse rib-vertebrae mutation is a hypomorphic Tbx6 allele. Mechanisms of Development 119, 251-256.
Wehn, A.K., Gallo, P.H., Chapman, D.L., 2009. Generation of transgenic mice expressing Cre recombinase under the control of the Dll1 mesoderm enhancer element. genesis 47, 309-313.

Weinmaster, G., Roberts, V.J., Lemke, G., 1992. Notch2: a second mammalian Notch gene. Development 116, 931-941.
Wellik, D.M., 2007. Hox patterning of the vertebrate axial skeleton. Dev Dyn 236, 2454-2463.
Wellik, D.M., Capecchi, M.R., 2003. Hox10 and Hox11 genes are required to globally pattern the mammalian skeleton. Science 301, 363-367.
White, P.H., Chapman, D.L., 2005. Dll1 is a downstream target of Tbx6 in the paraxial mesoderm. Genesis 42, 193-202.
White, P.H., Farkas, D.R., Chapman, D.L., 2005. Regulation of Tbx6 expression by Notch signaling. genesis 42, 61-70.
White, P.H., Farkas, D.R., McFadden, E.E., Chapman, D.L., 2003. Defective somite patterning in mouse embryos with reduced levels of Tbx6. Development 130, 1681-1690.
Williams, C.K., Li, J.-L., Murga, M., Harris, A.L., Tosato, G., 2006. Up-regulation of the Notch ligand Delta-like 4 inhibits VEGF-induced endothelial cell function. Blood 107, 931-939.
Wittler, L., Shin, E., Grote, P., Kispert, A., Beckers, A., Gossler, A., Werber, M., Herrmann, B., 2007. Expression of Msgn1 in the presomitic mesoderm is controlled by synergism of WNT signalling and Tbx6. EMBO Rep 8, 784-789.
Wong, P.C., Zheng, H., Chen, H., Becher, M.W., Sirinathsinghji, D.J., Trumbauer, M.E., Chen, H.Y., Price, D.L., Van der Ploeg, L.H., Sisodia, S.S., 1997. Presenilin 1 is required for Notch1 and DII1 expression in the paraxial mesoderm. Nature 387, 288-292.
Wray, G.A., 2007. The evolutionary significance of cis-regulatory mutations. Nature Reviews Genetics 8, 206-216.
Yang, W.J., Yang, D.D., Na, S., Sandusky, G.E., Zhang, Q., Zhao, G., 2005. Dicer is required for embryonic angiogenesis during mouse development. J Biol Chem 280, 9330-9335.
Yoo, A.S., Staahl, B.T., Chen, L., Crabtree, G.R., 2009. MicroRNA-mediated switching of chromatin-remodelling complexes in neural development. Nature 460, 642-646.
Yoshikawa, Y., Fujimori, T., McMahon, A.P., Takada, S., 1997. Evidence that absence of Wnt-3a signaling promotes neuralization instead of paraxial mesoderm development in the mouse. Developmental Biology 183, 234-242.
Zákány, J., Kmita, M., Alarcon, P., de la Pompa, J.L., Duboule, D., 2001. Localized and transient transcription of Hox genes suggests a link between patterning and the segmentation clock. Cell 106, 207-217.
Zhang, Z., O'rourke, J.R., Mcmanus, M.T., Lewandoski, M., Harfe, B.D., Sun, X., 2011. The microRNA-processing enzyme Dicer is dispensable for somite segmentation but essential for limb bud positioning. Developmental Biology.
Zhao, Y., Ransom, J.F., Li, A., Vedantham, V., von Drehle, M., Muth, A.N., Tsuchihashi, T., McManus, M.T., Schwartz, R.J., Srivastava, D., 2007. Dysregulation of cardiogenesis, cardiac conduction, and cell cycle in mice lacking miRNA-1-2. Cell 129, 303-317.
Zinzen, R.P., Girardot, C., Gagneur, J., Braun, M., Furlong, E.E.M., 2009. Combinatorial binding predicts spatio-temporal cis-regulatory activity. Nature 462, 65-70.